Modelling Brittle Fracture Propagation in the Next Generation CO$_2$ Pipelines

A thesis submitted to University College London for the degree of

Doctor of Philosophy

By

Peng Zhang

Department of Chemical Engineering

University College London

Torrington Place

London WC1E 7JE

April 2014

Table of Content

ABSTRACT

The development and testing of a fluid-structure interaction model for simulating the transition of an initial through-wall defect in pressurised CO_2 transmission pipelines employed as part of the carbon capture and storage chain into running brittle fractures is presented. The model accounts for all the important processes governing the fracture propagation process including the fluid/wall heat transfer, the resulting localised pressure stresses in the pipe wall as well as the initial defect geometry. Real fluid behaviour is considered using the modified Peng Robinson equation of state.

Hypothetical but nevertheless realistic failure scenarios involving the transportation of gas and dense phase CO_2 using existing natural gas steel pipelines are simulated using the model. The impacts of the pipe wall thickness, Ductile-Brittle-Transition Temperature (DBTT), initial defect geometry, feed temperature, stream impurities, surrounding backfill as well as flow isolation on brittle fracture propagation behaviour are investigated.

In all circumstances, the initial defect geometry in the pipeline is shown to have a major impact on the pipeline's propensity to brittle fracture propagation. For example, in the case of an initial through-wall defect in the form of a circular puncture where there is no stress concentration, fracture propagation is highly unlikely. The opposite applies to an elliptical through-wall defect embodying a hairline crack extending from its side.

Furthermore, gas-phase CO_2 pipelines are more prone to brittle fracture failures as compared to dense-phase CO_2 pipelines despite the higher starting pressure. This is due to the higher degree of expansion-induced cooling for gaseous CO_2. The emergency isolation of the initial flow in the pipeline following the formation of the initial defect promotes brittle fracture. For the ranges tested, typical CO_2 stream impurities are shown to have negligible impact on brittle fracture behaviour. Puncture in a buried pipeline where there is no blowout of the surrounding soil is more likely to lead to brittle facture propagation as compared to that for an exposed pipeline. This is due to the secondary cooling of the pipe wall by the surrounding soil cooled by the escaping gas.

ACKNOWLEDGEMENTS

List of Symbols

C: the volumetric specific heat

D_{in}:   thepipeline inner diameter

E: the Young's modulus

f_w: theFanning friction factor

G: the strain energy

g: the gravitational acceleration

g: the internal heat generation rate

$h(x,a)$ the weight function

h: the heat transfer coefficient

h: the specific enthalpy

J: the J integral

K: the stress intensity factor

K_c: the material critical stress intensity factor

K_f: the stress intensity factor under reference stress

M_g: themolecular weight of the gas components

M_l: themolecular weight of the liquid components

Nu: the Nusselt number

P: the pressure of the fluid

Pr: the Prandtl number

q_h: the heat transferred through the pipe wall

Re: the Reynolds number

s: the specific entropy

T: the temperature

U: the strain energy of the crack body

u: the velocity

V: the volume of the fluid

χ: the fluid quality

Y: thedimensionless shape factor

Z: the fluid compressibility

α: the half crack length

β_x: the fluid and the friction force

Γ: the plastic work per unit area of surface created

γ: the work required to form a unit new surface

γ: the ratio of specific heats

γ_p: the energy dissipated by the plastic deformation in the vicinity of the crack tip

ε: the pipe roughness

θ: the angle of inclination of the pipeline to the horizontal

κ: the isothermal coefficient of volumetric expansion

μ: the dynamic viscosity

ν: the Poisson's ratio.

ν: the kinetic viscosity

ρ: the density of the fluid

σ: the stress loading

σ_f: the critical stress

τ: the sheer

ω: the acentric factor

List of abbreviations

BTC: the Battelle Two Curve

CCS: the Carbon Capture and Storage

CFD: the Computational Fluid Dynamics

DBTT: the Ductile-Brittle-Transition Temperature

FVM: the Finite Volume method

FEA: the Finite Element Analysis

HEM: the Homogeneous Equilibrium Model

MOC: the method of Characteristics

SIF: the Stress Intensity Factor

CHAPTER 1: INTRODUCTION

As the planning for Carbon Capture and Storage (CCS) proceeds, the use of long distance networks of pressurised pipelines for the transportation of the captured CO_2 for subsequent storage is becoming inevitable. Given that CO_2 is toxic at concentrations higher than 7%, the safety of CO_2 pipelines is of paramount importance and indeed pivotal to the public acceptability of CCS as a viable means for tackling the impact of global warming.

It is noteworthy that CO_2 pipelines have been in operation in the US for over 30 year for enhanced oil recovery (Bilio et al., 2009; Seevam et al., 2008). However, these are either confined to low populated areas, mostly operating below the proposed supercritical conditions (73.3 bar and 31.18 ℃; Suehiroet al., 1996)that make CO_2 pipeline transportation economically viable. Additionally, given their small number, it is not possible to draw a meaningful statistical representation of the overall risk. Parfomak and Fogler(2007)propose that 'statistically, the number of incidents involving CO_2 pipelines should be similar to those for natural gas transmission pipelines'.

Clearly, given the heightened public awareness of environmental issues, even a single incident involving the large-scale escape of CO_2 near a populated area may have an adverse impact on the introduction of the CCS technology.

Propagating or running factures are considered as the most catastrophic type of pipeline failure given that they result in a massive escape of inventory in a short space of time. As such it is highly desirable to design pipelines with sufficiently high fracture toughness such that when a defect reaches a critical size, the result is a leak rather than a long running fracture. In the case of CO_2 pipelines such types of failure will be of particular concern in Europe as large pipeline sections will inevitably be onshore, some passing near or through populated areas(Serpa et al., 2011). In addition, there is significant financial incentive in using the existing stock of hydrocarbon pipelines for transporting CO_2(Serpa et al., 2011). Given the very different properties

of CO_2 as compared to hydrocarbons, all safety issues regarding pipeline compatibility must be addressed a prior.

In essence, a fracture may propagate in either a ductile or a brittle mode. However, there are subtle, yet important differences in the respective propagation mechanisms worthy of discussion. Ductile fractures, characterised by the plastic deformation of the pipeline along the tear are the more common of the two modes of failure and therefore best understood. These may commence following an initial tear or puncture in the pipeline, for example due to third party damage or corrosion. The likelihood of this initial through-wall defect transforming into a propagating ductile fracture may be assessed using the simple well-established Battelle Two Curve (BTC) methodology (Maxey, 1974). In essence the above involves the comparison of the pipeline decompression and the crack tip velocity curves. The crack will propagate as long as the decompression wave speed in the fluid is slower than the crack tip velocity. The BTC approach was recently extended by Mahgerefteh et al.,(2011) through the coupling the fluid decompression and the crack velocity curves. This enabled the prediction of the variation of the crack length with time and hence the crack arrest length. Given the almost instantaneous transformation of the initial tear into a ductile fracture running at high velocity (ca. 200-300 m/s), heat transfer effects between the escaping fluid and the pipe wall during the propagation process will be insignificant. As such the transient pressure stress is the only driving force for propagating a ductile fracture.

The propagation mechanism in the case of brittle factures is somewhat different. A situation may arise in which the pressure inside the pipeline at the time of formation of a puncture or a leak will be insufficient to drive a ductile fracture. However, with the passage of time, the Joule-Thomson expansion induced cooling of the escaping fluid will lower the pipe wall temperature in the proximity of the leak. In the event that the pipe wall temperature reaches its Ductile-Brittle-Transition Temperature (DBTT), for most pipeline materials, there will be an almost instantaneous and significant drop in the fracture toughness. In such cases, depending on the initial defect size and geometry, if the prevailing pressure and thermal stresses exceed the

critical facture toughness(Mahgerefteh and Atti, 2006),a running brittle fracture will occur.

As such the modelling of brittle fractures requires the consideration of both the transient thermal and pressure stresses in the proximity of the initial through-wall defect.

Three factors render CO_2 pipelines especially susceptible to brittle fractures as compared to hydrocarbon pipelines (Bilio et al., 2009). These include CO_2's unusually high saturation pressure and its significant sensitivity to the presence of even small amounts of impurities (Mahgerefeth et al., 2012), its 'slow' depressurisation following a leak especially during the liquid/gas phase transition and finally its high Joule-Thomson expansion induced cooling.

Although brittle fracture propagation in CO_2 pipelines has been raised as an issue of possible concern (Andrews et al., 2010), to date, no experimental test data or comprehensive mathematical modelling work on the topic hasbeen reported. This is of special concern given the economic incentives in using existing natural gas pipelines for transporting CO_2. Such pipelines are more susceptible to brittle fractures as compared to new pipeline materials given the fact that they were built under pipeline standards with much higher DBTT (cf.-10 ℃). Given the relatively short time frames being proposed for CCS introduction, the development of suitable mathematical models for assessing the susceptibility of CO_2 pipelines to brittle factures is very timely.

In a recent publication,Mahgerefteh and Atti (2006) presented a fluid-structure interaction model for simulating brittle fractures in pressurised pipelines. However, the simulation data reported was limited to hydrocarbon pipeline inventories. Given their very different thermodynamic decompression trajectories, it is impossible to extend the findings to CO_2 pipelines. Additionally, the model employed an over-simplified crack tip fracture model, only valid for an infinite plate with a puncture. Also, it only models the scenario wherethe pipeline is exposed to air. The heat transfer process when the pipeline is buried is not considered in the model.

Chapter 1: Introduction

In this thesis, the development and testing of a fully coupled fluid-structure interaction model for simulating brittle fracture propagation for gas and dense phase CO_2pipelines addressing the above limitations ispresented. Data based on the application of the model is reported in order to test the susceptibility tobrittle fracture propagation for CO_2 pipeline.

This thesis is divided into 7 chapters.

Chapter 2 presents relevant theories for thefracture mechanics used in this study. It provides a review of methods to determine the Stress Intensity Factor (SIF) and approximation of weight function.

In chapter 3, the theoretical basis for the pipeline outflow model employed in this study together with its assumptions and justifications are presented. The chapter presents the basic conservation equations for mass, momentum and energy.Furthermore, the Method of Characteristics (MOC) used for the resolution of the conservative equations is also presented.

In chapter 4, the development of theheat transfer sub-model to simulate the pipe wall temperature profile following rupture ispresented. The model accounts for all the heat transfer processes between the pipe wall, the fluid as well as the ambient conditions.

Chapter 5 presents the process of developing the crack tip fracture model which involves three steps: 1) Establishing the crack tip model using the Finite Element Method (FEA). 2) Deriving the corresponding parameters of weight function from the FEA results. 3) Curve fitting the weight function parameter datato polynomials. The performance of the fitted weight functions expressions isnext evaluated by comparing their predicted SIFvalues against those obtained using Abaqus.

In chapter 6, hypothetical but nevertheless realistic failure scenarios involving the transportation of gas and dense phase CO_2 using existing natural gas steel pipelines are simulated. The impacts of fluid phase, the pipe wall thickness,Ductile-Brittle-Transition Temperature (DBTT), the crack geometry, feed temperature, stream impurities as well as flow isolation on brittle fracture propagation behaviour are tested.

Chapter 7 deals with general conclusions and suggestions for future work.

CHAPTER 2: LITERATURE REVIEW

2.1 Introduction

Preventing unstable fractures in CO_2 pipelines is as important as that for natural gas pipelines.In the development of a rigorous mathematical model for simulatinglow-temperature-induced-brittle fracture, a rigorous Computational Fluid Dynamics (CFD)outflow model to determine the fluid release conditionsat the defect plane coupled with the relevantmaterialfracture considerations is essential.

In the first part of this chapter, mathematical models simulating outflow following pipeline failure are reviewed. In the second part, basic fracture mechanic theories employed in this study are also presented. For completeness, the basic theory of the UCL outflow model,along with its performance against real data, is presented in Chapter 3.This chapter presents a review of the background fracture mechanicstheories employed in this work.

2.2 Review of the CFD Outflow Models

Extensive reviews of the various pipeline outflow models ranging from the simple empirical correlations to the more sophisticated CFD models including, where possible, an evaluation of their performance against real data may be found in publications by Denton(2009)and Brown (2011). The merits and some of the drawbacks of these models, in terms of the degree of agreement with real data, range of applications and computational run time, have formed the basis for the development of the state of the art University College London (UCL) (Mahgerefteh et al., 2008a) pipeline rupture model employed in this study for determining the required CFD data. In this section, a brief review of four most-widely-used outflow simulation models is reviewed. The models reviewed include:

1. British Gas Model
2. OLGA

3. Imperial College London Models
4. University College London Models

2.2.1 British Gas Model (DECAY)

DECAY is a model that was reviewed by Jones et al.(1981), which is able to assess decompression of high-pressure natural gas that occurs once a pipeline has ruptured. The model stems from both homogenous and isentropic equilibrium fluid flow. Also, the model is only applicable to horizontal pipelines. Additionally, it utilises the Soave-Redlich-Kwong equation of state (abbreviated to the SRK EoS) to assess fluid property data. Furthermore, it can also address wave propagation that occurs along the pipeline length.

Jones et al.(1981) conducted shock tube experiments to validate the model, utilising different fluid compositions. A tube of 36.6 metres in length and 0.1 metres in diameter was tested. An explosive charge at the end of the tube was detonated to cause depressurisation. There was a good correlation between the experimental data and the simulated results.

However, in spite of the correlation that was noticed, critics of the model state that the model does not consider the blowdown of longer pipes, such as those that transport flashing fluids. Additionally, Kimambo et al. (1995) stated that the model failed to consider how friction and heat transfer could affect the process, which can distort the results and skew the simulated findings.

2.2.2 OLGA

Statoil initially utilized OLGA for the hydrocarbon industry in 1983, for the purpose of simulating slow transients that relate to slugging, shut-in, pipeline start-up and other induced problems. Initially, the model was designed for smaller pipelines, particularly for the flow of air and water at low pressures. OLGA was able to simulate the flow regime of bubbling or slugging, but could not measure stratified or annular

flow regimes. The model was addressed by Bendiksen et al. (1991), who was able to expand the capabilities of the model onto hydrocarbon mixtures.

The OLGA model uses different equations for liquid bulk, gas and liquid droplets. Interfacial mass transfer can assist the coupling process too. There are two momentum equations that are used:

1. Combination equation for liquid droplets and gas
2. Liquid film equation

A heat transfer coefficient that is specified by the user determines the heat transfer through pipe walls. Different factors of friction are applied for each separate flow regime. A numerical scheme can be applied to solve pertinent conservation equations. The outcomes are sharp slug front and tails, which can distort slug size predictions(Nordsveenand Haerdig, 1997). TheLangrangian type tracking scheme was later developed to overcome this issue. Phase behaviour cannot always be incorporated into the model, due to limitations on the methods and models that contribute to OLGA (Chen et al., 1993).

2.2.3 Imperial College London Models

BLOWDOWN Model

Researchers at Imperial College London pioneered the BLOWDOWN computer simulation, which aims to assess quasi-adiabatic expansion, which occurs once pressure vessels have experienced blowdown. The model is able to measure how weak vessels can affect a pipeline, through the simulations of low temperatures and fluid flow. It is considered to be the most useful method to measure vessel depressurization. Mahgerefteh and Wong (1999) expanded on the model, using alternate state equations.

The BLOWDOWN model considers many processes under different circumstances, such as heat transfer on the fluid wall between different phases, and evaporation/condensation induced fluxes on the sonic flow. There are many outcomes

of the process, including pressure fluctuations and differing temperatures. Pressure increments result in depressurization of vessels. An energy balance applied to the release orifice measures critical flow.

Chen et al.(1995a, 1995b) Model

Real fluid behaviour in pressurized pipeline outflow was initially measured by Picard et al. (1988). Chen et al. (1995a) expanded on these findings and also assessed how homogenous equilibrium compares against heterogeneous equilibrium, when considering constituent phases. The former suggests that the phases are at both mechanical and thermal equilibrium, as well as the contents travelling at the same speed. This belief allows for the maximum rate of mass transfer, which ultimately simplifies the process into an easier equation. The researchers proposed a model to further simplify the system, which assumed that fluid phases can be dispersed, meaning that concentration stratification does not affect the predictions made by OLGA or PLAC.

The researchers incorporated an explicit flow form, or alternatively used Reynolds' stress of kinetic energy; this allowed them to prove that departing from the equilibrium can be measured by addressing the differences between the vapour phase and the liquid phase. Hyperbolicity of the system is also measured by stabilizing the flow. The information that considers flow structure is not necessarily addressed with this model; especially when considering non dissipative flow.

Richardson et al. (2006) Model

Richardson et al. (2006)undertook many experiments in a British Gas bas in Cumbria, UK, which used highly volatile hydrocarbon combinations, such as commercial propane mixtures. These were placed under high pressures (100 bar) and rapid flow rates (4kg/s) to assess how the homogeneous equilibrium model (HEM) could predict pressurised hydrocarbon outflow through the pipe.

In research by Richardson et al.(2006), it was discovered that HEM assumptions are not always viable for compressed volatile liquids in a single phase upstream fluid, because of the inefficient gas nucleation process. The process is slow due to the phase equilibrium establishment. Therefore, the researchers state the fluid cannot be compressed, because the fluid density change is too small.

Richardson et al. (2006)continued to explain that HEM is useful for mixtures with a liquid mass fraction of less than 0.8. There is variation in the discharge coefficient, deviating from 0.9 for single phase flow of gas; it can reach 0.98 if the liquid fraction of the upstream is 0.8. Compressed volatile liquids are also suitable for the model; the discharge coefficient is approximately 0.6.

The researchers expanded by stating that two phase mixtures are harder to apply with HEM, as the >0.8 to <0.97 range is too difficult to measure. Also, API recommendation comparisons indicated that API predictions are less accurate for measuring restricted flow rates.

2.2.4 University College London Models

Mahgerefteh et al.(1997, 1999, 2000) Models

Mahgerefteh et al. produced much research surrounding modelling transient outflows, once a pipeline has been ruptured. The research focused on one-dimensional flow and its associated equations, to address associated MOC properties (Zucrow & Hoffman, 1976).

Check and ball valves were also measured to determine emergency isolated; these were simulated in research by Mahgerefteh et al. (1997)which used an inventory to determine ideal gas in an attempt to assess associated dynamic effects.A real case study in the North Sea used a methane pipeline of 145km in length and 0.87m in diameter; it assessed valve responses after emergency isolation was applied.

Peng-Robinson Equation of State (EoS) was applied with Mahgerefteh et al. (1999) to assess long term hydrodynamic equations of two phase flows. Additionally, characteristics of curves were assessed and modified using arc parabolas. These additions overcome the issues associated with linear pipelines and their associated characteristics, ultimately reducing variation in thermo physical properties. Chen et al. (1995a) stated that the HEM maintains assumptions of thermal and mechanical equilibrium.

Mahgerefteh et al. (1999) published the document that worked in accordance with the Piper Alpha riser. Two test results supported these findings, which stemmed from the Isle of Grain depressurisation experiments.

A real fluid model was applied to simulate how phase transition occurs on the emergency shutdown of valves, which was assisted by a MOC model(Mahgerefteh et al., 2000).

A transition from a gas phase to a two phase flow results in a delayed activation of valves. Consequently, the content of the pipeline is lost more rapidly, compared with permanent gas content. The Joukowsky equation(Joukowsky, 1990) was applied to simulate the pressure surge of the upstream closed valve.

Oke et al.,(2003, 2004) Model

Modelling outflow characteristics after ruptures on pipelines has been extensively studied(Oke et al., 2003;2004). These predictions use MOC models and maintain assumptions of homogeneous equilibriums. However, to assess the accuracy and run times, conservation equations were applied to assess combinations of velocity, pressure and enthalpy/entropy. Usually, pressure, velocity and density are solely measured (Mahgerefteh et al., 1997; Zucrow & Hoffman, 1976). Additionally, quadratic interpolation effects along space coordinates were measured to determine their effects.

The Isle of Grain and the Pipe Alpha data was used to triangulate the model by Oke(2004). All of aforementioned parameters were assessed with equations that measured depressurisation in pipelines, to establish which of these variables most greatly affect accuracy and run time. The model testing velocity, pressure and enthalpy was proven to be the most effective, compared with combinations that replaced enthalpy with either entropy or density.

The depressurization of a pipeline is heavily affected by the distance that the expansion waves travel, from the rupture to the intact end (Oke, 2004). Faster depressurization occurs when the distance is reduced. There are two different network configurations, both of equal length, yet one has a greater number of branched pipes, resulting in faster depressurization. Therefore, with extensively branched pipes, quicker emergency responses are required in case of a failure, as secondary escalation is higher and personnel need to be evacuated quicker.

The aaforementioned models can predict the outcomes of pipeline punctures; however the boundary conditions need modification. Atti (2006) explained that these can overcome the problems associated with boundary condition formulation.

Atti(2006)Model

An interpolation technique was developed by Atti(2006) to reduce the runtime for Mahgerefteh et al.(2000) HEM model. The equations for conservation that were applied were based on velocity, enthalpy and pressure (PHU). The inverse marching MOC provided parameters to measure time and distance: 1) pressure (P), 2) speed of sound (a), 3) enthalpy (h), 4) density (r) and 5) velocity (u). The pipeline was divided into elements for both distance (Δx) and time (Δt).Compatibility equations were expressed in a finite manner, in accordance with Courant stability criteria with regards to maximum levels (Courant et al., 1952; Zucrow & Hoffman, 1976). The equations were solved using spatial axis iteration and interpolation, along with pressure and enthalpy flash calculations. These occurred at the intersections of linear regions.

Isolating the maximum and minimum fluid enthalpies (h_{max}, h_{min}) in association with the appropriate temperatures (T_{max}, T_{min}) and pressures (P_{max}, P_{min}) resulted in a reduction in computational workload. Inlet and ambient pressures were extracted for these measurements. The greater value was the T_{max}, while the isentropic flash from both P_{max} and T_{max} to P_{min} (while neglecting pipewall-environment heat transfer) provided the T_{min}value.Figure 2.1shows the corresponding interpolation space domain.
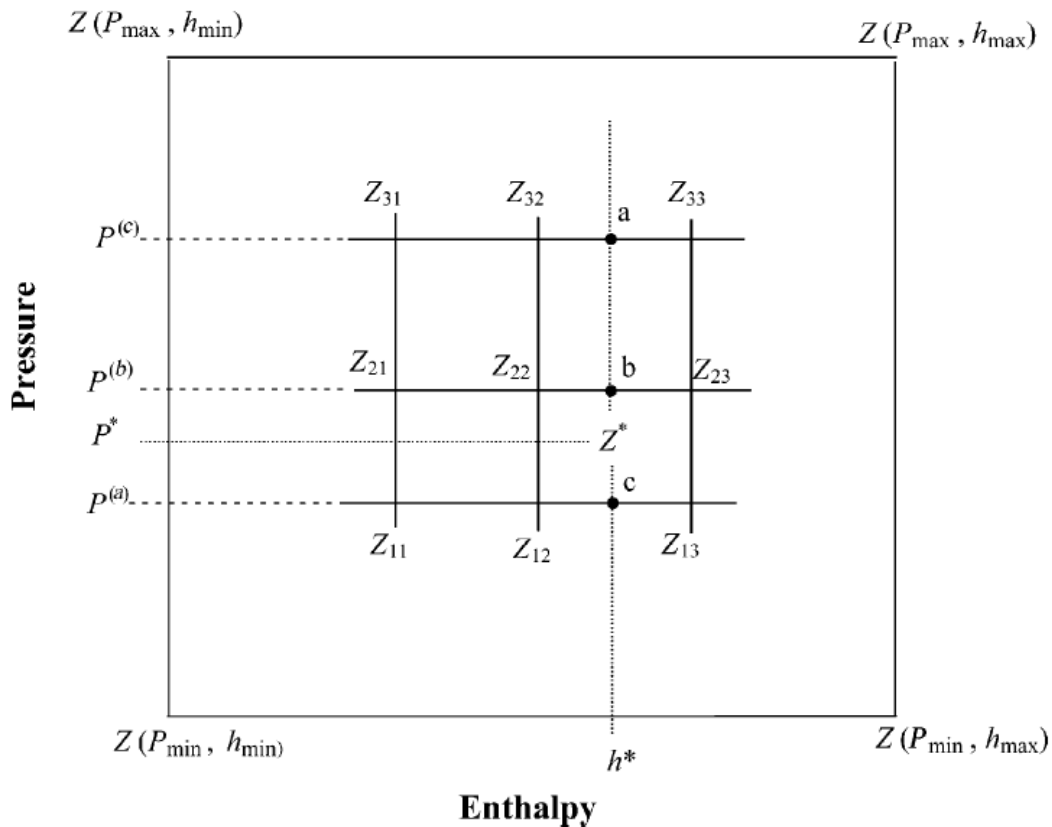
Figure 2.1.Schematic representation of the depressurizing fluid pressure/enthalpy interpolation domain (Atti, 2006).

Applying this method to a variety of compositions produces a difference value of 0.01%, with regards to the predicted fluid properties; interpolated data, rather than direct flash calculations, provided this information. This difference, however, was found to be negligible in terms of its effect on the following profiles following rupture: time variant pressure, mass flow rate, discharge velocity, and discharge temperature.

The model was further validated by Atti (2006), who compared the results with those of pipeline rupture experiments that were conducted by Shell Oil and BP. Additionally, data from the MCP-01 rupture and the Piper Alpha incident were

utilized. The simulated results are effectively in correlation with the experimental data. Additionally, the model causes a 70% reduction in runtime. The initial runtime was 12 minutes, whereas the new model runtime was 3.5 minutes (70-80% reduction).

Mahgerefteh et al.(2008) Model

A hybrid outflow model was produced by Mahgerefteh et al. (2008) to consider how the HEM failed to address depressurization liquid discharge that is noted in pipelines that have ruptured, especially for those transporting condensable or two-phase gas combinations.

A representation of a reduced pipeline with a mixture of gas and liquid is depicted in figure 2.2; it illustrates the effects after depressurization has occurred. The HEM model fails to address the liquid discharge that results. A simulation was conducted where the liquid discharge was released as a result of an energy balance; the idea was that any liquid left in the pipeline was detached from vapour composites (Mahgerefteh et al., 2008).
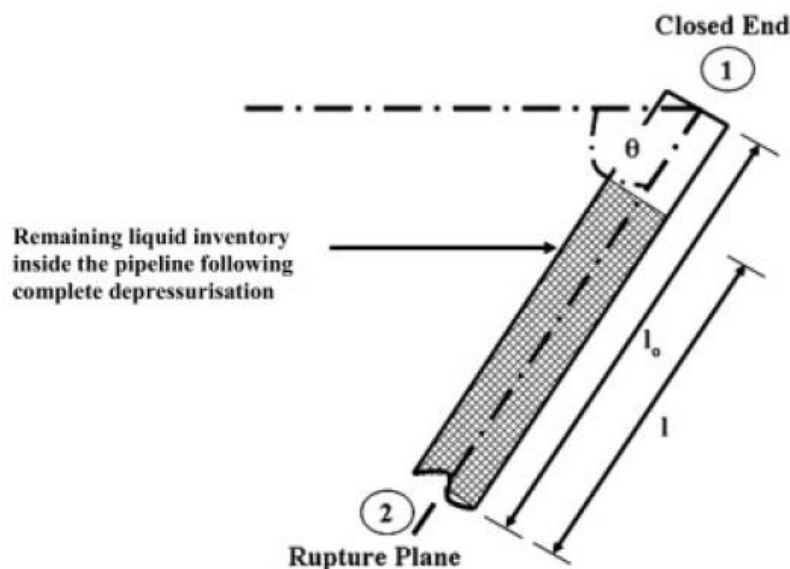
Figure 错误！文档中没有指定样式的文字。**.2.Schematic representation of a pipeline declined at an angle θ (Mahgerefteh et al., 2008).**

A comparison of the temporally released mass variations between the HEM (curve A) (Atti, 2006) and the hybrid model (curve B) (Mahgerefteh et al., 2008) has been illustrated in figure2.3. It considered a 100 metre by 0.154 metre pipeline, transporting pure hexane in liquid form, under 21 bar pressure and $20^{o}C$ temperature. Curve A clearly underestimates the total discharge of mass, due to the disregards of outflow after depressurization.
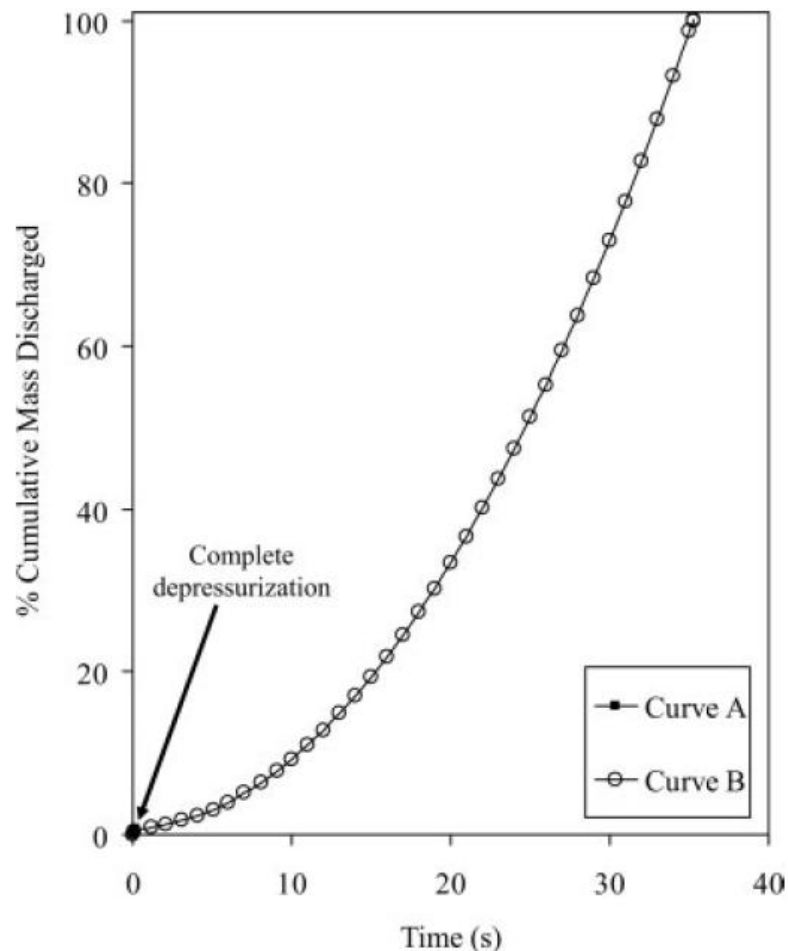
Figure 错误！文档中没有指定样式的文字。.3.Variation of % cumulative mass discharged with time for a pipeline transporting 100% hexane at a decline angle of -10° following FBR (Mahgerefteh et al., 2008).

Curve A: Atti (2006)

Curve B: Hybrid model

Brown(2011) Model

All the previous University College London Models are based on the Method of Characteristics (MOC). MOC models are often criticized for having particularly high computational costs per simulation. Much research has been conducted into alternative methods of simulation prediction(Mahgerefteh et al., 1999; Oke et al., 2003) , but the issue remains.

Existing research into this topic has typically aimed to reduce the costs and calculations that are associated with computational procedures. However, Atti (2006) explained that iterations are often needed in the correction stages of the MOC models, which tend to elongate the duration of CPU runtimes. Therefore, a technique that does not use numerical iterations could improve the efficiency of the system by reducing the operational runtime. Finite Volume (FV) systems are examples of such models, where a finite number of calculations are applied to the model. The accuracy of the system is maintained, while the runtime is reduced extensively.

Brown (2011) applied the Finite Volume Method (FVM) to solve the conservation equations in the University College London Model with the aim to discuss how the FVM could provide suitable alternatives for resolving such equations, in the hope of reducing the computational runtime.

The model was assessed through a comparison of the predicted outcomes and the actual outcomes, in terms of a hypothetical rupture along a pipeline that was transporting a range of different combinations. Gas, two-phase and liquid hydrocarbon mixtures were all assessed in this context. For all of the examples, the FVM models were compared against predictions made by MOC models. The FVM was found to generally produce good results. Figure 2.4 shows one of the test cases:
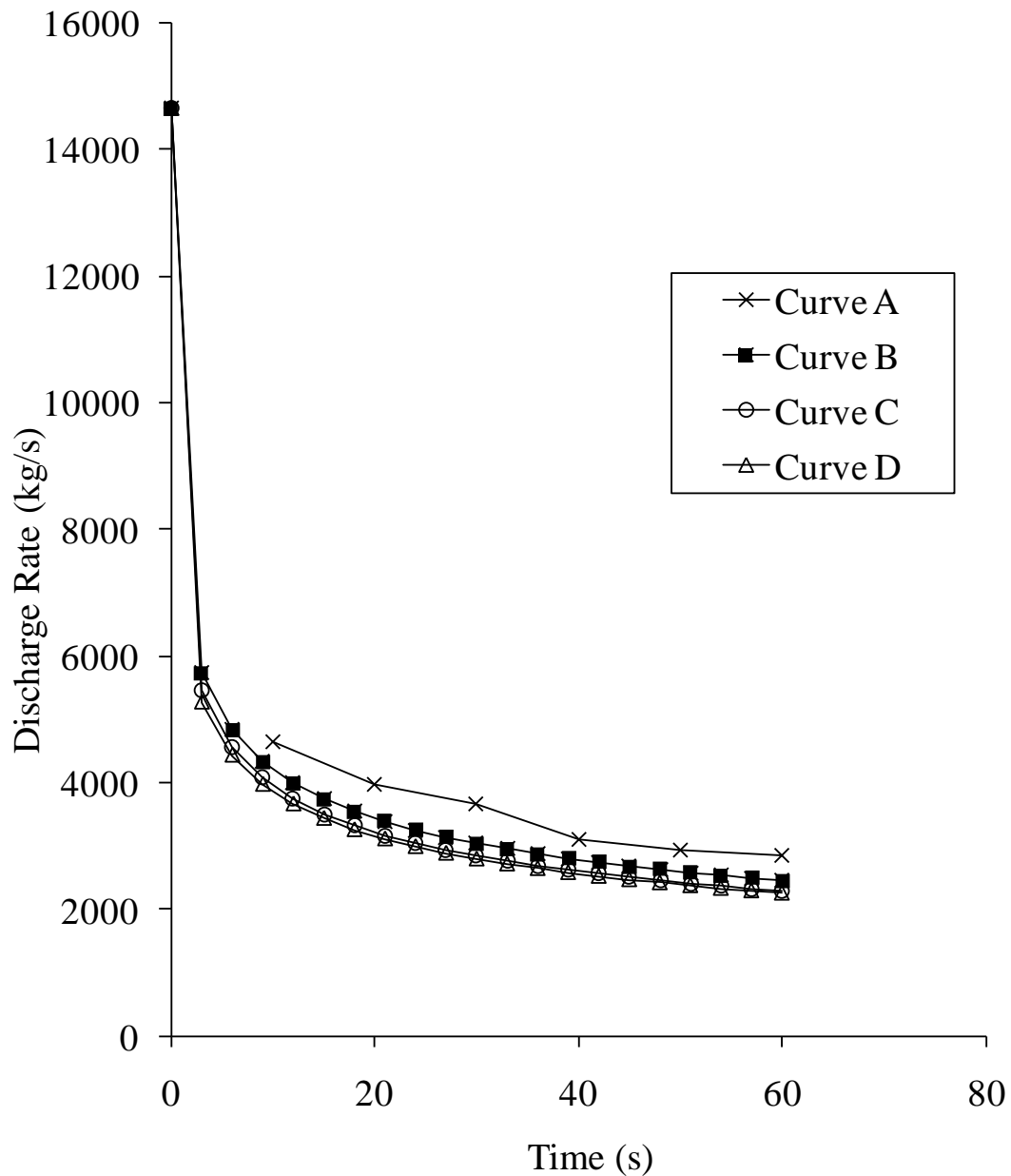
Figure 2.4.Comparison of variation of release rate with time following the FBR TransCanada pipeline. (Brown,2012)

Curve A: Experimental data (HSE,2004)

Curve B: MOC, CPU runtime = 627 s

Curve C: PRICE-1 method, CPU runtime = 414 s

Curve D: PRICE-2 method, CPU runtime = 725 s

However, FVM cannot always be applied to simulate bore ruptures, where the inventory is initially in a liquid form. Large fluctuations in the properties of the fluid resulted in numerical instabilities, ultimately hindering the application of the models to real life scenarios (Brown,2011).

It is also found that the CPU runtimes were significantly reduced by using the FVM. The reductions ranged from 23 to 78% using the FVM as compared to the MOC (Brown,2011). Table 2.1 presents the comparison of CPU runtimes for the MOCand FVM.

	CPU runtime (s)		% CPU runtime reduction
	MOC	FVM	
Experimental tests			
TransCanada	627	414	33.97
Piper Alpha	20685	11762	43.14
P45	1027	694	32.42
P47	2351	1625	30.88
Case Study			
Full Bore Rupture			
Permanent Gas	901	366	59.38
Two-phase Mixture	1233	274	77.78
Puncture			
Permanent Gas	1631	1255	23.05
Two-phase Mixture	1283	874	46.80
Liquid	3135	31048	-890.37

Table 2.1.Comparison of CPU runtimes for the MOC and FVM for all simulations presented(Brown,2011).

2.2.5 Validation of the University College London Model

The University College London outflow model employed in this study was validated against intact end pressure data for the Piper Alpha riser and two sets of test resultsobtained from the Isle of Grain depressurisation tests (P40 and P42). The results of the Piper Alpha simulation and test P40 are reviewed herewith.

Figure 2.5 shows the measured intact end pressure-time history following the FBR of the Piper Alpha to MCP-01 subsea line. Curve A shows measured data whereas curve B shows the predictions using Compound Nested Grid System Method of Characteristics (CNGS-MOC). Curve C shows the corresponding data (CNGS-ideal) with the ideal gas assumption.
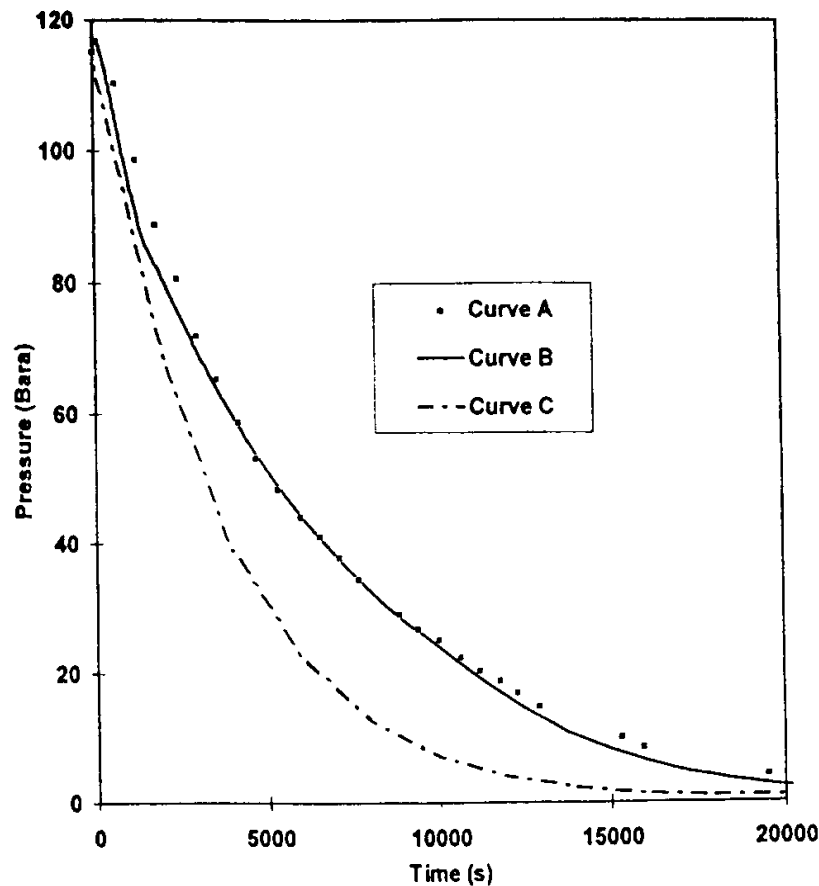
Figure 2.5. Intact end pressure vs. time profiles for the Piper Alpha-MCP pipeline (Mahgerefteh et al., 1999). Curve A: Field Data Curve B: CNGS-MOC,Curve C: CNGS-MOC ideal gas

Figures 2.6 and 2.7 show predictions for the open and closed end temperature and pressure data against time the LPG mixture test P40 as compared to experimental data. Curves A and B show the measured data whereas curves C and D represent the corresponding simulated data using CNGS-MOC.
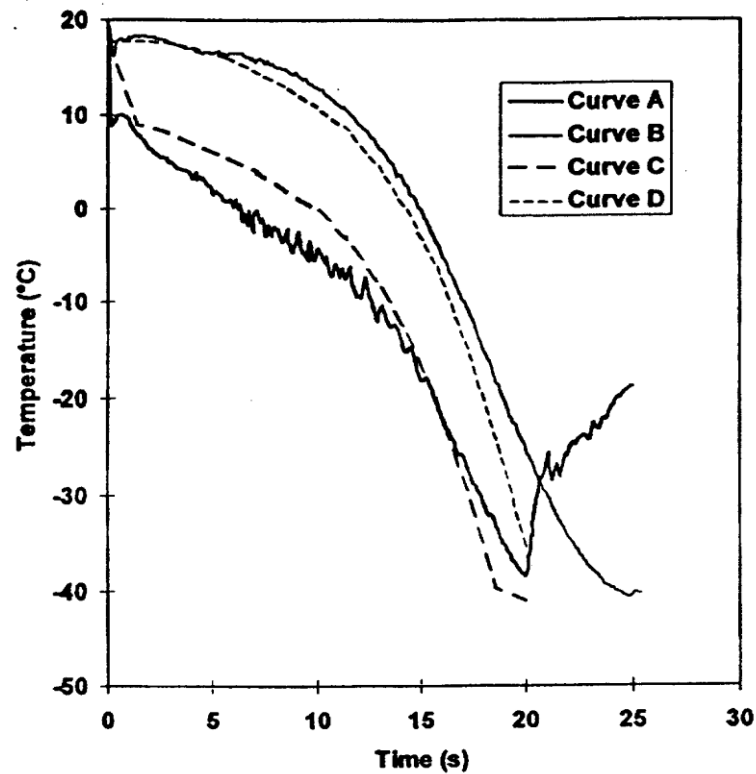
Figure 2.6. Temperature-time profiles at the open and closed ends for the P40 (LPG) test (Magerefteh et al., 1999).

Curve A: Field data (open end)Curve B: Field data (closed end)

Curve C: CNGS-MOC (open end) Curve D: CNGS-MOC (closed end).
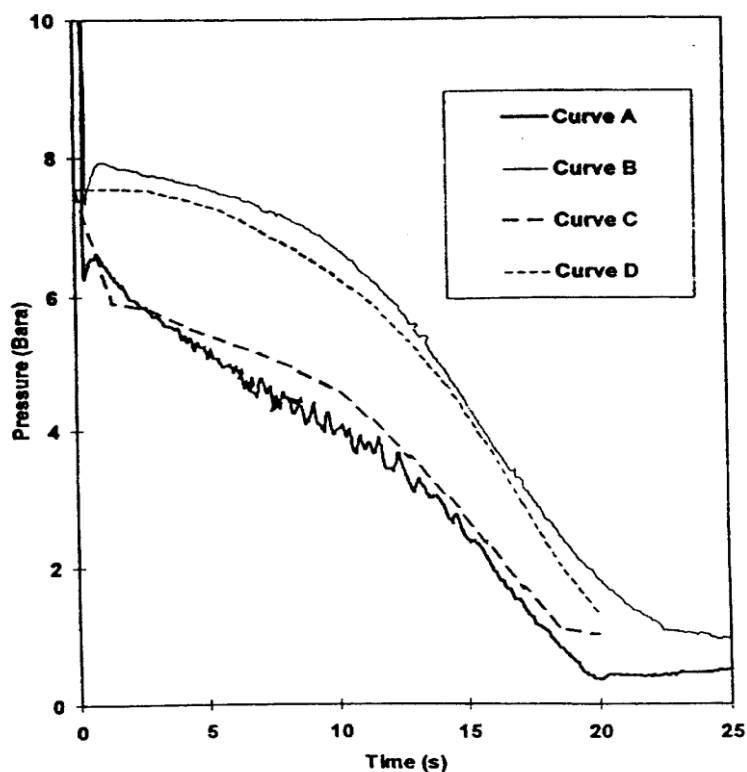
Figure 2.7. Pressure-time profiles at the open and closed ends for the P40 (LPG) test (Magerefteh et al., 1999).

Curve A: Field data (open end)Curve B: Field data (closed end)

Curve C: CNGS-MOC (open end) Curve D: CNGS-MOC (closed end).

2.2.6 Concluding remarks – CFD Outflow

Given the catastrophic consequences of pipeline rupture and the important role that the fluid pressure and temperature plays in such scenario, the precise prediction of the releasing fluid property becomes the basis of this study. Based on the above review, it is clear that significant progress has been done to improve the model accuracy without compromising the computational run time. The University College London Models are employed in this study.

2.3 Review of Fracture Mechanics

Fracture mechanics, as a branch of engineering, has been developed for strength estimation of structural components in the presence of cracks or crack-like flaws. It focuses on assessing the behaviour of cracks in structural components and material in a quantitative manner. It is widely accepted that crack growth must be considered in both the design and analysis of failures. In this section, some of the important concepts of fracture mechanics are reviewed with an emphasis on Linear Elastic Fracture Mechanics (LEFM).

2.3.1 Origin of Fracture Mechanics - Griffith's Energy Theory for Fracture

The first systematic study of fracture on a solid body was presented by Griffith(1921),who laid the foundation for fracture mechanics. Griffith carried out a series of experiments to measure the strength of glass rods with different sizes. He observed that thin rods havehigher unit strengths than thick rods. To explain this, Griffith suggested that the existence of crack-like flaws on material surfaces would weaken the glass rod.

Griffith(1921) applied anenergy balance to the formation of a crack. He suggested that the criterion of failure of a structure was determined by the balance between the energy stored in the structure and the surface energy of the material. The crack in a brittle material becomes unstable if the strain energy released per unit increment in the crack area is greater than or equal to the energy required to form a unit new surface. This criterion can be expressed as:

$$G \geq 2\gamma \qquad \qquad \textbf{(2.1)}$$

where G and γ are the strain energyand the work required to form a unit new surface respectively.

By studying a plate subjected to constant stress with a crack, the following respective expressionsfor the critical stress, σ_f, and the critical crack length, a, can be derived (Anderson, 2005):

$$\sigma_f = \left(\frac{2E\gamma}{\pi a}\right)^{1/2} \tag{2.2}$$

$$a = \frac{2E\gamma}{\pi\sigma^2} \tag{2.3}$$

where E, γ and α are the total energy, the work required to form a unit new surface and the half crack length respectively. σ and σ_farethe stress applied and the critical stressrespectively.

Equation (2.2) gives the critical stress for a crack with the given length becomesunstable. Equation (2.3) gives the critical crack length at thegiven stress.

Equations (2.2) and (2.3) are valid only for purely brittle materials. They producegood agreement with experimental datafor critical fracture stress of glass, but severely underestimate the critical fracture stress for metals. This limits the application of Griffith's theory to engineering problems, because hardly any crack in practice is purely brittle,given that some plastic deformation is always present in the vicinity of the crack tip.

Modified Griffith Theory

Thirty years after Griffith's theory, Orowan(1949) studied the crack growth in metals, and suggested that Griffith's crack criterion can be extended to ductile materials by accounting for the additional energy dissipated by the plastic deformation in the vicinity of the crack tip. Thus, the corresponding criterion becomes:

$$G \geq 2\gamma + \gamma_p \tag{2.4}$$

whereγ_p is the energy dissipated by the plastic deformation in the vicinity of the crack tip.

Orowan gave the following respective expressions for critical stress, σ_f and crack length, a :

$$\sigma_f = \left(\frac{2E(\gamma + \Gamma)}{\pi a} \right)^{1/2} \qquad \textbf{(2.5)}$$

$$a = \frac{2E(\gamma + \Gamma)}{\pi \sigma^2} \qquad \textbf{(2.6)}$$

where Γ is the plastic work per unit area of surface created. For metals, Γ is typically much larger than γ (Anderson, 2005).

Although Orowan's work extends Griffith's theory to metals, it can only be applied to linear elastic material behaviour. Any plasticity must be confined to a small region near the crack tip. Therefore, it is not valid for any global non-linear deformation behaviour.

2.3.2 Classification of Fracture

For engineering materials, depending on the ability of the material to undergoplastic deformation prior to crack propagation, two primary modes of fracture prevail: brittle and ductile.

Brittle Fracture

A brittle fracture involves crack propagation at high crack velocities with no significant plastic deformation.Since there is low energy absorption by deformation prior to crack propagation, brittle cracks tend to continue to grow and increase in size, without increase in the applied stress.

Linear Elastic Fracture Mechanics (LEFM) is applied to brittle fracture problems. It assumes that the material is isotropic and linear elastic (Anderson, 2005). The condition for a crack to grow based on LEFM theory is that the stresses near the crack tip exceed the material fracture toughness. The crack tip stresses can be evaluated by the crack tip stress field, which is a function of crack geometry and loading. In

addition, the crack tip stress field can be characterised by the Stress Intensity Factor(SIF) to be discussed in section 2.2.4.

LEFM is valid only when plastic deformation is confined to the vicinity of the crack tip. However, if the fracture is ductile, i.e., the material is subject to a large global non-linear plastic deformation before the crack growth, an alternative fracture mechanics theory is required.

Ductile Fracture

A ductile fracture is characterised by the extensive plastic deformation ahead of the crack and its associated energy dissipation. It is caused by the nucleation, growth and coalescenceof voids(Anderson, 2005). In practice, ductile failures are preferred over brittle failures,since in the former, the material may undergo large deformation without breaking. Furthermore, once a ductile fracture isinitiated, it tends to resist further extension unless the applied stress is increased. Additionally, the crack propagation speed for a ductile fracture is much slower than for a brittle fracture because most of the energy is dissipated in plastic deformation.

As LEFM is no longer valid for a ductile fracture, Elastic-Plastic Fracture Mechanics (EPFM) is proposed. In EPFM, two primary parameters are used as crack criterion, the strain energy release rate, J integral, and the Crack Tip Opening Displacement (CTOD). Boththe J integral and CTOD are functions of crack geometry and loading. The material critical CTOD and J integral can be measured experimentally. When the J integral or CTOD exceed the critical value of the material, the crack will propagate.

Ductile-to-brittle Transition

The characteristics of a material to resist a ductile fracture are defined by the material fracture toughness, which is in turn defined by the energy absorbed by the plastic deformation prior to fracture. The fracture toughness is strongly dependent on temperature. As temperature decreases, a material's ability to absorb energy on impact decreases, which reduces its ductility. Over some small temperature ranges, the ductility may suddenly decrease to almost zero, while the toughness also decreases to

a much lower level, as figure 2.8 illustrates. The Ductile-Brittle Transition Temperature (DBTT) is defined by the small temperature range in which the material energy absorbed on impact (fracture toughness) drops significantly. This temperature is normally the lowest working temperature of a structural engineering material. The DBTT of a material can be measured experimentally by conducting Charpy V-notch impact testing at various temperatures.
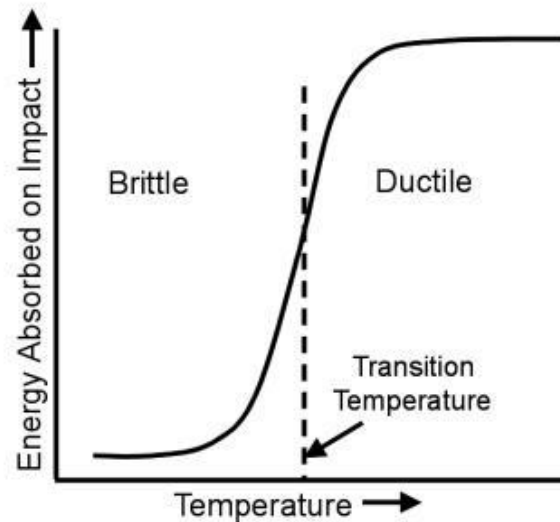
Figure2.8. Ductile-to-brittle transition (Anderson, 2005)

2.3.3 Modes of Fracture

To distinguish different separation directions, fractures can be classified into three modes: opening (mode I), sliding (mode II) and tearing (mode III), as illustrated in figure 2.9. Mode I is associated with the crack faces separating directly apart. Mode II is defined by the crack faces sliding apart from each other in a direction perpendicular to the crack front. Mode III is identified by the crack faces tearing apart parallel to the crack front. Most crack problems of engineering interest in pressurised pipelines involve mode I(Anderson, 2005).

Mode I   Mode II   Mode III
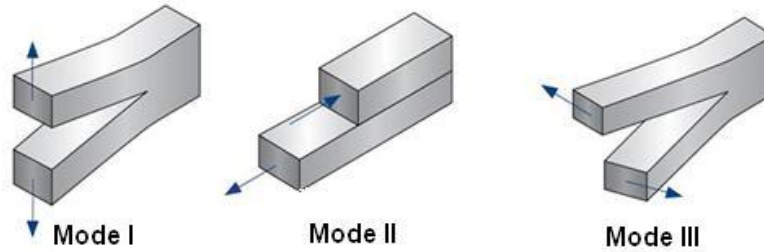
Figure 2.9.Different modes of fracture (Anderson, 2005)

2.3.4 The Stress Intensity Factor (SIF)

The SIFisthe main fracture parameterinlinear elastic fracture mechanics(Pook, 2000). The concept arises from linear elastic stress analysis of cracks of various configurations. Westergaard(1939), Irwin(1957), Sneddon(1946) and Williams(1957)solved several cracked structures subject to external forces in linear elasticity and showed that the stress field in the vicinity of the crack-tip was always of the same form. The stress field near the crack-tip, σ_{ij}, in any linearly elastic body with a crack is given in the following form(Anderson, 2005):

$$\sigma_{ij} = \left(\frac{K}{\sqrt{r}}\right)f_{ij}(\theta) + \sum_{m=0}^{\infty} A_m r^{\frac{m}{2}} g_{ij}^{(m)}(\theta) \tag{2.7}$$

where r and θ are the polar coordinates of a point with respect to the crack tip respectively.σijand f_{ij} are the stress tensor and the dimensionless function of θ in the leading term respectively.K is a constant.Detailed expressions for the stress field of mode I crack are given as follows (Anderson, 2005):

$$\sigma_{xx} = \left(\frac{K}{\sqrt{2\pi r}}\right)\cos\left(\frac{\theta}{2}\right)\left[1 - \sin\left(\frac{\theta}{2}\right)\sin\left(\frac{3\theta}{2}\right)\right] \tag{2.8}$$

$$\sigma_{yy} = \left(\frac{K}{\sqrt{2\pi r}}\right)\cos\left(\frac{\theta}{2}\right)\left[1 + \sin\left(\frac{\theta}{2}\right)\sin\left(\frac{3\theta}{2}\right)\right] \tag{2.9}$$

$$\tau_{xy} = \left(\frac{K}{\sqrt{2\pi r}}\right)\cos\left(\frac{\theta}{2}\right)\sin\left(\frac{\theta}{2}\right)\sin\left(\frac{3\theta}{2}\right) \tag{2.10}$$

$$\sigma_{zz} = 0 \text{ (Plane stress)} \quad \sigma_{zz} = \nu(\sigma_x + \sigma_y) \text{ (Plane strain)} \tag{2.11}$$

$$\tau_{xz}, \tau_{yz} = 0 \tag{2.12}$$

where σ_{xx}, σ_{yy} and σ_{zz} are the stress in x , y and z directions respectively. τ_{xy}, τ_{xz} and τ_{yz} are the sheer in x-y, x-z, and y-z directions respectively.v is Poisson's ratio.

The constant, K, in the first term of equation 2.7is defined by Irwin (1957) as the SIF.Thus, the stress and strain field at the vicinity of the crack tip can be characterised by equation (2.8-12) if K is known. The value of the SIF, K is a function of the applied stress and geometry of the structural component, including the global geometry and the crack geometry.

The SIFcan be determined from the local crack tip stress fieldor the crack tip displacement field. Some indirect methods can also be applied to obtain the SIF through the energy release rate or J-integral. A number of SIF solutions are available for various configurations(Tada et al., 2000).In general, the expression fortheSIF,K is often written in the following form:

$$K = Y\sigma\sqrt{\pi a} \tag{2.13}$$

whereY is thedimensionless shape factor, which is a function of crack geometry and applied loads. σand a are the stress loading and the half crack length respectively.

Since the linear crack growth is controlled by the stress field at the crack tip, if it is assumedthat the crack will grow under some critical stress, it follows that the material must fail at a critical stress intensity, K_c orthe material fracture toughness(Anderson, 2005), which can be obtained experimentally. Following this, the failure criteria for a linear fracture under a plane strain condition can be written as:

$$K > K_c \tag{2.14}$$

Equation(2.14) indicates that structuralfailure occurs when the applied crack tip SIF, K exceeds the material fracture toughness, K_c.

The SIFprovides a reasonable description of the crack tip stress field only when global yielding is small. Anderson(2005)suggests that it is essential to ensure the net section stress does not exceed $0.8\sigma_y$.Further, the presence of unknown residual stresses can be a serious limitation in the practical application of fracture mechanics(Pook, 2000).

2.3.5 Methods for Calculating the Stress Intensity Factor

The calculation of the SIF has been thesubject of extensive investigations over the past decades.Although a large number of solutions for various crack geometries and loading conditions can be found in the literature (Tada et al., 2000), existing solutions (e.g. through wall crack on a infinite plate, or longitudinal line crack on a cylinder) are still inadequate to meet need of solutions required in this study: a round puncture with an initial crack on a cylinder).Many methods can be used to determine SIF, including:

Analytical:

1. Superposition(Anderson, 2005)
2. Green's function(Anderson, 2005)
3. Weight function method (Rice, 1972)

Numerical:

1. Boundary element method (Cruse, 1969)
2. Finite element method (FEM) (Wilson, 1973)

The analytical methods were developed based on known reference stress fields;therefore, their accuracy depends on the reference stress used. However, for complicated problems, where reference stress fields are unavailable, the numerical methods are needed. Among them, the FEM is the most commonly applied.

2.3.6Determination of the Stress Intensity Factor by Finite Element Method (FEM)

The close-form SIF solutions are only available for some limited geometries and loadings. The numerical methods are widely applied to determine the SIFs. FEM is one of the most powerful tools for the solution of crack problems in fracture mechanics. A wide range of finite elements has been developed to determine the SIFs, which can be extracted from energy-based methods or displacement-based methods.

Energy-based Methods

By definition, the strain energy release rate, Gis given by

$$G = -\frac{\partial U}{\partial L}$$ (2.15)

where U and L are the strain energy of the crack bodyand the crack lengthrespectively.

Irwin (1957) demonstrated the relationship between the SIF,Kand the strain energy release rate, G as follows:

$$G = \frac{K^2}{H}$$ (2.16)

$$H = E \quad \text{(Plane stress)} \quad H = \frac{E}{1-v^2} \quad \text{(Plane strain)}$$ (2.17)

Thus, from equation (2.16),K can be determined by the following expression if the energy release rate, Gis known.

$$K = \sqrt{-\frac{\partial U}{\partial L} H}$$ (2.18)

Chan et al. (1970) approximated the derivative of the energy release rate by a finite difference method as:

$$\frac{\partial U}{\partial L} \approx \frac{U_{L+\Delta L} - U_{L-\Delta L}}{2\Delta L}$$ (2.19)

The major disadvantage of this technique is that two finite element analyses are required to obtain the strain energy values. Parks (1974) modified this technique so that only one analysis is required by writing the strain energy release rate as:

$$G = -\frac{1}{2}\{u\}^T \frac{\partial [K]}{\partial L}\{u\}$$ (2.20)

where {u} and [K] are the nodal displacement vector and the global stiffness matrix respectively.

Both {u} and [K] can be determined by the FEM. Parks further showed that the derivative of [K] can be expressed by:

$$\frac{\partial [K]}{\partial L} \approx \frac{[K]_{L+\Delta L} - [K]_L}{\Delta L} \approx \sum_{j=1}^{n} \frac{[k_j^{ct}]_{L+\Delta L} - [k_j^{ct}]_L}{\Delta L}$$ (2.21)

where j and k_j^{ct} are the total number of crack tip elements and the element stiffness matrices of crack tip elementsrespectively.

Although this technique is accepted to be the most accurate method for extracting the SIF from the FEM(Banks-Sills and Sherman, 1986),it is of little value since the extraction of the element stiffness matricesare usually not available in commercial finite element software.

Another energy-based approach is the J-integral method. For an arbitrary counter clockwise path (Γ) around the crack tip, the J-integral was defined by Rice (1968) as

$$J = \int_\Gamma (Wdy - T_i \frac{\partial u_i}{\partial x})ds$$

(2.22)

where W, T_i, u_i and ds are the strain energy density, the components of the traction vector, the displacement vector components and the length increment along the contour Γ respectively.

Rice(1968)showed that the value of J is independent of the integration path, and it is a more general form of the energy release rate, G. Thus, the SIFcan be obtained using the following relations:

$$K_{planestrain} = \sqrt{\frac{JE}{1-v^2}} \quad \text{(Plane strain)}$$

(2.23)

$$K_{planestress} = \sqrt{JE} \quad \text{(Plane stress)}$$

(2.24)

whereE is the Young's modulus.

Cracks on pressurised pipelines satisfy the plane strain condition given by equation (2.23).

Displacement-based Methods

Apart from the energy-based methods, a number of methods are also available to extract theSIFs from nodal displacements near the crack tip. These methods arerelativelysimpler than energy-based methods, since the required displacement can be obtained through commercial finite element software. The following displacement-based techniques are described below: the displacement extrapolation (Chan et al.,

1970), the displacement correlation (Shih et al., 1976) and the quarter point displacement (Barsoum, 1976).

The Displacement Extrapolation Technique

For any cracked body, Irwin (1957) demonstrated that the crack tip displacement can be expressed as:

$$v = \frac{K_I}{2G}\sqrt{\frac{r}{2\pi}}\sin\frac{\theta}{2}\left[(\kappa+1)-2\cos^2\frac{\theta}{2}\right] + \text{higher order terms in r} \tag{2.25}$$

$$\kappa = (3-\nu)/(1+\nu) \quad \text{(Plane stress)} \quad \kappa = 3-4\nu \quad \text{(Plane strain)}$$

where K_1 and G are the mode I SIF and the shear modulus respectively, andr and θ are the polar coordinates of a point with respect to the crack tip respectively.The higher order terms in r can be neglected when r approaches 0; thus, rearranging equation (2.25)to become:

$$K_I = 2Gv\sqrt{\frac{2\pi}{r}}\left[\sin\frac{\theta}{2}\left[(\kappa+1)-2\cos^2\frac{\theta}{2}\right]\right]^{-1} \tag{2.26}$$

$$\kappa = (3-\nu)/(1+\nu) \quad \text{(Plane stress)} \quad \kappa = 3-4\nu \quad \text{(Plane strain)}$$

where all variables are as defined in (2.25).

Chan et al. (1970) proposed the displacement extrapolation technique by substituting the values of v and r for the nodal points of fixed θ. The resulting expressions are as follows:

$$K_I = \lim_{r^i \to 0} K_I^i \tag{2.27}$$

$$K_I^i = \frac{G}{\kappa+1}\sqrt{\frac{2\pi}{r^i}}\upsilon(r^i) \tag{2.28}$$

$$\kappa = (3-\nu)/(1+\nu) \quad \text{(Plane stress)} \quad \kappa = 3-4\nu \quad \text{(Plane strain)}$$

whereυ and r^{i}arethe local displacement normal to crack axis of point i and the distance between ith node and the crack tip respectively.

The process is illustrated in figure 2.10. The curve is plotted by a number of calculated K_1^i against the radial distance, r. Thus, by extrapolating the straight-line portion of the K_1^i-r curve to r=0, $\lim_{r^i \to 0} K_1^i$ can be obtained at the intersectionof the straight line and the y-axis. $\lim_{r^i \to 0} K_1^i$ is regarded an estimation of the actual K_I.
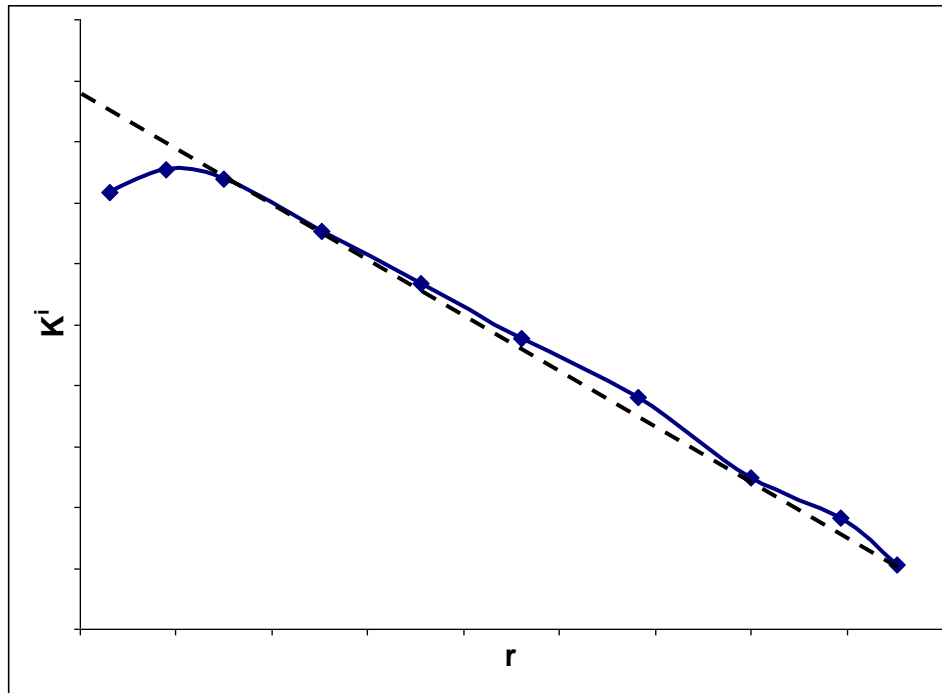
Figure 2.10.Illustration of the displacement extrapolation technique

Solid line: the nodal K^iagainst the radial distance, r
Dotted line: the linearly extrapolated line between K^i and r.

This technique is based on the assumption that the nodal, K^i is linear along the crack face. Carpenter (1983) showed that the displacements along anyangle,θ, do not vary linearly. However, this technique is only valid for a single edge crack under uniform tension. For analysis involving complex crack geometry and loadings, the linearity cannot be satisfied.

The Displacement Correlation Technique

Shih et al. (1976) proposed the displacement correlation technique from the nodal displacement using the quarter point element at the crack tip. In this technique, the displacement normal to the crack face along the edge ABC of the quarter point element can be written as:

$$v = \left(4(v_B - v_D) - (v_C - v_E)\right)\sqrt{\frac{r}{L_Q}} + \left(-4(v_B - v_D) + 2(v_C - v_E)\right)\frac{r}{L_Q}$$

(2.29)

where v_B, v_C, v_D and v_E are the local nodal displacements normal to the crack face of nodes B,C,D and E, as illustrated in figure 2.11. L_Q, and r are the length of the quarter point element along the crack face and the polar coordinates of a point with respect to the crack tip respectively.
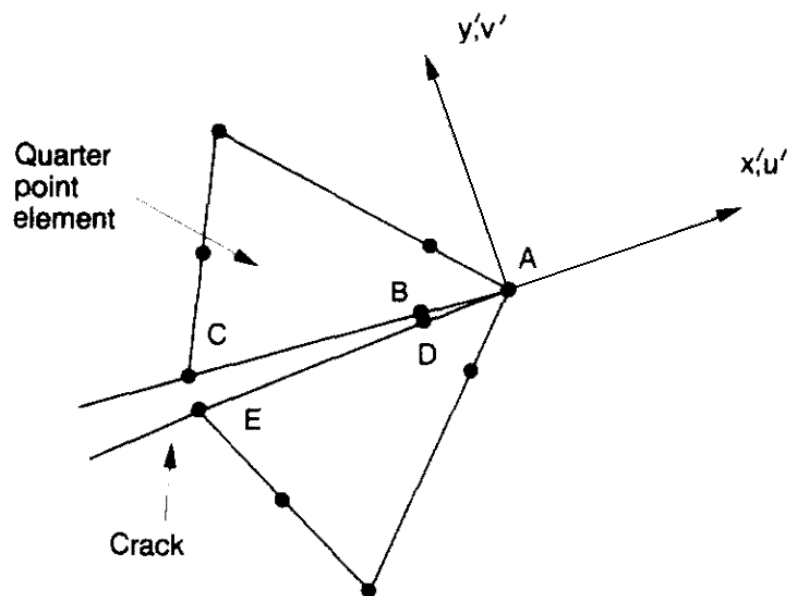
Figure 2.11.Crack tip element mesh (Lim & Choi, 1992)

By taking θ=π in equation (2.25), the crack tip displacement can also be written as:

$$v = \frac{K_I(\kappa+1)}{2G}\sqrt{\frac{r}{2\pi}} + \text{higher order terms in r}$$

(2.30)

$$\kappa = (3-v)/(1+v) \quad \text{(Plane stress)} \quad \kappa = 3 - 4v \quad \text{(Plane strain)}$$

where all variables are as defined in (2.25).

By equating(2.29) and (2.30) to eliminate $\sqrt{r}$ term, the mode I SIF can be calculated by:

$$v = \frac{G}{(\kappa+1)}\sqrt{\frac{2\pi}{L_Q}}\{4(v_B - v_D) - (v_C - v_E)\}$$

(2.31)

$\kappa = (3-\nu)/(1+\nu)$ (Plane stress) $\kappa = 3-4\nu$ (Plane strain).

The accuracy of this technique is shown by Shih et al.(1976) to be 1.2% and 1.1% for double edge crack strips and three point bending specimens respectively.

The Quarter Point Displacement Technique

Following Shih et al.(1976), Barsoum(1976) proposed a technique using only the nodal displacement of the quarter point element. By neglecting higher order terms in equation (2.30)as $r \rightarrow 0$, the displacement in the vicinity of the crack tip can be written as:

$$v = \frac{K_I(\kappa+1)}{2G}\sqrt{\frac{r}{2\pi}}$$ **(2.32)**

$\kappa = (3-\nu)/(1+\nu)$ (Plane stress) $\kappa = 3-4\nu$ (Plane strain)

where all variables are as defined in (2.30).

Substituting r with the local nodal displacement $(v_B - v_D)$, the estimated mode I SIF can be written as:

$$K_I = \frac{2G}{\kappa+1}\sqrt{\frac{2\pi}{L_Q}}(v_B - v_D)$$ **(2.33)**

$\kappa = (3-\nu)/(1+\nu)$ (Plane stress) $\kappa = 3-4\nu$ (Plane strain).

The accuracy of this technique is shown to be generally better than the displacement correlation technique, given the fact that it is easier to implement and more efficient computationally (Lim and Choi, 1992).

2.3.7 Theoretical Background of Weight Function Method

The implementation of the FEM requires significant computer coding or the use of existing commercial finite element packages such asAbaqus(SIMULIA, 2011)or ANSYS(ANSYS® Academic Research, 2011). In addition, theFEM requires a great amount of computation run time. On the other hand, the weight function method can

provide an analytical solution to the SIFunder arbitrary loading and achieve remarkable computational efficiency,without compromising the solution accuracy. The weight function method was first proposed by Bueckner(1970) and Rice (1972) and has been widely used inthe past decades.

Rice (1972) showed that the SIF, K can be expressed as:

$$K = \int_{\Gamma_c} \sigma(x)h(x,a)dx \qquad (2.34)$$

where $\sigma(x)$, $h(x,a)$ and $\Gamma_c$are the stress distribution along the crack face in the uncracked geometry, the weight function of the cracked geometry and the perimeter of the crack respectively.

Rice (1972) showed that the weight function is a universal function for cracked body of given geometry and is independent of loading. Thus, given the weight function for a given crack configuration, which can be determined from a reference loading,the SIFof the same geometry for any body loading can be easily determined using equation (2.34).

In the following section, the theoretical development of the weight function method followed byvarious methods for evaluating weight functions are reviewed.

The expression for the weight function $h(x,a)$was first derived by Bueckner(1970) based on analytical function representation of elastic fields for isotropic materials.Rice (1972) independently developed a similar version of equation (2.34), expressing the weight function for mode I deformation in terms of the partial derivative of the crack opening displacement (COD) field in respect to crack length. This simplification is more practical and suitable for engineering applications. Rice's weight function expression is as follows:

$$h(x,a) = \frac{H}{2K}\frac{\partial u_r(x,a)}{\partial a} \qquad (2.35)$$

$$H = E \text{ (Plane stress) } H = \frac{E}{1-v^2} \text{ (Plane strain)}$$

where $u_r(x,a)$ is the COD field.

From equation (2.35), the weight function can be determined by knowing a reference SIF, K_r for a specific geometry and loading in addition to the corresponding COD field, $u_r(x,a)$. Since analytical expression of $u_r(x,a)$ is available only for a few ideal cases, the weight function method did not attract much attention initially. However, some authors have proposed approximate expressions for the COD field, $u_r(x,a)$, which have greatly broadened the use of the weight function method.

2.3.8 Methods of Approximating Weight Functions

A number of methods have been proposed for the approximation of the weight functions. In these methods, known SIFand corresponding geometrical boundary conditions are used to evaluate the weight functions. These are reviewed in the following.

Petroski-Achenbach Method

Petroski and Achenbach (1978) first proposed a series of expansion methodsfor approximating the reference COD field to estimate the weight function. They proposed the following approximate expression:

$$u_r(x,a) = \frac{\sigma_0}{H\sqrt{2}}\left[4F\left(\frac{a}{L}\right)\sqrt{a(a-x)} + \frac{G\left(\frac{a}{L}\right)(a-x)^{\frac{3}{2}}}{\sqrt{a}} \right] \tag{2.36}$$

$$H = E \text{ (Plane stress) } \quad H = \frac{E}{1-v^2} \text{ (Plane strain)}$$

where σ_0 and L are the characteristic stress and length for the specific problem, respectively, and a is the crack length. $F\left(\frac{a}{L}\right)$ and $G\left(\frac{a}{L}\right)$ are geometry related functions respectively defined as:

$$F\left(\frac{a}{L}\right) = \frac{K_r}{\sigma_0\sqrt{\pi\alpha}} \tag{2.37}$$

$$G\left(\frac{a}{L}\right) = \frac{\left[I_1 - 4F\left(\frac{a}{L}\right)a^{\frac{1}{2}}I_2\right]a^{\frac{1}{2}}}{I_3} \tag{2.38}$$

where

$$I_1 = \pi\sqrt{2}\sigma_0\int_0^a\left[F\left(\frac{a}{L}\right)\right]^2 a\,da$$

$$I_2 = \int_0^a\sigma(x)(a-x)^{\frac{1}{2}}dx$$

$$I_3 = \int_0^a\sigma(x)(a-x)^{\frac{3}{2}}dx$$

where K_r is the reference SIFof the geometry under reference stress loading $\sigma_r(x) = \sigma_0 p(x)$ in which $p(x)$ is the non-dimensional reference stress distribution.

Thus, by knowing K_r the functions $F\left(\frac{a}{L}\right)$ and $G\left(\frac{a}{L}\right)$ depend only on the geometrical parameters. By substituting equation (2.36) into equation (2.35), the following weight function can be derived:

$$h(x,a) = \frac{2}{\sqrt{2\pi(a-x)}}\left[1 + M_1\left(1-\frac{x}{a}\right) + M_2\left(1-\frac{x}{a}\right)^2\right] \tag{2.39}$$

where

$$M_1 = \frac{8\dfrac{\partial F\left(\frac{a}{L}\right)}{\partial a} + 4F\left(\frac{a}{L}\right) + 3G\left(\frac{a}{L}\right)}{4F\left(\frac{a}{L}\right)}$$

$$M_2 = \frac{2\dfrac{\partial G\left(\frac{a}{L}\right)}{\partial a}a - 3G\left(\frac{a}{L}\right)}{4F\left(\frac{a}{L}\right)}$$

Petroski and Achenbach's approach requires only one reference SIF solution with corresponding stress load. The method has been found sufficient for the approximation of weight functions of many 2D and 3D cracked problems (Wu andCarlsson, 1991). However, it is recommended (Wu and Carlsson, 1991; Niu and Glinka, 1990)to use a uniform load as the reference loading, because segment loads, point loads and self-equilibrating loads can cause erratic results. Non-uniform loading may be used if the whole crack surface is loaded corresponding to a continuous monotonic function, which does not increase towards the crack tip. Furthermore, Wu and Carlsson(1991) found that the weight function will fail with a large crack length, e.g., $a/w > 0.6$ for edge crack in a finite width strip.

Shen-Glinka Method

In order to obtain more accurate weight functions, several authors have proposed other weight function approximations. Petroski-Achenbach's method was extended by Fett et al. (1989) by adding more terms to the COD approximation as:

$$u_r(x,a) = \frac{\sqrt{8}\sigma_0}{H} \cdot a \cdot F\left(\frac{a}{L}\right) \cdot \sum_{i=0}^{n} M_i \left(1 - \frac{x}{L}\right)^{n+\frac{1}{2}}$$ **(2.40)**

$$H = E \text{ (Plane stress)} \quad H = \frac{E}{1-v^2} \quad \text{(Plane strain)}$$

where $M_0 = 1$ and M_i are functions of $\frac{a}{L}$.

Similarly, Shen and Glinka (1991) proposed approximated general expressionsgiven by:

$$h(x,a) = \frac{2}{\sqrt{2\pi(a-x)}} \left[1 + M_1\left(1 - \frac{x}{a}\right)^{\frac{1}{2}} + M_2\left(1 - \frac{x}{a}\right) + M_3\left(1 - \frac{x}{a}\right)^{\frac{3}{2}}\right]$$ **(2.41)**

where M_1, M_2 and M_3 are geometry dependent parameters.

Shen and Glinka also gave the general expression of the weight function for the surface and the deepest point of a semi-elliptical crack in a finite thickness plate, as shown in figure 2.12 below.
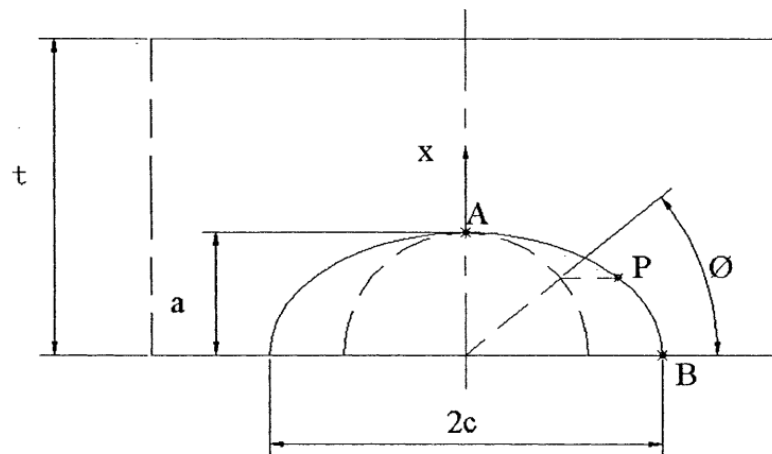
Figure 2.12.Semi-elliptical crack in a finite thickness plate, where t, c, a, A, B are the thickness of the plate, the half length of the crack, the depth of the crack,the crack mouth on the surface of the plate and the crack tip respectively.

The weight function can be expressed as:

$$h_A(x,a) = \frac{2}{\sqrt{2\pi(a-x)}}\left[1 + M_{1A}\left(1-\frac{x}{a}\right)^{\frac{1}{2}} + M_{2A}\left(1-\frac{x}{a}\right) + M_{3A}\left(1-\frac{x}{a}\right)^{\frac{3}{2}}\right] \quad \textbf{(2.42)}$$

$$h_B(x,a) = \frac{2}{\sqrt{\pi x}}\left[1 + M_{1B}\left(\frac{x}{a}\right)^{\frac{1}{2}} + M_{2B}\left(\frac{x}{a}\right) + M_{3B}\left(\frac{x}{a}\right)^{\frac{3}{2}}\right]. \quad \textbf{(2.43)}$$

The parameters, M_1, M_2 and M_3, for a particular cracked body can be determined from equation (2.34), which in turn requires the knowledge of three reference SIF solutions with corresponding stress states. However, the number of reference SIFs can be reduced by applying an extra boundary condition. It is observed that the slope of the COD of central through edge cracks under symmetrical loading is zero at the crack tip where x = 0, i.e.

$$\frac{\partial u(x,a)}{\partial x}\bigg|_{x=0} = 0 \quad \textbf{(2.44)}$$

$$\left.\frac{\partial h(x,a)}{\partial x}\right|_{x=0} = 0 \tag{2.45}$$

Thus, by applying the conditions in equation(2.45), only two reference SIF solutions with corresponding stress states are required to solve the weight function. The respective constitutive equations for determining parameters M_1, M_2 and M_3 are thus:

$$K_{r1} = \int_0^a \sigma_{r1}(x) \frac{1}{\sqrt{2\pi(a-x)}} \left[1 + M_1 \left(1 - \frac{x}{a}\right)^{\frac{1}{2}} + M_2 \left(1 - \frac{x}{a}\right) + M_3 \left(1 - \frac{x}{a}\right)^{\frac{3}{2}} \right] dx \tag{2.46}$$

$$K_{r2} = \int_0^a \sigma_{r2}(x) \frac{1}{\sqrt{2\pi(a-x)}} \left[1 + M_1 \left(1 - \frac{x}{a}\right)^{\frac{1}{2}} + M_2 \left(1 - \frac{x}{a}\right) + M_3 \left(1 - \frac{x}{a}\right)^{\frac{3}{2}} \right] dx \tag{2.47}$$

$$\left.\frac{\partial}{\partial x} \left\{ \frac{1}{\sqrt{2\pi(a-x)}} \left[1 + M_1 \left(1 - \frac{x}{a}\right)^{\frac{1}{2}} + M_2 \left(1 - \frac{x}{a}\right) + M_3 \left(1 - \frac{x}{a}\right)^{\frac{3}{2}} \right] \right\} \right|_{x=0} = 0 \tag{2.48}$$

Solving the above equations simultaneously, the three parameters, M_1, M_2 and M_3, specific to a particular cracked geometry can be found.

Ojdrovic and Petroski Method

Ojdrovic and Petroski(1991) introduced a different approach to approximate the weight function by directly defining the derivative of COD, which is needed for the weight function. The derivative of the COD can be expressed in the form of a power series as:

$$\frac{\partial h(x,a)}{\partial a} = \frac{4\sigma_0}{H} \sqrt{2} \sum_{j=0}^{m} C_j \left(1 - \frac{x}{a}\right)^{j-1/2} \tag{2.49}$$

where $C_0 = \dfrac{F\left(\dfrac{a}{L}\right)}{2}$ and $F\left(\dfrac{a}{L}\right)$ are as defined in equation (2.37). C_j are unknown coefficients to be determined, which depend on geometry only, whilem is the number of symmetrical reference loading stress.

Substituting equation (2.49) into (2.35) gives the weight function expression:

$$h(x,a) = \frac{H}{2K_1(a)} \frac{\partial u\,(x,a)}{\partial a} = \frac{2\sigma_0}{HK_1(a)} \sqrt{2} \sum_{j=0}^{m} C_j \left(1 - \frac{x}{a}\right)^{j-1/2} \tag{2.50}$$

The unknown coefficient, C_j, can be solved by knowing at least two reference SIF solutions with corresponding reference stress loading. Considering the situation where two reference cases are available:

$$C_1 = \frac{q_1 W_{22} - q_2 W_{12}}{W_{11} W_{22} - W_{21} W_{12}} \tag{2.51}$$

$$C_2 = \frac{q_2 W_{11} - q_1 W_{21}}{W_{11} W_{22} - W_{21} W_{12}} \tag{2.52}$$

where q_i and W_{ij} are respectively defined as

$$W_{ij} = \int_0^a \sigma_i(x) \sum_{j=0}^{m} \left(1 - \frac{x}{a}\right)^{j-1/2} dx \tag{2.53}$$

$$q_i = \frac{F_1\left(\dfrac{a}{L}\right)}{2} \left[K_i(a) \sqrt{\frac{\pi a}{2}} - W_{i0} \right] \tag{2.54}$$

where $K_i(a)$ is the SIF of ith loading case.

The above Ojdrovic and Petroski method significantly reduces the computational effort compared to the Petroski-Achenbach method(Petroski and Achenbach, 1978). Furthermore, Brennan (1994) demonstrated that Ojdrovic and Petroski'sapproach gives more accurate and stable results. Such improvement in accuracy and stability is because,when applying Petroski-Achenbach method, small inaccuracies in displacement values can result in large errors in the derivative values obtained (NG, 1998). In contrast, Ojdrovic and Petroski's method approximates the derivative directly. The main disadvantage of implementing this method is that it generally requires at least two known solutions whereby one reference solution is often difficult to solve(Brennan, 1994). This disadvantage can be overcome by incorporating the FEM, which can provide numerical solutions to the specific geometry under several reference loadings.

2.4 Pipeline Fracture Modelling

Propagating fractures are considered the most catastrophic type of pipeline failure. Such failures involve the rapid axial splitting or tearing of the pipeline, sometimes running over distances of several hundred meters resulting in massive loss of inventory in a very short time. Therefore, the modelling of pipeline fractureshas led to many studies (see for example Leis et al., 2005; Maxey, 1974). Such interest has intensified recently (Cosham and Eiber, 2008; Mahgerefteh et al., 2008c) given the prospect of using pressurised pipelines for transporting CO_2 in Carbon Capture and Storage (CCS) projects. Given that exposure to CO_2 at a concentration of >10% v/v is likely to be instantly fatal (Kruse and Tekiela, 1996), a ruptured CO_2 pipeline near a populated area can lead to catastrophic consequences.

Fractures are initiated from defects introduced by mechanical damage, geological movement, corrosion or adverse operating conditions. Such defects can grow when the stresses acting on the defect overcome the pipe wall fracture initiation tolerance. When defect length reaches a critical size, based on the pipeline material properties and the prevailing thermal and pressure stresses, fractures occur and propagate. Thus, it is highly desirable to design pipelines such that when a defect reaches a critical size and fails, the result is a leak, rather than a long running fracture. This can be achievedthrough the following steps:

- providing sufficient fracture initiation resistance by specifying the required pipeline material toughness, pipe wall thickness and operating conditions

- ensuring sufficient fracture propagation resistance such that if a running fracture occurs, its length is limited to a short distance.

Fracture initiation can be controlled a priori by specifying the required pipeline material toughness, minimum wall thickness and the maximum operation pressure. However, controlling fracture propagation, once a leak has formed, is more complex. The fracture propagation velocity and arrest length depend on material fracture

toughness, ambient backfill conditions, depressurisation rate and the minimum pipe wall temperature relative to its ductile-to-brittle transition temperature.

A leak in the pressurised pipeline results in a series of expansion waves within in the pipe inventory that propagate from the rupture plane towards the intact end of the pipeline at the speed of sound(Picard and Bishnoi, 1988). During fracture propagation, the crack tip pressure is the main driving force. Therefore, the precise tracking of the expansion waves, and their effect on the pressure profile along the pipeline, is essential for the proper modelling of fracture propagation.

Additionally, when phase change occurs during depressurisation, the transition from the gaseous to the two-phase region results in a significant drop in the speed ofsound and hence the depressurization rate. Such analysis must also take real fluid behaviour into account by employing an appropriate equation of state. In addition,the temperaturedrop because of the Joule-Thomson expansion coolingof the fluid within the pipeline during discharge can besignificant. In the case of CO_2, depending on the startingconditions, such temperatures can reach as low as -70 ℃resulting in very significant localised cooling of the pipewall in contact with the escaping fluid.

2.4.1 Pipeline Ductile Fracture Modelling

To model the pipeline ductile fracture, the Battelle-Two-Curve (BTC) approach byMaxey(1974) expresses the criterion for thepropagation by the comparison between the fluid decompression-wave velocity and the pipeline crack-propagation velocity. If the fluid decompression-wavevelocity is larger than the crack velocity, the crack tipstress will decrease, eventually dropping below the arreststress and causing the crack to arrest. Conversely, if thedecompression-wave velocity remains smaller than the crackvelocity, the crack tip pressure will remain constant resultingin indefinite propagation.

Several studies have since been conducted for modellingductile fractures based on the BTC approach (Inoue et al., 2003). Some employ sophisticated FEMs for simulating

material deformationbut use over-simplistic transient fluid flow models forpredicting the rupture plane pressure and, hence, the crackdriving force(Odonoghue et al., 1991; Zhuang and Guo, 1999). Others, onthe other hand, although accounting for the transientdepressurization profile within the pipeline, do notdeal with the impact of pipe wall heat transfer andfriction effects on the fluid decompression behaviour(Makino et al., 2001; Terenzi, 2005).Additionally a reliabledecompression model must also incorporate a suitableequation of state. This is especially important in thecase of CO_2 pipelines given the unique depressurizationthermodynamic trajectory.

Mahgerefteh et al. (2010) developed a rigorous model which simulates the dynamic interaction between the rapidly changing crack tip opening area and the pressure loading as the crack propagates. The model coupled a semi-empirical fracture model with the transient real fluid decompression model considering all of the important transient fluid/structure interactions governing the ductile fracture process. The authors validated the model against some of the full-scale burst tests including theHigh-Strength Line Pipe Committee Tests (Inoue et al., 2003), the ECSC X100 Pipeline Test (Takeuchi et al., 2006)and Alliance Pipeline Tests (Johnson et al., 2000)for pipes containing citherair or rich gas mixtures. Following its successful validation, Mahgerefteh et al. (2010)applied their model to a hypothetical but realistic pressurised CO_2 pipeline to test its ductile-fracture-propagation susceptibility.

2.4.2 Low-Temperature-Induced Brittle Fracture Modelling

As described in the previous section, a crack can initiate and grow from defects that developin a structural part as a result of fatigue, creep or stress corrosion. In case of a pressurised pipeline, such fractures are likely formed from one surface and grow to the other. Depending on the internal pressure, material toughness and pipe wall thickness, there are two possible fracture modes. In the first scenario, the crack may become unstable after it reaches the critical length. In this case, a ductile fracture propagation described in the previous section occurs. The other scenario involves the crack growing steadily through the wall forming a stable through-wall crack, which is called "leak-before-break"(LBB). However, the rapid expansion of the pressurised

inventory through the stable leak may cause a significant temperature drop at the puncture. If the minimum pipe wall temperature drops below its DBTT, the pipeline, depending on the magnitude of the localised thermal and pressure stresses, as compared to the pipe wall fracture toughness, mayfail in the brittlefracture manner. The only model available for simulating the above failure mechanism through the coupling of fracture and fluid mechanics considerations is that reported by Mahgerefteh and Atti(2006). A review of the model and its limitations is presented as follows.

2.4.3 Review of the Mahgerefteh and Atti(2006)Brittle Fracture Model

The fluid dynamics model employed inMahgerefteh and Atti's(2006) study was the University College London decompression model, the details of which are presented in chapter 3. Briefly, the outflow model involves the numerical solution of mass, momentum and conservation equations using the Method of Characteristics (MoC), taking account of fluid/wall friction and heat transfer effects. In addition, the Homogeneous Equilibrium Model is employed in which the constituent fluid phases are assumed to remain in thermal and mechanical equilibrium during the depressurisation process.

The Peng-Robinson Equation of State (PR EoS)(Peng and Robinson, 1976) is used to determine the required phase equilibrium and thermodynamic data. Although this EoSperforms relatively well for hydrocarbons, its application to CO_2, produces relatively large errors(Li and Yan, 2009). In this study, the modified PREoS(Wu and Chen, 1997)is chosento obtain the relevant fluid thermodynamic and phase equilibrium data of CO_2. The modified PREoShas been shown(Mahgerefteh et al., 2008) to produce generally good agreement with the well-established but computationally demanding GERG-2004 EoS(Kunz et al., 2007)for CO_2 and its mixtures.

Fracture Modelling

The fracture component of Mahgerefteh and Atti's(2006)modelemploys an analytical shape function to calculate the SIF using the standard SIF equation (2.13). Yet, theshape functions employed in the previous studyare only valid for puncture on an infinity plate. There is significant error by applying it to pipe wall where there is curvature for the cylindrical pipe wall. The shape functions underestimate the crack tip SIF when the curvature is large. A more rigorous fracture model is required, which accounts for the precise geometry of the pipe wall and the initial crack.

In this study, a FEMapproach combined with the weight function method will be employed.

PipeWall Heat Transfer Modelling

In the heat transfer module of Mahgerefteh and Atti's(2006) work, the following heat transfer sub-processes were considered,as depicted in figure 2.13:

i)   Conductive heat transfer within the pipe wall (H_1).
ii)   Natural/forced convective heat transfer between the outside ambient and the pipe wall (H_2).
iii) Axial forced convective heat transfer between the escaping fluid and the puncture plane (H_3).
iv)   Convective heat transfer between the flowing fluid and the pipe wall (H_4).
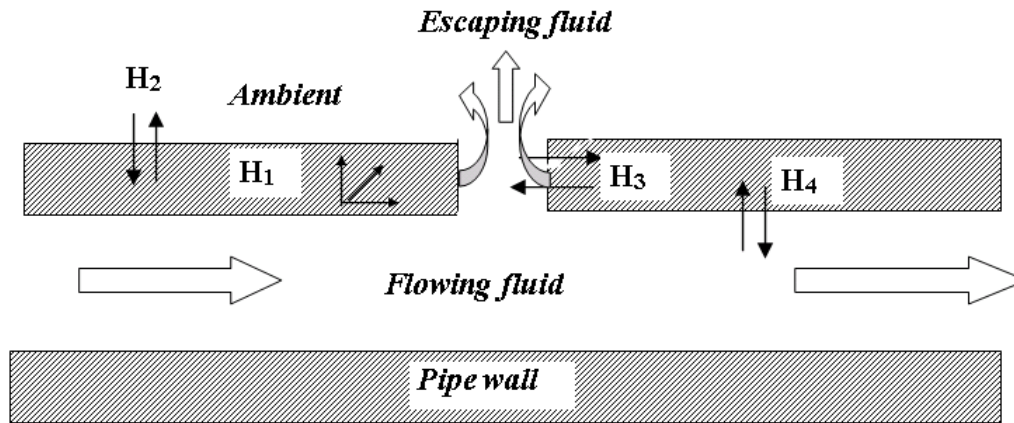
Figure 2.13.A schematic representation of the various heat transfer boundaries following pipeline puncture (Atti, 2006).

Two ambient conditions were considered in the study: pipeline exposed to air and pipeline buried where a large crater is formed. In the latter case, the pipe wall temperature is assumed to be instantly the same as the released fluid. The heat transfer process between the trapped fluid and the pipe wall is not considered, and thus, the fluid/structural interaction is oversimplified. In this study, a more rigorous heat transfer model will be further developed.

2.5Concluding Remarks

After reviewing the three sub-modules of the current low-temperature-induced brittle fracture model, the following conclusion can be made. Although the model successfully depicts the low-temperature-induced brittle fracture concept, significant improvements need to be made in the heat transfer module and fracture mechanics module to model actual CO_2 pipelines. The main development in this study will be:

1) In the fracture model, a rigorous method to determine the crack tip SIF, which accounts for real pipeline geometry, is required.In this study, a FEM approach combined with the weight function method will be employed.

2) In the heat transfer model, further development has to be made to incorporate the fluid/soil/pipe wall interaction when the pipeline is buried.

CHAPTER 3: BACKGROUND THEORY FOR MODELLING TRANSIENT FLOW IN PIPELINES

3.1 Introduction

As described in the previous chapter, the modelling of low-temperature-induced brittle fracture in a pressurised pipeline requires the following elements:

i)   A transient fluid flow model for predicting the fluid temperature and pressure during the decompression process following the initial leak;

ii)   A heat transfer model for predicting the localised cooling of the pipe wall at and near the rupture plane caused by the expansion of the escaping fluid;

iii)   A fracture model for evaluating the propagation of the crack under the pressure stress.

This chapter deals with (i) above, i.e the review of the background theory for simulating the transient outflow following pipeline rupture, including its validation against real data. Given that the model has been presented elsewhere (Brown, 2011; Denton, 2009), only the main features are given here.

Model Assumptions

i)   The flow in the pipeline is predominantly one-dimensional. However, a two-dimensional approximation is used in puncture cases where the flow is in both normal and axial directions.

ii)   Steady state flow in the pipeline prior to rupture

iii)   Homogeneous Equilibrium Model (HEM) where the consentient phases are assumed to be at thermal and mechanical equilibrium

iv)   Uniform pipeline cross-sectional

3.2 Governing Conservation Equations

Based on the above assumptions, the governing conservation equations for mass, energy and momentum for the unsteady transient one-dimensional fluid flow can be respectively written as (Zucrow and Hoffman, 1976) :

$$\frac{d\rho}{dt} + \rho\frac{\partial u}{\partial x} = 0 \quad \text{(Mass)} \tag{3.1}$$

$$\rho\frac{\partial u}{\partial t} + \rho u\frac{\partial u}{\partial x} + \frac{\partial P}{\partial x} = \alpha \quad \text{(Momentum)} \tag{3.2}$$

$$\rho\frac{dh}{dt} - \frac{dP}{dt} = q_h - u\beta_x \quad \text{(Energy)} \tag{3.3}$$

where

$$\beta_x = -\frac{2f_w\rho u|u|}{D_{in}} \tag{3.4}$$

where u, h, ρ and P are the velocity, specific enthalpy, density and pressure of the fluid as a function of time, t, and space, x, along the pipeline respectively. q_h and β_x are the heat transferred through the pipe wall to the fluid and the friction force term, in which D_{in} and f_w are the pipeline inner diameter and the Fanning friction factor is given by (Chen, 1979):

$$\frac{1}{\sqrt{f_w}} = -2\log\left(\frac{\varepsilon/D_{in}}{3.7065} - \frac{5.0452}{\text{Re}} \cdot \log\left(\frac{\left(\varepsilon/D_{in}\right)^{1.1098}}{2.8257} + \frac{5.8506}{\text{Re}^{0.8901}}\right)\right) \tag{3.5}$$

where ε and Re are the pipe roughness and Reynolds number respectively.

Also

$$\alpha = -(\beta_x + \rho g sin\theta) \tag{3.6}$$

where g and θ are the gravitational acceleration and the angle of inclination of the pipeline to the horizontal respectively.

3.2.1 Cubic Equation of State

In the case of hydrocarbon mixtures, the Peng-Robinson Equation of State (PR EoS) (Peng and Robinson, 1976) is used to predict the required vapour/liquid phase equilibrium data for hydrocarbon mixtures. This equation has been shown to produce good agreement with experimental data (Walas, 1985).

$$P = \frac{RT}{V - b_V} - \frac{a_V \alpha}{V^2 + 2b_V V - (b_V)^2} \tag{3.7}$$

$$a_V = 0.45724 \frac{R^2 T_c^2}{P_c^2} \tag{3.8}$$

$$b_V = 0.07780 \frac{RT_c}{P_c} \tag{3.9}$$

where P, V, T are pressure, volume and temperature respectively, and subscript c stands for critical. R and α are the universal gas constant and alpha function respectively. The alpha function used in conjunction with Peng-Robinson EoS is given by (Soave, 1972):

$$\alpha = \left(1 + \kappa \left(\frac{T}{T_c} \right)^{0.5} \right)^2 \tag{3.10}$$

$$\kappa = 0.48 + 1.574\omega - 0.175\omega^2 \tag{3.11}$$

where ω is the acentric factor.

However, in the case of CO_2, the PR EoS performs poorly, as shown by Mahgerefteh et al. (2008) . The authors have shown that the Modified PR EoS produces much better predictions. The EoS is expressed as (Wu and Chen, 1997):

$$P = \frac{RT}{V - b_V} - \frac{a_V \alpha}{V(V + b_V) + 0.645 b_V (V - b_V)} \tag{3.12}$$

where all variables are defined in equations (3.8–11).

3.2.2 Fluid Properties Determination

In this section, the main equations for determining the single and two-phase mixture density, speed of sound, thermal conductivity and viscosity as well as the friction factor are presented.

Density

In the case of a two-phase mixture, based on the homogeneous equilibrium model assumption, the pseudo-mixture density, ρ is given by:

$$\rho = \frac{\rho_g \rho_l}{\rho_g(1 - \chi) + \rho_l \chi} \tag{3.13}$$

$$\rho_g = \frac{PM_g}{Z_g RT} \tag{3.14}$$

$$\rho_l = \frac{PM_l}{Z_l RT} \tag{3.15}$$

where χ refers to the fluid quality, which is the mass of vapour per unit mass of bulk fluid, and M_g and M_l are the molecular weight of the gas and liquid components respectively. ρ_l , ρ_g and Z are the liquid and gas densities and the fluid compressibility respectively.

Single and Two-phase Speed of Sound (Atti, 2006)

The speed of sound, a through single-phase fluid can be expressed as (Picard and Bishnoi, 1988):

$$a^2 = \frac{\gamma}{\kappa\rho} \tag{3.16}$$

where γ and κ are the ratio of specific heats and the isothermal coefficient of volumetric expansion respectively, given by (Walas, 1985):

$$\gamma = \frac{C_P}{C_V} \tag{3.17}$$

$$\kappa = -\rho \left(\frac{\partial V}{\partial P}\right)_T \tag{3.18}$$

where C_P and C_V are the specific heats at constant pressure and volume respectively. V is the fluid specific volume. The term $\left(\frac{\partial V}{\partial P}\right)_T$ in equation (3.18) can be obtained analytically by differentiating the Peng-Robinson and Modified Peng-Robinson equations of state:

$$\left(\frac{\partial V}{\partial P}\right)_T = \left(\frac{-RT}{(V - b_V)^2} - \frac{2a_V\alpha(V + b_V)}{(V^2 + 2b_V V - (b_V)^2)^2}\right)^{-1} \tag{3.19}$$

$$\left(\frac{\partial V}{\partial P}\right)_T = \left(\frac{-RT}{(V - b_V)^2} - \frac{a_V\alpha(2V + 1.645b_V)}{\left(V(V + b_V) + 0.645b_V(V - b_V)\right)^2}\right)^{-1} \tag{3.20}$$

For two-phase flows, analytical expressions for determining a and C_p are not available (Mahgerefteh et al., 1999). The numerical expression of the speed of sound is given as (Mahgerefteh et al., 1999):

$$a^2 = \left(\frac{\Delta P}{\rho(T, P) - \rho(T^*, P - \Delta P)}\right)_s \tag{3.21}$$

where $T, P, \Delta P$ and ρ are fluid temperature, pressure, an infinitesimal change in pressure $\Delta P = 1 \times 10^{-6}$ bar and density respectively. The subscript, s, denotes a constant entropy condition and T^* represents the fluid temperature after the increment of pressure, ΔP, which can be obtained by a pressure-entropy flash.

Thermal Conductivity and Viscosity

In order to determine the Reynolds, Nusselt and Prandtl numbers for the fluid flow calculations, the vapour thermal conductivity and viscosity are needed. These can be calculated from Ely and Hanley's method (Ely and Hanley, 1981, 1983) by using the principle of corresponding states, using methane as a reference fluid. This method is one of the few schemes available to give a prediction of the viscosity and thermal conductivity of many non-polar components as well as mixtures with reasonable accuracy (Assael et al., 1996). For alkanes, the viscosities and thermal conductivities are calculated by Assael et al.'s (1996) semi-empirical scheme. The authors measured over 2,000 viscosities and thermal conductivities to optimise the coefficients of the scheme. It has a proven uncertainty of not greater than 5 per cent in the temperature

range of 280 K to 400 K and pressure range from saturation to up to 990 atm (Assael et al., 1996). For mixtures of various classes of components, the correlations given by DIPPR (Design Institute for Physical Property Data) (Daubert and Danner, 1990) are employed.

In the case of two-phase fluids, the viscosity and thermal conductivity is given by

$$\frac{1}{c_m} = \frac{\chi}{c_g} + \frac{1-\chi}{c_l} \tag{3.22}$$

where c_m is the mixture property, either viscosity or thermal conductivity. c_g and c_l are the gas and liquid properties respectively.

3.3 Fluid / Wall Heat Transfer

Unless the pipeline is perfectly insulated, the temperature of the fluid within the pipeline will be affected by the pipe wall and surrounding ambient. In practice, the pipeline may either be buried in soil or exposed to air. Therefore, the heat transfer between the ambient, pipe wall and fluid has to be considered.

In the CFD model employed in this study, a transient energy balance is employed by Atti (2006) to model the heat transfer process. The method uses an energy balance between fluid-wall-ambient interfaces. In every time step, the wall temperature will be updated, which will be used to carry out the heat transfer between the fluid and pipe wall in the next time step. Figure 3.1 shows the heat transfer parameters.
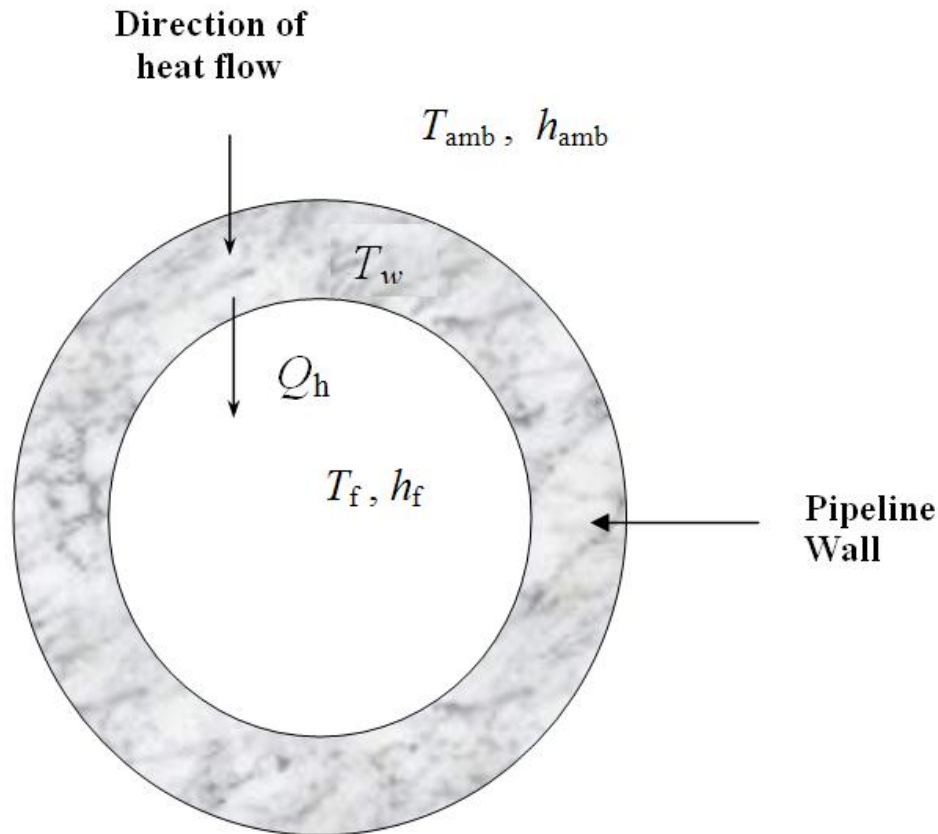
Figure 3.1. Schematic representation of the heat flow across the cross-section of a pipeline wall based on the lumped body approach (Atti, 2006).

T_{amb}, h_{amb} and T_w are the ambient temperature, heat transfer coefficient of the ambient and wall temperature respectively. T_f, h_f and q_h represent the fluid's temperature, heat transfer coefficient, and the quantity of heat transferred to the fluid respectively.

The heat transfer model has the following assumptions:

- The pipe wall to ambient heat transfer coefficient (h_{amb}) and the pipe wall to fluid heat transfer coefficient (h_f) are determined from the fluid properties at the beginning of a given step and remain constant during the time step.
- The pipe wall properties including density (ρ_w), specific heat capacity (C_{pw}) and thermal conductivity (κ_w) are constant.
- The ambient and fluid temperature is constant during a given time step.
- Only the heat transfer in the radial direction across the pipe wall is considered. The tangential and longitudinal heat conduction are neglected.

The rate of transient heat transfer to the fluid, Q_h, within a time step may be approximated by applying Newton's cooling law. The rate of heat transferred to the fluid (Q_h) in a given time step can be approximated by (Atti, 2006):

$$Q_h = \frac{4}{D_{in}} h_f \left(T_w - T_f\right)$$

(3.23)

3.4 The Steady State Non-Isothermal Flow Model (Brown, 2011)

In order to model the transient flow following pipeline rupture, it is essential to obtain the fluid flow profile along the pipeline prior to the rupture. The steady state flow model for obtaining this data is presented in this section. The model was first developed by Oke (2004) based on the isothermal assumption such that the temperature of the fluid remains the same along the pipe during normal flow. In reality, this will not hold, due to the inevitable drop in the fluid temperature due to the line pressure drop. The above was accounted for by Brown (2011) through the presentation of the mass, momentum and energy conservation equations in the following form:

$$\frac{\partial \rho u}{\partial x} = 0$$

(3.24)

$$\frac{\partial \rho u^2 + P}{\partial x} = -\rho g \sin(\theta) - \beta$$

(3.25)

$$\frac{\partial s}{\partial x} = \frac{Q_h - u\beta}{\rho u T}$$

(3.26)

where ρ, u, s, T and P are the fluid's density, velocity, specific entropy, temperature and pressure respectively. x and θ are the space and the angle of inclination respectively. Q_h is the heat transferred between the pipe wall and the fluid, calculated from equation (3.23). β is the friction term given by equation (3.4).

3.5 Solving the Transient Conservation Equations Using the Method of Characteristics (MOC)

In the above section, the transient CFD model for simulating the transient outflow following pipeline rupture was described. The mass, momentum and energy conservation equations coupled with the fluid equation of state together with the steady state and heat transfer forms the foundation of the transient fluid flow model. In this section, the technique for solving the above system of equations is presented.

3.5.1 Hyperbolic PDEs Solving Technique

There are three numerical techniques which are commonly used for resolving hyperbolic partial differential equations as follows:

- Finite Difference Methods (FDM)
- Finite Volume Methods (FVM)
- Method of Characteristics (MOC)

The Finite Difference Method (FDM) discretises the spatial domain into smaller nodes. The derivatives in the Partial Differential Equations (PDE) are substituted by finite approximations at the series of nodes. The method has been widely applied to solving PDEs as a general mathematical technique. However, Mahgerefteh et al. (2009) showed that the numerical diffusion associated with the method makes it unsuitable for modelling the transient flow following pipeline rupture.

Instead of discretising into nodes, the Finite Volume Method (FVM) divides the system into a set of small cells. The approximation is taken by integrating the PDEs over each cell. FVM has been employed to solve many hyperbolic PDEs (see for example Leveque, 2002; Toro, 2009). Brown (2011) also presented a method based on FVM for the resolution of the conservation equations of transient outflow following pipeline rupture.

The most suitable mathematical technique for solving the quasi-linear hyperbolic PDEs is the Method of Characteristics (MOC). The MOC expresses the system into a set of ordinary differential equations (compatibility equations) through a particular coordinate change. The compatibility equations are only valid along that coordinate, which can then be solved by standard FDM. The method is suitable for systems with different and complex boundary conditions. The implementation of the MOC for solving the system of equations modelling the transient outflow from a ruptured pipeline is presented in the following sections.

3.5.2 The MOC's Discretisation Methods

For implementing the MOC, there are two main discretisation methods: the Inverse Marching method (Flatt, 1986) and the Characteristic Grid method (Wylie and Streeter, 1993). The Inverse Marching method is also known as the Method of Specific Time Intervals. In this method, the locations of the discretised points in the space and time grid are predefined. Hence the characteristic lines can be extended backwards in time to intersect the previous timeline. The initial data of the characteristics line is approximated by interpolation between the two defined solutions on the previous time step, which compromises the accuracy of this method. Figure 3.2 shows the systematic approach for this method, where x and y axes represent the space and time discretisation respectively. The crossover lines shows the characteristic line. A more detail explanation of the grids will be given in figure 3.4 in the next section.
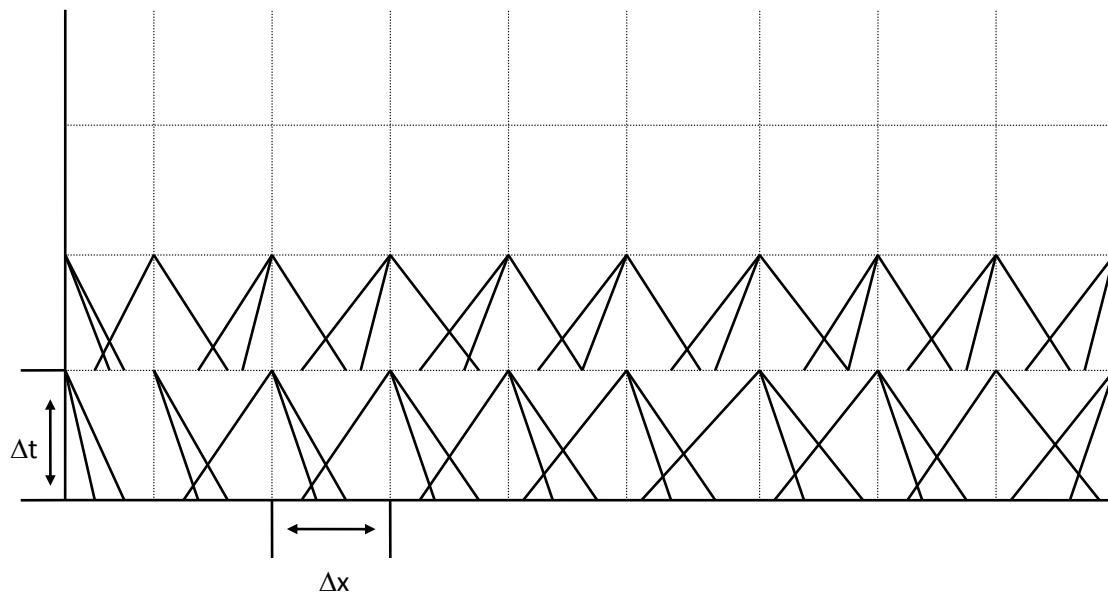
Figure 3.2. The Method of Specified Time Intervals

In contrast, in the Characteristic Grid Method, which is also known as the Natural Method of Characteristics, the position of the new solution is not specified but is determined from the intersection of the left and right characteristics lines extended from solution points in the previous time step. Hence a free growing grid is developed in the space-time plane shown as figure 3.3 below.
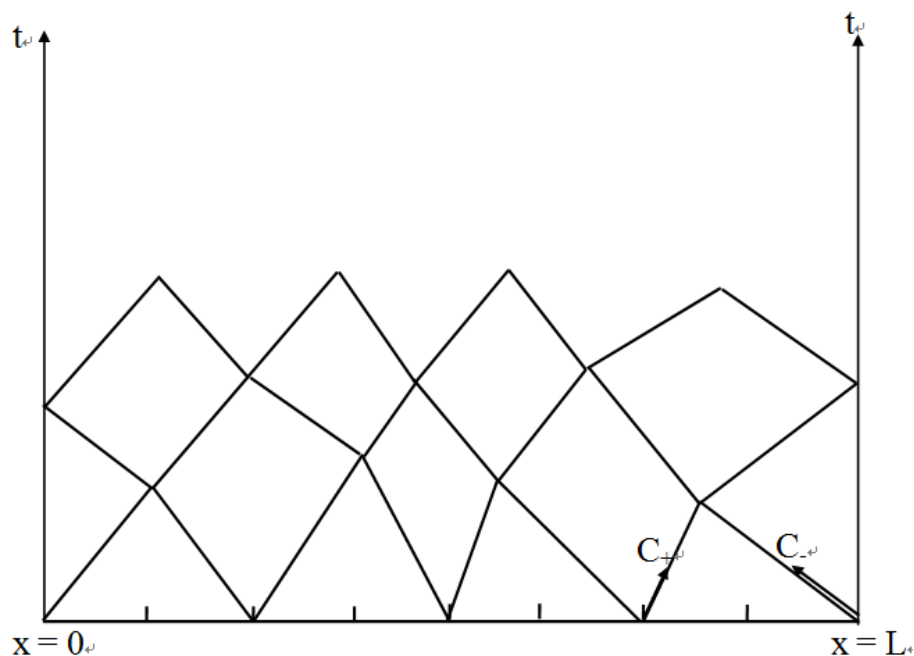
Figure 3.3. The Characteristic Grid

The Characteristic Grid Method is more accurate than the Method of Specified Time Intervals because the solution progresses along the characteristic lines where the

initial data is known and no interpolation is required. However, in contrast to the Method of Specified Time Intervals, the Characteristic Grid Method does not allow the introduction of boundary conditions at predefined times. Hence the Method of Specified Time Intervals is employed in this study.

3.5.3 Solving PDEs Using the MOC

There are two steps for solving the PDEs by the MOC:

1. Convert the partial differential equations into a set of ordinary differential equations, which are also known as compatibility equations.

2. Solve the compatibility equations based on the Method of Specified Time Intervals, employing the Euler predictor-corrector technique (Zucrow and Hoffman, 1976).

Step 1: Converting the PDEs to ODEs.

There are two common methods to convert the PDEs into Ordinary Differential equations (ODEs): the matrix transformation methods by Tiley (1989) and the multiplication of the basic equations by an unknown parameter. Atti (2006) demonstrated that the latter method is more rigorous. Hence this method is adapted in this study.

Atti (2006) introduced $\frac{1}{\lambda}$ to represent the slope of the characteristics lines. The conservation equations ($3.1 - 3.3$) may be replaced by three compatibility equations which are valid along the characteristic curves and can be solved by finite difference approximation. The compatibility equations are as follows (Atti, 2006):

$$\rho_0 d_0 h - d_0 P = \psi d_0 t \quad along \quad \frac{d_0 t}{d_0 x} = \frac{1}{u} \tag{3.27}$$

(Path line characteristic, C_0)

$$d_+ P + \rho a d_+ u = \left(a\alpha + \frac{\varphi\psi}{\rho T} \right) d_+ t \quad along \quad \frac{d_+ t}{d_+ x} = \frac{1}{u + a} \tag{3.28}$$

(Positive Mach Line charactersistic, C_+)

$$\rho a d_- u - d_- P = \left(a\alpha - \frac{\varphi\psi}{\rho T} \right) d_- t \quad along \quad \frac{d_- t}{d_- x} = \frac{1}{u - a} \qquad (3.29)$$

$$\text{(Negative Mach Line, } C_-)$$

The positive Mach lines govern the speed of the expansion waves from the low pressure end, while the negative Mach lines govern the compression wave speed from the high pressure end. The path line dictates the rate of flow along the pipeline at any given point.

Step 2: Resolving the Compatibility Equations

As described above, the Method of Specified Time Intervals is employed in this study to resolve the compatibility equations. Figure 3.4 gives a schematic representation of the characteristics lines at a grid point along the space (x) and time (t) plane.
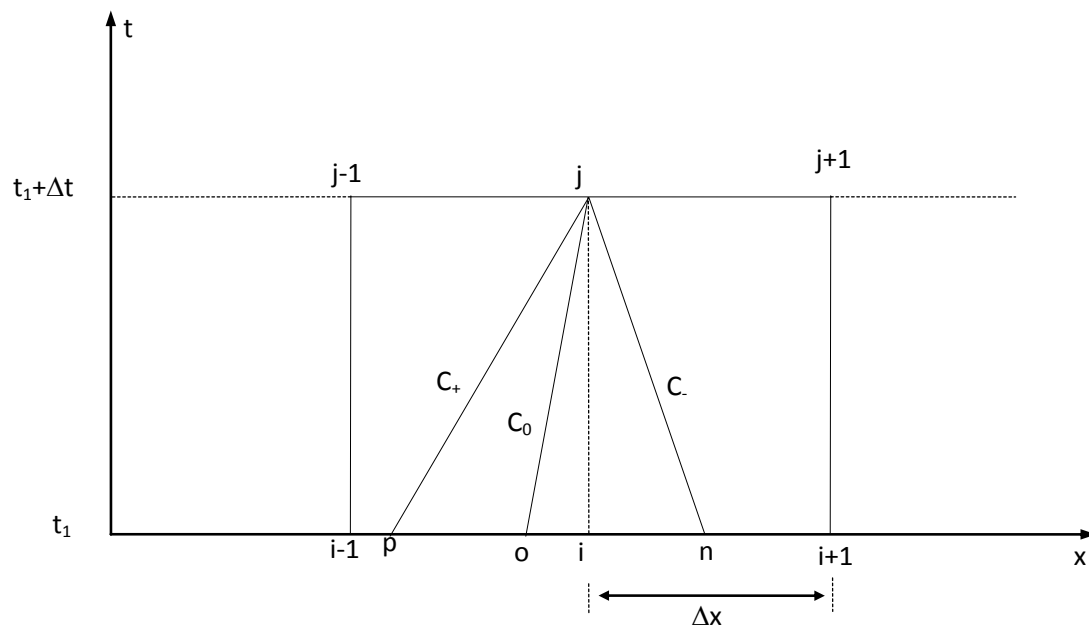
Figure 3.4. A schematic representation of Path line (C0) and Mach lines (C+, C-) characteristics at a grid point along the time (t) and space (x) axes.

In figure 3.4, t_1 represents the current time step, in which the fluid properties are known along the grid points including point i, i-1 and i+1. In the next time step, the fluid properties of point j can be calculated by following the three characteristics lines backwards. The intersections of the three characteristics lines C_+, C_0 and C_- are point p, o and n respectively, of which the initial conditions are evaluated by linear

interpolation between point i-1, i and i+1. From the initial conditions, the compatibility equations can be solved by a finite difference scheme to obtain the flow properties at point j in the next time step $t_1 + \Delta t_1$.

To ensure the numerical stability, the time step Δt has to be carefully defined, subject to the Courant-Friedrichs-Lewy (CFL) criterion (Courant et at., 1967; Mahgerefteh et al., 2009). The criterion is given by:

$$\Delta t \leq \frac{\Delta x}{|u + a|_{max}} \tag{3.30}$$

Validation:

Data relating to the validation of the outflow model presented is given in other publications (see for example Denton, 2009; Mahgerefteh et al., 2008b). These, in the main, relate to tests involving the full bore rupture of a 100 m pipeline containing LPG, where the measured rupture and intact plane temperatures and pressures as well as the mass flow rate are compared against the simulated data, in each case producing reasonable agreement. Appendix I shows such data.

3.6 Concluding Remarks

In this chapter, the development of the CFD model for simulating transient flow following pipeline failure was reviewed. This model is employed in this study to provide the necessary fluid profile for modelling low-temperature-induced brittle fracture. The mass, momentum and energy conservation equations in terms of pressure, enthalpy and velocity were presented. The conservations were coupled with the Modified Peng-Robinson Equation of State. The methods to obtain hydrodynamic and thermodynamic properties of the fluid such as fluid speed of sound, thermal conductivity and viscosity were described.

In addition, the method to incorporate the fluid phase-dependent heat transfer effects including fluid/pipe wall and pipe wall/ambient into the CFD model was described. Finally, the numerical technique to solve the partial differential conservation

equations using MOC was described. Among the two types of MOC's, the Method of Specified Time Intervals was chosen, and the corresponding formulations were shown.

In the next chapter, a rigorous heat transfer model for obtaining a detailed pipe wall temperature profile in the vicinity of the puncture will be presented. The corresponding heat transfer model will be used to determine whether the crack tip temperature will drop below the Ductile-brittle-Transition Temperature, the main factor governing the risk of brittle fracture propagation.

CHAPTER 4: DEVELOPMENT OF THE TRANSIENT HEAT TRANSFER MODEL

This chapter deals with the development of a 3-D transient heat transfer model for predicting the pipewall temperature in the proximity of the through-wall defect prior to the fracture propagation process. The modelling involves discretisation of the pipe-wall into cubic cells, followed by numerical solution of theheat conduction equations for each cell to obtain thetemperature at the next time step. The Finite Volume Method is used to resolve the equations.

4.1 Governing Equations for 3-D Transient Heat Transfer in the Pipeline

Considering a cubical cell of length,Δxwidth,Δy and height, Δz as shownin figure 4.1, the energy balance on this cubic cell during a short time interval, Δt can be written as(Cengel, 2003):

$$Q_x + Q_y + Q_z - Q_{x+\Delta x} - Q_{y+\Delta y} - Q_{z+\Delta z} + G_{cell} = \frac{\Delta E_{cell}}{\Delta t} \tag{4.1}$$
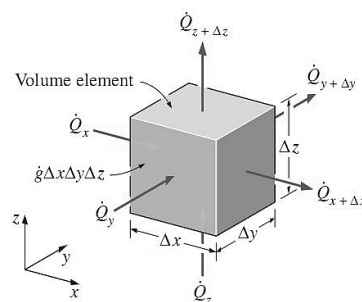

Figure 4.1.Three-dimensional heat conduction through a rectangular cell (Cengel, 2003)

For heat conduction, $Q_{x,y,z}$ can be expressed as:

$$Q = kA\frac{dt}{dx} \tag{4.2}$$

where k, A, ΔE_{cell} and G_{cell} are the thermal conductivity of the material, the cross section area, the change in the energy content of the cell and the rate of heat generation within the cell respectively. Also, ΔE_{cell} and G_{cell} can be expressed as:

$$\Delta E_{cell} = \rho C \Delta x \Delta y \Delta z T_{t+\Delta t} - T \qquad \textbf{(4.3)}$$

$$G_{cell} = g \Delta x \Delta y \Delta z \qquad \textbf{(4.4)}$$

where g, ρ and C are the internal heat generation rate, the body density and the volumetric specific heat respectively.

Figure 4.2 shows a cell (i,j,k) with side lengths Δx, Δy and Δz. For each cell, there are six adjacent cells. One adjacent cell (i,j,k+1) is also shown in figure 4.2. $K_{i,j,k+1/2}$ is expressed as the thermal conductivity between the cells (i,j,k) and (i,j,k+1). $T_{i,j,k}$ and $T_{i,j,k+1}$ are the temperatures of the two cells respectively.
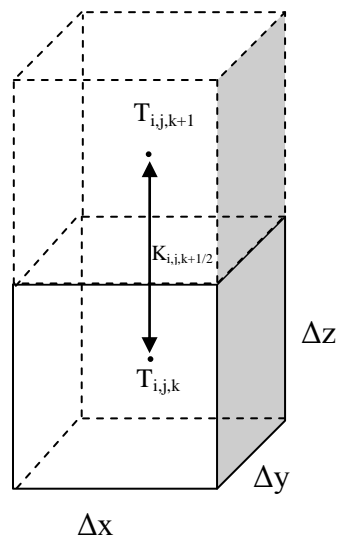
Figure 4.2. Discretised cube cells (i,j,k) and (i,j,k+1)

The 3-D heat transfer for the pipe wall is governed by the following heat conduction equation:

$$\rho C \frac{\partial T}{\partial t} + \frac{\partial}{\partial x}\left(\kappa \frac{\partial T}{\partial x}\right) + \frac{\partial}{\partial y}\left(\kappa \frac{\partial T}{\partial y}\right) + \frac{\partial}{\partial z}\left(\kappa \frac{\partial T}{\partial z}\right) = 0 \qquad \textbf{(4.5)}$$

where κ and C are the thermal conductivity and the specific heat respectively. Equation (4.5) is solved numerically using FVM by discretising the pipe wall into small elements. The heat balance for each element, e.g., for the cell (i,j,k), is given by:

$$k_{i-1/2,j,k}\Delta y\Delta z\frac{T_{i-1,j,k}-T_{i,j,k}}{\Delta x}+k_{i,j-1/2,k}\Delta x\Delta z\frac{T_{i,j-1,k}-T_{i,j,k}}{\Delta y}+k_{i,j,k-1/2}\Delta x\Delta y\frac{T_{i,j,k-1}-T_{i,j,k}}{\Delta z}$$

$$-k_{i+1/2,j,k}\Delta y\Delta z\frac{T_{i,j,k}-T_{i+1,j,k}}{\Delta x}-k_{i,j+1/2,k}\Delta x\Delta z\frac{T_{i,j,k}-T_{i,j+1,k}}{\Delta y}-k_{i,j,k+1/2}\Delta x\Delta y\frac{T_{i,j,k}-T_{i,j,k+1}}{\Delta z}$$

$$+g\Delta x\Delta y\Delta z=\rho C\Delta x\Delta y\Delta z\frac{T^{t+\Delta t}_{i,j,k}-T^{t}_{i,j,k}}{\Delta t}$$

(4.6)

Thus, by knowing the temperature of cell (i,j,k) along with its six adjacent cells at time t, the temperature of cell (i,j,k) at time $t+\Delta t$ can be calculated from equation (4.6).

The stable time-step, Δt is determined using the following stability criterion:(Cengel, 2003)

$$\Delta t<\frac{C_{i,j,k}\Delta x\Delta y\Delta z}{k_{i-1/2,j,k}+k_{i,j-1/2,k}+k_{i,j,k-1/2}+k_{i+1/2,j,k}+k_{i,j+1/2,k}+k_{i,j,k+1/2}}$$

(4.7)

To guarantee stability, this criterion must be satisfied for all cells (i,j,k). Hence, the smallest stable time-step among the cells is used.

Equation (4.6) is valid for all internal cells that have at least one cell on each side. For the modelling of the heat transfer process along the convective boundaries, the boundary heat transfer, $Q_{boundary}$ can be written as:

$$Q_{boundary}=h_{boundary}A\Delta T$$

(4.8)

where $h_{boundary}$ and A are the boundary heat transfer coefficient and the cross sectional area respectively.

The determination of various heat transfer coefficients as dictated by the fluid phase or flow characteristics is required next. The relevant correlations employed at various fluid-wall boundaries are given below.

4.2 Boundary Heat Transfer Coefficient

To evaluate the boundary heat transfer coefficient, $h_{boundary}$ in equation (4.8), the following modes of heat transfer must be considered:

i)   heattransfer between the escaping fluid and the puncture plane

ii)   ambientair-to-outer-pipe-wall heat transfer

iii) convectiveheat transfer between the flowing fluid within and the inner pipe wall

iv)   where applicable, heat transfer conditions for buried pipelines

4.2.1 Heat Transfer between the Escaping Fluid and the Puncture Plane

Considering the high Reynolds numbers ($>10^6$), the flow through the puncture is assumed to befully developed and turbulent. Therefore, the heattransfer between the flow through the punctureis forced turbulent convection, as opposed to natural convection. The Nusselt number for forcedconvection can be determined fromGnielinski (1976):

$$Nu = \frac{(f/8)(\text{Re}-1000)\text{Pr}}{1+12.7(f/8)^{0.5}(\text{Pr}^{2/3}-1)} \tag{4.9}$$

$$\left(\begin{array}{c} 0.5 \leq \text{Pr} \leq 200 \\ 3*10^3 < Re < 5*10^6 \end{array}\right)$$

wherePr and Re are the PrandtlandReynolds numbers respectively. The fanning friction factor is f, which can be calculated from (Chen, 1979):

$$\frac{1}{\sqrt{f}} = -2\log\left(\frac{\varepsilon/D}{3.7065} - \frac{5.0452}{\text{Re}} \cdot \log\left(\frac{(\varepsilon/D)^{1.1098}}{2.8257} + \frac{5.8506}{\text{Re}^{0.8901}}\right)\right) \tag{4.10}$$

where ε and D are the pipe roughness and the pipe internal diameter respectively.

Once the Nusselt number is determined, the convection heat transfer coefficient is obtained from the definition of the Nusselt number as follows:

$$h = \frac{kNu}{D} \tag{4.11}$$

For two-phase flow, the heat transfer coefficient, h_f can be calculated from(Steiner andTaborek, 1992):

$$\frac{h_f}{h_l} = \left[\left(1-x\right)^{1.5} + 1.9x^{0.6}\left(\frac{\rho_l}{\rho_g}\right)^{0.35} \right]^{1.1} \tag{4.12}$$

wherex, ρ_gandρ_l are the vapour mass fraction, vapour density and liquid density respectively.The heat transfer coefficient for the liquid phase, h_l is given by:

$$\frac{h_l D}{k_l} = 0.023 \left[\frac{\rho_{mix} u\left(1-x\right)D}{\mu_l} \right]^{0.8} \left[\frac{\mu_l C_{pl}}{k_l} \right]^{0.4} \tag{4.13}$$

where k_l, ρ_{mix}, u, C_{pl}, and μ_l arerespectively the thermal conductivity of the liquid, the two-phase mixture density, the mixture velocity, the liquid specific heat and the liquid viscosity.

4.2.2 Ambient Air-to-Outer-Pipe-Wall Heat Transfer

The ambient-to-outer-pipe-wall heat transfer can be by natural (no wind) or forced (wind) convection. The heat transfer coefficient, h_{amb} between the pipe wall and the ambient is given by(Janna, 2000):

$$h_{amb} = (h_{nat}^3 + h_{for}^3)^{1/3} \tag{4.14}$$

whereh_{nat} and h_{for} are the natural and forced (in the case of wind)heat transfer coefficients respectively.

The empirical correlation for the average Nusselt number for natural convection over the entire surface of a horizontal cylinder is given by Churchill and Chu (1975) as:

$$Nu_{nat} = \left\{ 0.6 + \frac{0.387 Ra_D^{1/6}}{\left[1 + \left(0.559/\Pr_{film}\right)^{9/16}\right]^{8/27}} \right\} \tag{4.15}$$

$$(Ra_D < 10^{12})$$

$$Ra = Gr_{Lfilm} \Pr_{film} \text{ (Reyleigh number)} \tag{4.16}$$

$$Gr_L = \frac{g\beta_{film}(T_s - T_{amb})D^3}{v_{film}^2} \text{ (Grashof number)} \tag{4.17}$$

$$\Pr = \frac{C_{pfilm}\mu_{film}}{\kappa_{film}} \text{ (Prandtl number)} \tag{4.18}$$

$$\beta_{film} = -\frac{1}{\rho_{film}}\left(\frac{\partial \rho_{film}}{\partial T_{film}}\right) \tag{4.19}$$

$$T_{film} = \frac{T_s + T_{amb}}{2} \tag{4.20}$$

where β, D, v and μ are the coefficient of volume expansion, pipe diameter and kinematic and dynamic viscosity respectively. The subscript film represents the ambient air properties at the film temperature.

Using the equation (4.15), the heat transfer coefficient fornatural convection, h_{nat} can be calculated fromthe definition of the Nusselt number as:

$$h_{nat} = \frac{k_{film}Nu_{nat}}{D} \tag{4.21}$$

where k_{film} is the thermal conductivity of the fluid at the film temperature.

For forced convection, the correlation forthe average heat transfer coefficient over the entire surface is providedby Churchill and Bernstein (1977):

$$Nu_{for} = \frac{h_{for}D_{pipe}}{k_{film}} = 0.3 + \frac{0.62\,\mathrm{Re}_{film}^{1/2}\,\Pr_{film}^{1/3}}{\left[1+\left(0.4/\Pr_{film}\right)^{1/4}\right]}\left[1+\left(\frac{\mathrm{Re}}{282000}\right)^{5/8}\right]^{4/5} \tag{4.22}$$

(for Re Pr> 0.2)

where Nu_{for}, Re_{film} and $\Pr_{film}$ are the force convection Nusselt number, the Reynolds numberandthe Prandtl number at the film temperature respectively.

4.2.3 Convective Heat Transfer between the Flowing Fluid and the Inner Pipe Wall

Depending on the puncture diameter and the flow conditions,the heat transfer between the flowing fluid and the pipe wall away from a puncture may be either laminar or turbulent convection. For turbulent flow, equation (4.9)applies. For laminar flow, the Nusselt number can be determined from(Edwards et al., 1979):

$$Nu = 3.66 + \frac{0.065(D/L)\,\mathrm{Re}\,\mathrm{Pr}}{1 + 0.04\left[(D/L)\,\mathrm{Re}\,\mathrm{Pr}\right]^{2/3}} \tag{4.23}$$

$$(\text{for } \mathrm{Re} < 2000)$$

where L is the pipe length.

4.2.4 Heat Transfer Conditions for Buried Pipelines

In the case of a puncture in a buried pipeline,the worst case scenario is assumed in which there is no blowout of the surrounding soil. In such case, the rapid quasi-adiabatic depressurisation of CO_2 into the soil can result insignificant cooling of the escaping fluid to temperatures as low as$-80\,^{0}C$(Mahgerefteh et al., 2008). This low temperature fluid is expected to cool the surrounding soil, effectively forming a cold blanket around the pipeline. The heat transfer mode between the buried pipeline and the surrounding soil is via conduction. To model this, a heat transfer coefficient approximation, h_{soil} for a horizontal cylinder in a semi-infinite medium is used as given byequation (4.24)(Bai and Bai, 2005):

$$h_{soil} = \frac{k_{soil}}{\left(\dfrac{D}{2}\right)\cosh^{-1}\left(\dfrac{2Z}{D}\right)} \tag{4.24}$$

where h_{sol} and k_{soil} are the heat transfer coefficient and thermal conductivity of the soil respectively. D and Z are respectively the outer pipe diameter and the distance between the top of the soil and the centre of the pipe as shown in figure 4.3.
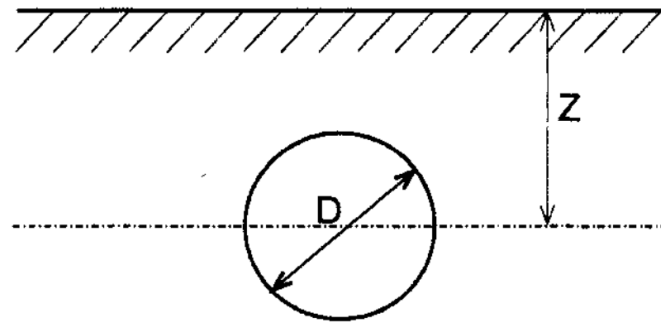
Figure 4.3.Horizontal cylinder buried soil showing the characteristic dimensions,

Referring to equation (4.24), when Z is greater than D/2, the $\cosh^{-1}$term can be simplified as

$$\cosh^{-1}\left(\frac{2Z}{D}\right) = \ln\left[x + \left(x^2 - 1\right)^{0.5}\right].$$

Hence,equation ((4.24)) can be rewritten as:

$$h_{soil} = \frac{2k_{soil}}{D\ln\left[\dfrac{2Z + \sqrt{4Z^2 - D^2}}{D}\right]} \tag{4.25}$$

The soil thermal conductivity in equation (4.25) may be found by experimentation or the literature. Empirical correlations, expressed as a function of dry soil density, water content, temperature, mineralogy, soil particle size distribution and the volumetric proportions of solid, liquid and airare available in the literature (Bai and Bai, 2005). Kersten(1949) proposed the following correlations for some typical types of soil:

$$k_{soil} = [0.9 \cdot \log(\omega) - 0.2] \times 10^{0.01 \times \rho} \qquad \text{(unfrozen silt-clay)} \tag{4.26}$$

$$k_{soil} = 0.01 \cdot 10^{0.022 \times \rho} + 0.085 \cdot 10^{0.008 \times \rho} \omega \qquad \text{(frozen silt-clay)} \tag{4.27}$$

$$k_{soil} = [0.7 \cdot \log(\omega) - 0.4] \times 10^{0.01 \times \rho} \qquad \text{(unfrozen sand)} \tag{4.28}$$

$$k_{soil} = 0.076 \cdot 10^{0.013 \times \rho} + 0.032 \cdot 10^{0.0146 \times \rho} \omega \qquad \text{(frozen sand)} \tag{4.29}$$

where ω and ρ are the moisture content in percentage of dry soil weight and soil dry density respectively.

As the thermal conductivity of the soil changes during the pipeline depressurisation, a constant value of 0.9 W/mK is used for each soil as thermal conductivity. This assumption is need as the real soil properties such as voidage, moisture content and density is not available and may varies by position.

4.3 Application of the Model

The complete 3-D heat transfer model covers 1 meters of the pipe wall in the vicinity of the crack. Further pipe wall temperature profile is not need as the critical crack length before unstable growth is normally found to be less than 20 cm. To reduce the computational runtime by symmetry, only a quarter of the pipe wall around the puncture is modelled, shown as the shaded area in figure 4.4. The mesh size ranges from 0.2 cm to 1 cm according to the requirement of the crack increment resolution.
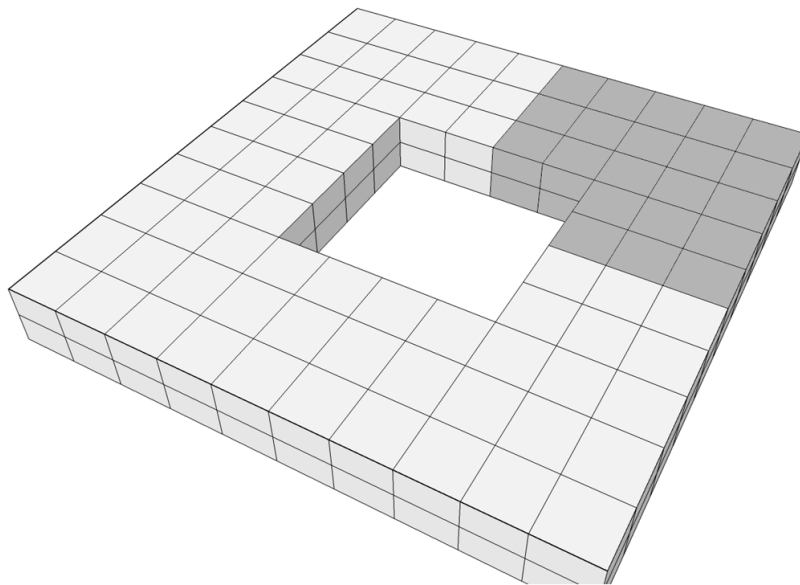
Figure 4.4. Presentation of the mesh used in the heat transfer model.

The model was validated against the Finite Element Method results givenAbaqus by applying constant heat flux at the puncture.

4.4 Summary

In this chapter, the heat transfer module for required for simulatingthe low-temperature induced brittle fracture was presented. This model accounts for various heat transfer processes taking place during depressurisation including ambient to pipe wall, fluid to pipe wall and soil to pipe wall heat transfer.

In the next chapter, a rigorous crack tip fracture model is presented to enable the determinationwhether the crack will propagate or arrest under various pressure and temperature conditions.

CHAPTER 5: DEVELOPMENT OF THE FRACTURE MODEL

5.1 Introduction

In the development of an integrated model for evaluating low-temperature brittle fracture, a rigorous crack tip fracture model is essential in order to account for the pertinent parameters, including pipeline characteristics, crack geometry, hoop stresses andmaterial toughness. The criterion for low-temperature-induced brittle fracture propagation is characterised by the crack tip Stress Intensity Factor (SIF). Previous work conducted by Atti(2006)employed an analytical shape function tocalculatethe SIF. However, the shape function employed in Atti's work is only valid for an infinite plate with a through-wall defect or a puncture.In the case of a through-wall defect in a pipe wall, however, the above assumption results in a significant error (Rahman et al., 1998) since the impact of the pipe wall curvature on the resulting stresses is ignored. This chapter presents the development of a rigorous fracture model to simulate the transition of an initial through-wall defect in a pressurised pipeline into a running brittle facture, taking into account the pipe wall curvature and the defect shape. The above involves the following main steps:

1. the development of a finite element model usingthe commercial software, Abaqus(SIMULIA, 2011),to calculatethe SIF;
2. the determination of the weight function parameters usingthe results of the Abaqus-generated model and
3. the approximation of the weight function parameters using available data.

5.1.2 Introduction to Finite Element Method

Finite Element Analysis (FEA) is a special numerical analysis technique used to obtain various approximate solutions to a wide variety of engineering problems (Huebner, 2001). It has become the most popular method of solving real-life problems in mechanical, heat transfer, magnetic and other fields of analysis. A finite element model is set up using a system of points known as 'nodes'. Connecting specific nodes forms the 'elements' that create the finite mesh and contain the structural and material

properties of the structure.Such process results in a set of simultaneous algebraic equations as

$$[K]\{u\} = \{F\} \qquad\qquad (5.1)$$

where [K], {u}, and {F} are the property, behaviour and action matrixes respectively.

By using FEA, Many engineering problems can be expressed by such set of simultaneous algebraic equations. The various variables of these engineering problems are described in Table 5.1.

	Property[K]	Behaviour {u}	Action {F}
Elastic	stiffness	displacement	force
Thermal	conductivity	temperature	heat source
Fluid	viscosity	velocity	body force
Electrostatic	permittivity	potential	charge

Table 5.1.Corresponding property, behaviour and action variables of various engineering problems using FEA.

The unknown variables {u} can be obtained by solving the equations

$$\{u\} = [K]^{-1}\{F\} \qquad\qquad (5.2)$$

5.2 Finite Element Analysis Using Abaqus

The commercial FEA package Abaqus(SIMULIA, 2011)employed in this studyis capable of solving problems ranging from relatively simple linear ones to complex non-linear simulations. The Abaqus/CAE environment is divided into modules where each module defines a logical aspect of the modelling process, such as geometry, material properties, mesh and boundary conditions. The process of solving a general problem using Abaqus involves three stages(SIMULIA, 2011), as follows.

1. The Abaquspreprocessor provides a compatible input file that includes all model data for the solver.

2.The Abaqussolver solves the problem based on an implicit algorithm for static problems or an explicit algorithm for dynamic problems.

3. The Abaqus postprocessor displays the results.

The above process is illustrated in figure 5.1.
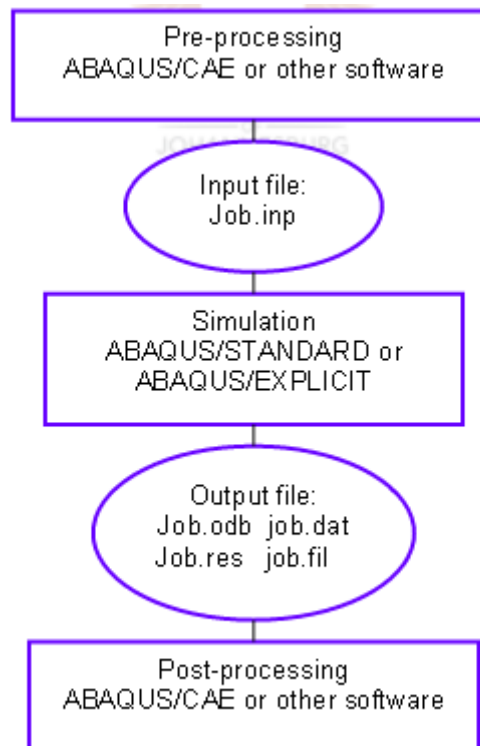
Figure 5.1.The three stages of analysis using Abaqus.

The following section presents the development of the fracture model in Abaqus. The FEA model calculates the mode I Stress Intensity Factor (SIF) at the crack tip.

5.2.1 Geometry of the FEA Model

The problem in this study consists of a cylindrical tube of defined diameter and thickness, a through-wall puncture hole of a given diameter and a longitudinal crack that starts from the edge of the puncture, as shown in figure 5.2.
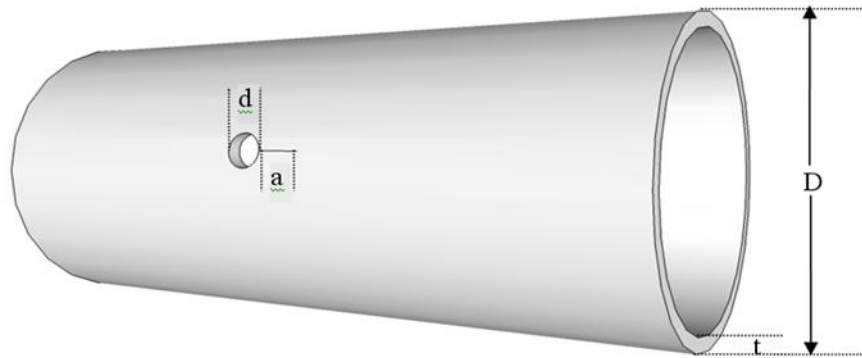
Figure 5.2.Geometry of the problem in this study.

In this study, only half of the pipe is modelled due to the symmetry of the geometry so that the computational runtime is reduced. The model geometry in Abaqus is shown in figure 5.3.
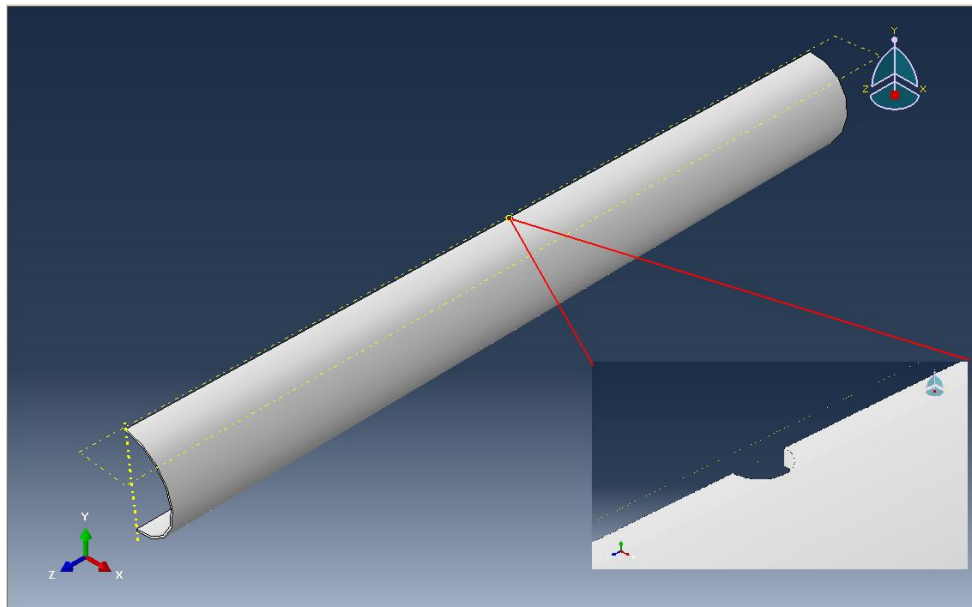
Figure 5.3.Model geometry in Abaqus.

5.2.2 The Mesh of the FEA Model

FEA involves the division of a large structure into a finite numberof subregions.The accuracy and performance of FEA depends heavily on the geometric characteristics of the generated mesh. Hence, the mesh generation is one of the most important

procedures in FEA.A good mesh must be able to preserve the features of the physical model and must be highly adaptable.

Given that stress and strain gradients become large as the crack propagates, the mesh in the vicinity of the crack must be refined to obtain accurate results. Also, the singularity at the crack tip must be satisfied.

A number of elements are supported by Abaqus to model the elastic deformation. The 20-node quadratic brick with reduced integration element (C3D20R) is employed in this study. It provides sufficient accuracy without compromising the computational runtime. The final mesh is shown in figures 5.4 and 5.5. The latter shows the mesh refinement in the vicinity of the crack tip. A coarser mesh was firstly used, and the mesh size was optimised later in the study which will be described in section 5.2.6. The red line in figure 5.5 represents the position of the crack.
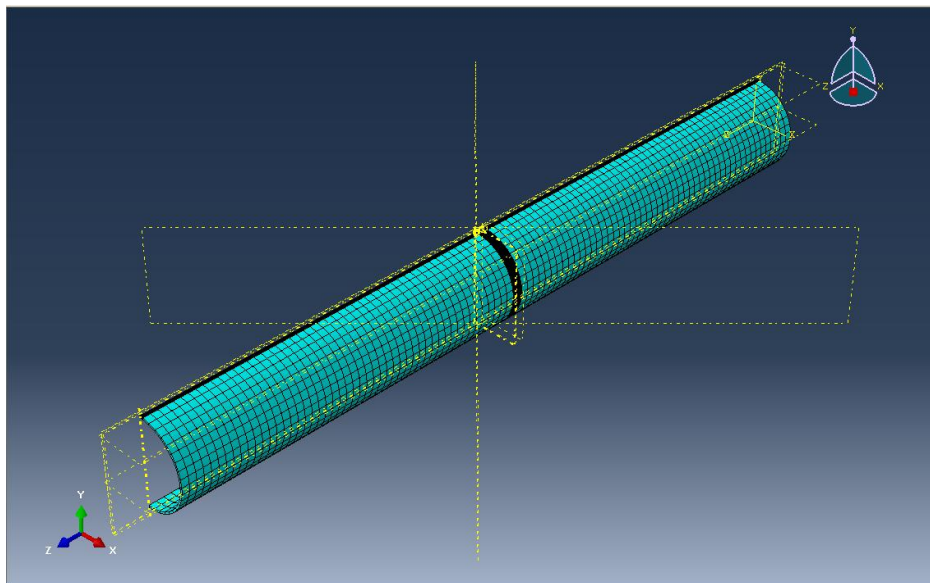
Figure 5.4.The mesh of the completed model.
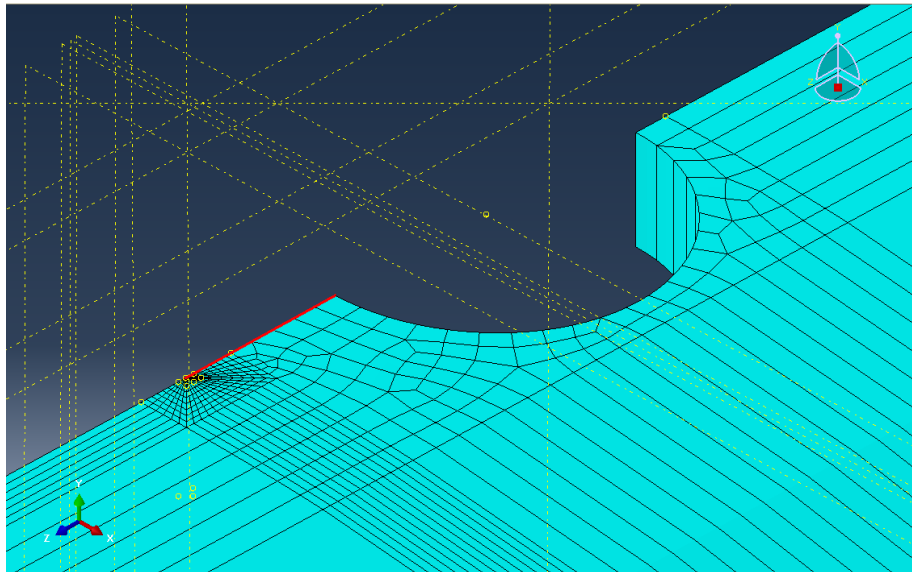
Figure 5.5.The zoom-in representation of the mesh in the vicinity of the crack.

5.2.3 The Boundary Conditions forthe FEA Model

In Abaqus three-dimensional analysis, each node has six degrees of freedom. They are the displacements and rotations in the x-, y-and z-axes, respectively. In this study, two sets of boundary conditionsare defined, as follows.

1. All nodes on the symmetrical plane except for those within the puncture and crack are fixed in x-axis displacement and y-z-axis rotation.
2. All nodes on both ends of the pipehave no degrees of freedom.

Figure 5.6 shows the boundary condition at the puncture and the crack. The red rectanglerepresents the crack face, while the small triangles towards each node represent a fixed displacement.
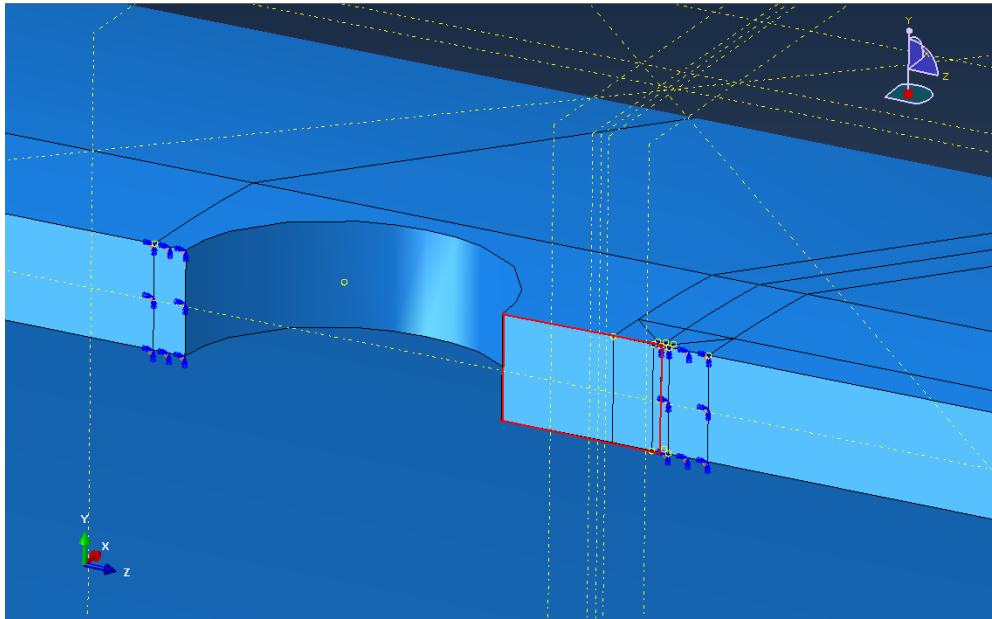
Figure 5.6.Boundary condition at the puncture and crack.

5.2.4 The Loadings of the FEA Model

The multiple reference method used to evaluate the weight function described in the next section requires the geometricSIFsunder two independent loadings. Hence, in the FEA, both uniform and linear loadings are applied to the crack surface as surface traction. Figure 5.7 shows the two independent loading profiles.
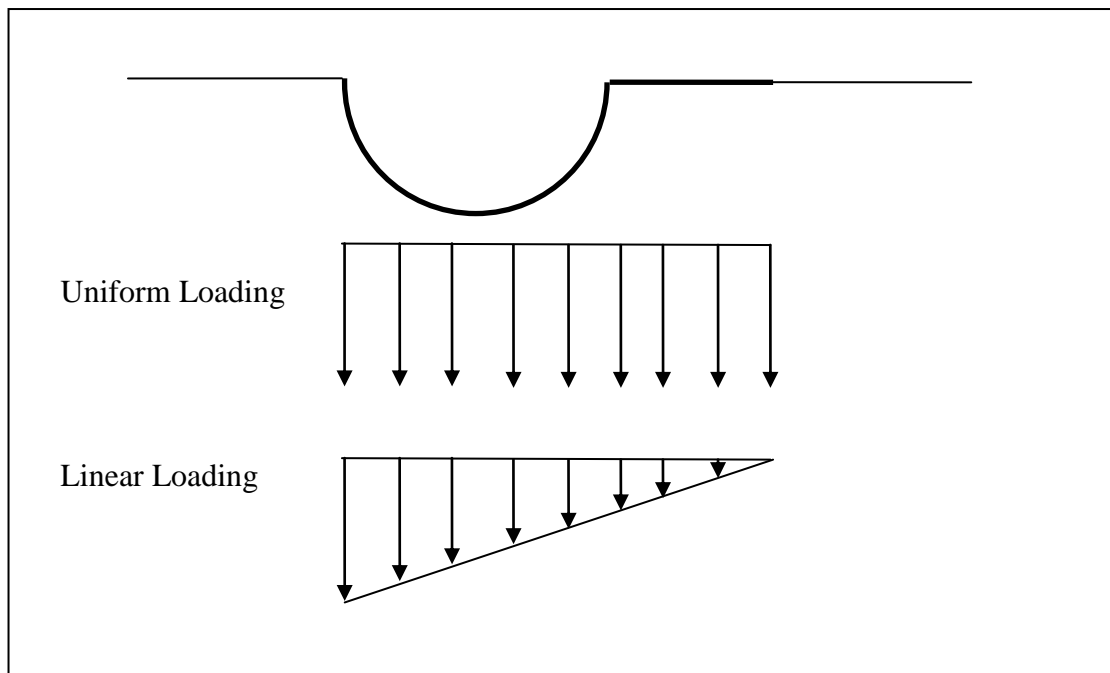
Figure 5.7.Schematic diagram of the two independent surface tractions,with the bold line indicating the crack surface.

5.2.5Evaluation of the Stress Intensity Factor in Abaqus

In this study, the mode I SIF, K_I, is employed as the fracture criterion.Abaqusemploys the interaction integral method by Shih and Asaro (1988)to compute the SIFs directly for a crack under mixed-mode loading. This capability is available for linear isotropic and anisotropic materials. The pertaining theory can be found in detail in the Abaqus Theory Manual 6.10(SIMULIA, 2010).

Figure 5.8 presents the relevant parameter settings for the crack integral method. The crack tip singularity is accomplished by collapsing the element's side witha single node. The integral contour required by this method is indicated by the red line in figure 5.9. The red arrow represents the crack extension direction defined by q vector (0,0,1).
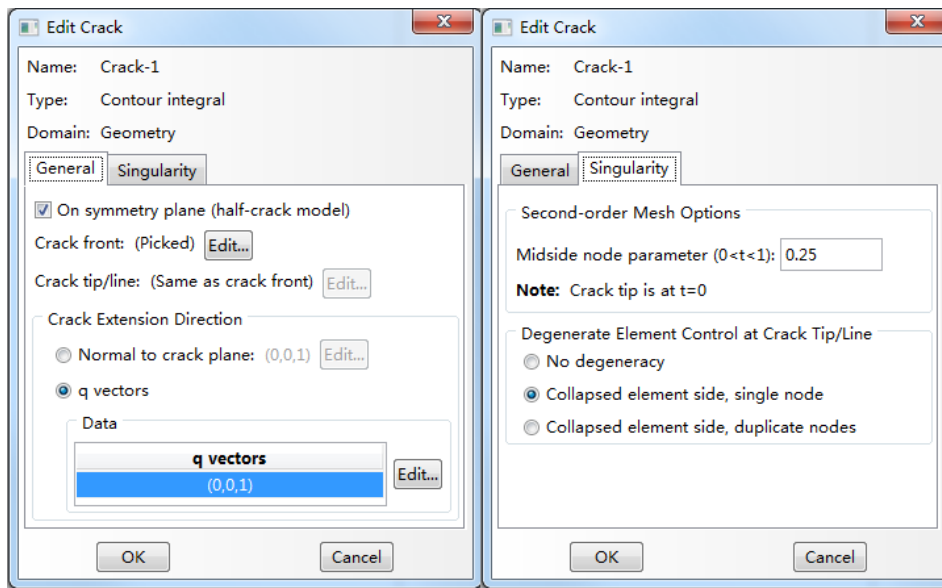
Figure5.8.Crack integral parameters in Abaqus.
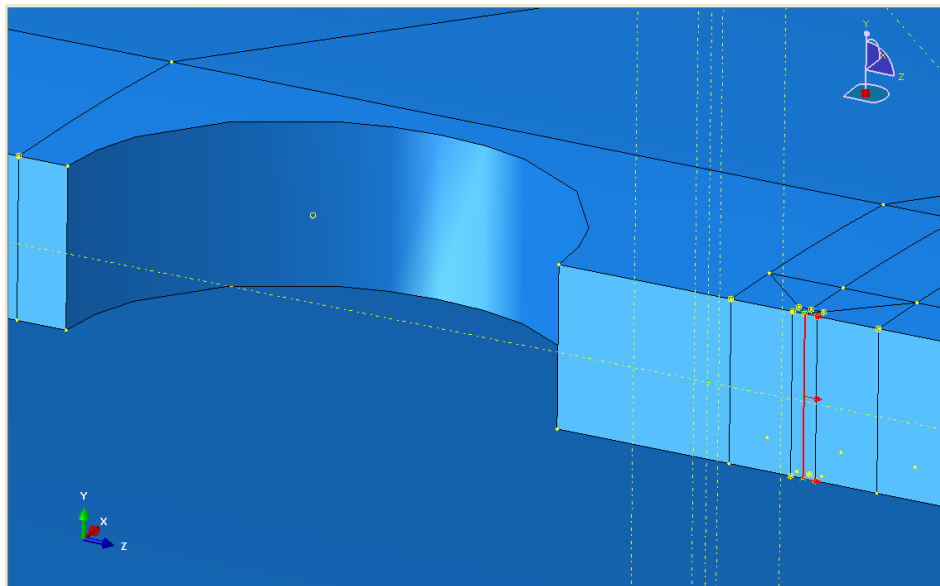
Figure 5.9.Region of contour integral and crack extension direction.

5.2.6 Optimisation of Crack Tip Mesh Size and Validation

As pointed out in the previous section, the accuracy of the FEAdepends on the quality of mesh in the vicinity of the crack tip. Finer mesh normally leads to more accurate results but requires higher computational runtime. As such, it is essential to determine the balance between the crack tip mesh size and the computational runtime without compromising the accuracy. The optimisation of the crack tip mesh size is carried out

by obtaining the FEA resultsfor various crack tip mesh sizes. Figure 5.10 and figure 5.11 show coarse mesh and fine mesh with mesh sizesof 3.3 mm and 0.8 mm,respectively.
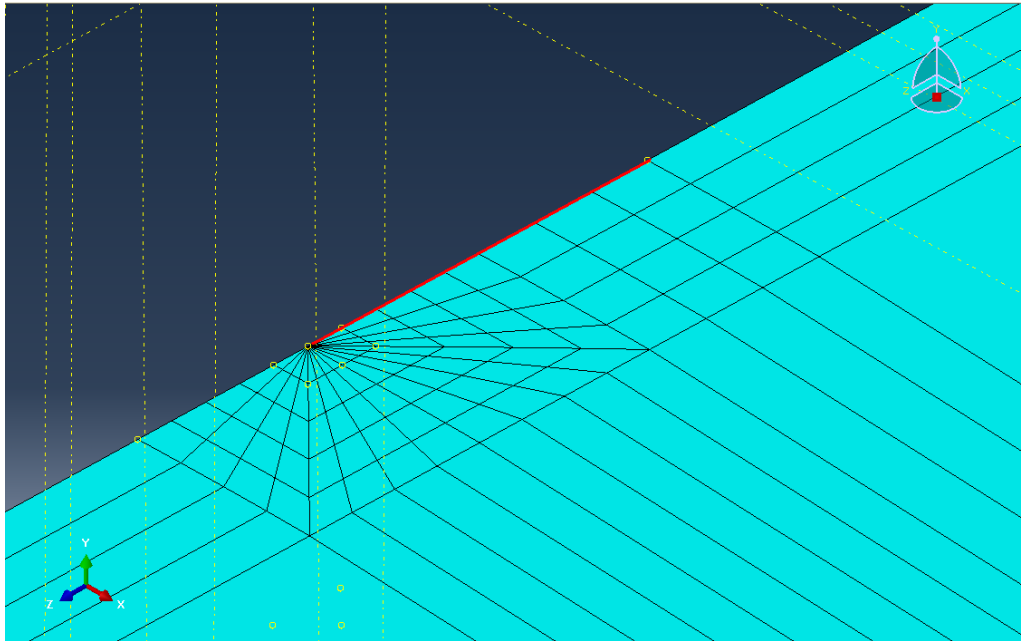
Figure 5.10. Coarse mesh near crack tip; mesh size 3.3 mm.
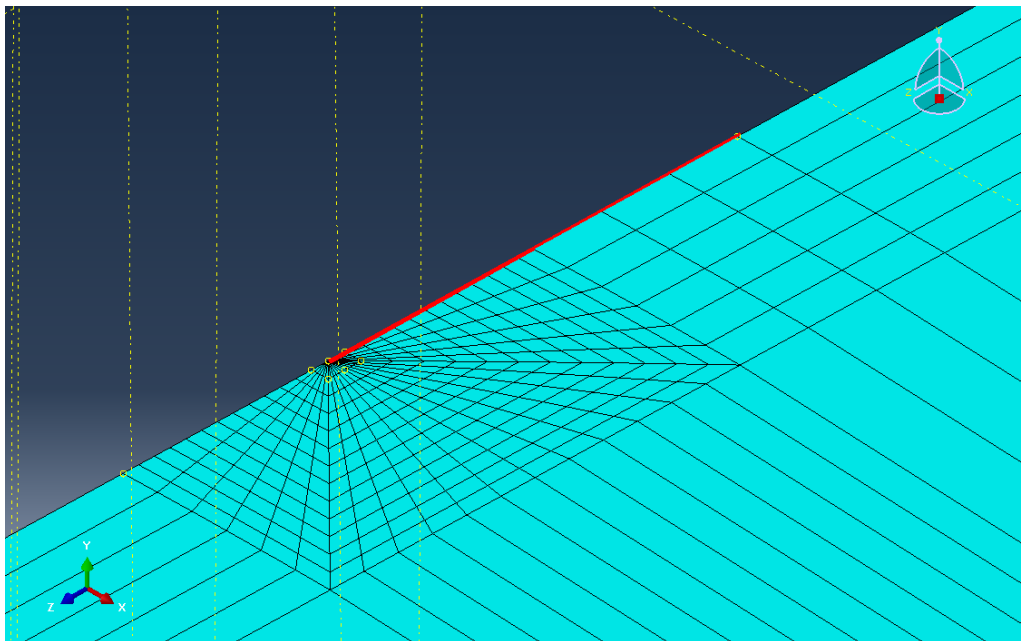
Figure 5.11.Fine mesh near crack tip; mesh size 0.8 mm.

The FEA results foreach mesh size are compared and validated againstavailable analytical results. However, the analytical result for the geometry in this study is not available in the literature.Hence,the optimisation process is carried out on a simplified

geometry: a longitudinal through-wall crack in a cylindrical shell structure, as shown in figure5.12.
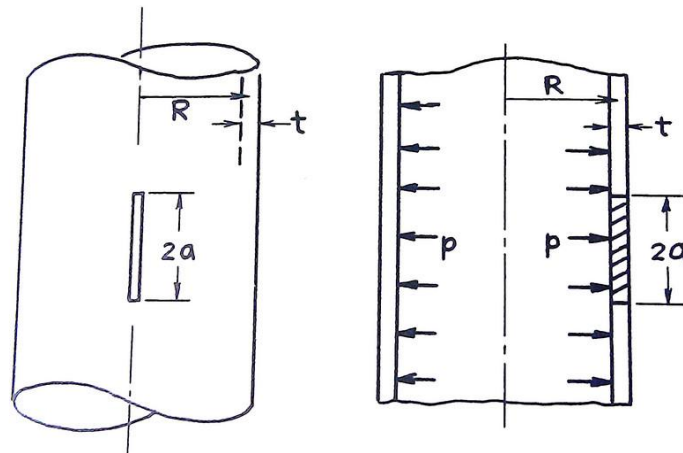
Figure 5.12. Through-wall crack in a cylindrical shell (Tada et al., 2000).

The analytical solution for the mode I SIF, K_I is givenby Tada et al.(2000),as follows.

$$\sigma = p\frac{R}{t}, \tag{5.1}$$

$$\lambda = \frac{a}{\sqrt{Rt}}, \tag{5.2}$$

$$K_I = \sigma\sqrt{\pi a} \cdot F(\lambda), \tag{5.3}$$

$$F(\lambda) = (1 + 1.25\lambda^2)^{1/2} \; 0 < \lambda < 1 \text{ and} \tag{5.4}$$

$$F(\lambda) = 0.6 + 0.9\lambda \; 1 < \lambda < 5$$

where σ, p, a, R, t are the hoop stress, the internal pressure, the half crack length, the pipe radius and thickness respectively. $F(\lambda)$is the shape function.

Figure 5.13 shows the variation of the mode I SIFwith a crack tip mesh size obtained using FEA. The result ofthe analytical solution is shown as the red dot. It can be seen that the result of the FEA converges to the analytical solution when the crack tip mesh size is smaller than 1 mm. Therefore, a crack tip mesh size of 1 mm will be used later in this work.
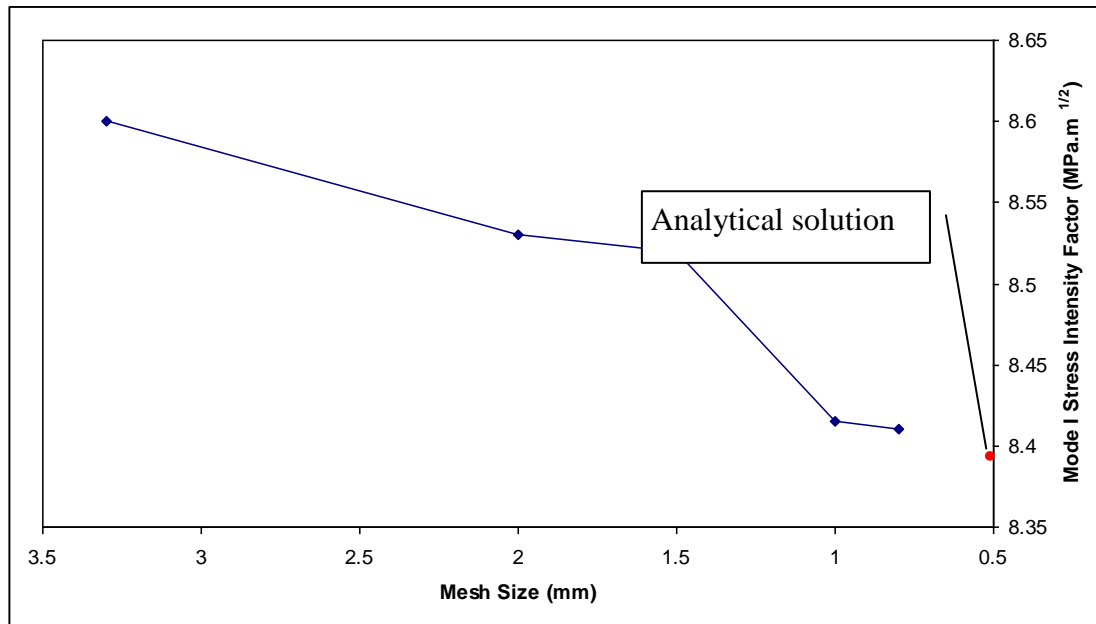
Figure 5.13.The variation of the mode I SIF obtained by FEA with crack tip mesh size.

5.3 Calculation of Stress Intensity Factor Using the Weight Function

The quasi-adiabatic expansion of the escaping fluid will result in the cooling of the pipe wall in the proximity of the puncture. If the temperature at the crack tip falls below the pipeline material Ductile-Brittle-TransitionTemperature (DBTT), depending on the prevailingthermal and pressure stresses, the material may fail in a brittle manner, in which case linear–elastic fracture mechanics become applicable. As such, the mode 1 SIF, $K_I$is used as the fracture parameter(Pook, 2000; Westergaard, 1939).

In the absence of an analytical solution for non-uniform defect geometries considered in this study, the weight function method (Rice, 1972) is used to evaluate K_I at the crack tip.

The weight function at any distance, x, along the crack length,a, is given by

$$h(x,a) = \frac{H}{2K_I} \frac{\partial u_r(x,a)}{\partial a},$$ **(5.5)**

where for plane stress, $H = E$, and for plane strain, $H = \dfrac{E}{1-v^2}$.

E, v and $u_r(x,a)$ are the Young's modulus, Poisson's ratio and crack displacementrespectively.

Using equation (5.5), the SIF, K_I, can be expressed as

$$K_I = \int_{\Gamma_c} \sigma(x)h(x,a)dx \; .$$

(5.6)

where $\sigma(x)$ and Γ_c are the stress distribution along the crack face in the uncracked geometry and the perimeter of the crack respectively.

Following Brennen (1994), the weight function can be expressed in the form of a power series given as

(5.7)

$$h(x,a) = \frac{H}{2K_1(a)} \frac{\partial u(x,a)}{\partial a} = \frac{2\sigma_0}{HK_I(a)} \sqrt{2}\sum_{j=0}^{m} C_j \left(1 - \frac{x}{a}\right)^{j-1/2} {}_{(m \geq 2)} \text{ and}$$

$$C_0 = \frac{F\left(\dfrac{a}{L}\right)}{2} \quad F\left(\frac{a}{L}\right) = \frac{K_r}{\sigma_0 \sqrt{\pi \alpha}} \; ,$$

(5.8)

where$C_j$represents unknown coefficients to be determined, which depend on the defect geometry only. *m* is the number of symmetrical reference loading stresses.

The coefficients C_j can be found using at least two reference SIF solutions with corresponding reference stress loading. Consider a situation where two reference cases are available,

$$C_1 = \frac{q_1 W_{22} - q_2 W_{12}}{W_{11}W_{22} - W_{21}W_{12}} \text{ and}$$

(5.9)

$$C_2 = \frac{q_2 W_{11} - q_1 W_{21}}{W_{11}W_{22} - W_{21}W_{12}} \; ,$$

(5.10)

whereq_i and $W_{ij}$are defined as

$$W_{ij} = \int_0^a \sigma_i(x) \sum_{j=0}^{m} \left(1 - \frac{x}{a}\right)^{j-1/2} dx \qquad \textbf{(5.11)}$$

$$q_i = \frac{F_1\left(\dfrac{a}{L}\right)}{2} \left[K_i(a)\sqrt{\frac{\pi a}{2}} - W_{i0} \right], \qquad \textbf{(5.12)}$$

where $K_i(a)$ is the SIF of the ith loading case.

For a given defect geometry, four parameters need to be calculated in each weight function: C_1, C_2, $F\left(\dfrac{a}{L}\right)$ and $\dfrac{\sigma_0}{K_I(a)}$ in equations (5.9), (5.10), (5.8) and (5.7), respectively. At least two SIF solutions under independent stress loadings are required to calculate the above parameters.The FEA model using Abaqusis employed for this purpose. Here, the pipeline is modelled as a cylindrical tube of defined diameter and thickness, incorporating a puncture of a given geometry on its wall.

As discussed in the previous section, the weight function is geometry-specific. The parameters for a givendefect geometry are unique. In order to calculate the SIF incorporating various possible geometries during crack propagation, a weight function look-up table is required. The look-up table gives the corresponding weight function parameters (C_1, C_2, $F\left(\dfrac{a}{L}\right)$ and $\dfrac{\sigma_0}{K_I(a)}$) for specific pipeline and defect geometries. The variables for the geometries involve the pipeline external diameter, pipe wall thickness, puncture size and crack length extending from its side. The weight function parameters of 720 pipeline and defect geometries are calculated as the grid point source data. The geometry rangesconsidered for a circular puncture with an extended crack are given in Table 5.2.

Pipe diameter(mm)	457.2, 508.5, 609.6
Pipe thickness(mm)	5,6,9,14.7
Puncture diameter(mm)	5,10,15,20,25,30
Initial crack length (mm)	10,20,30,40,50,60,70,80,90,100

Table 5.2. The geometry range employed to generate the weight function parameters look-up table.

Oneexample set of the look-up data is presented in Table 5.3.

Pipeline Diameter (mm)	Thickness (mm)	Puncturediameter (mm)	Crack Length (mm)	C_1	C_2	$F\left(\dfrac{a}{L}\right)$	$\dfrac{\sigma_0}{K_I(a)}$
457.2	5	30	10	7.980124	-5.836161	2.150388	0.991667
457.2	5	30	20	4.507997	-0.919186	2.055615	0.970386
457.2	5	30	30	3.193559	0.752279	1.996277	0.942083
457.2	5	30	40	2.579110	1.642739	1.980636	0.900797
457.2	5	30	50	3.239341	0.622467	1.990033	0.854820
508.5	9	15	10	3.106877	-3.879657	1.268879	2.223214
508.5	9	15	20	1.516639	-1.749679	1.145053	2.203540
508.5	9	15	30	1.227253	-1.330340	1.128538	2.040984
508.5	9	15	40	1.244369	-1.319041	1.139029	1.872180
508.5	9	15	50	1.400757	-1.427928	1.177618	1.693878
609.6	14.7	5	10	-0.123449	-0.023861	0.796528	5.008588
609.6	14.7	5	20	-0.219228	0.063413	0.756610	4.305254
609.6	14.7	5	30	-0.224631	0.061363	0.750045	3.761096
609.6	14.7	5	40	-0.161101	-0.024407	0.761888	3.311734

Table 5.3. The weight function parameters look-up tableexample.

In order to interpolate the data between the grid points in the look-up table, the MatlabCurve Fitting Toolbox is employed.The toolboxis a collection of highly useful graphical user interfaces and functions for curve and surface fitting. The process of curve fitting involves the use of interpolation in which an exact fit of data is needed for smoothing (Guest,1961). Fitted curves and surfaces are employed in this study as aidsto calculate the weight function parameters between the grid data points. In this process, the fitted surfaces are used to effectively infer values of a given function in cases where there is no available data.

In this study, four parameters:C_1, C_2, $F\left(\dfrac{a}{L}\right)$ and $\dfrac{\sigma_0}{K_I(a)}$ were fitted against the puncture diameter and crack length. Figures5.14 tofigure 5.17 show one example of the fitting results for a specific pipeline diameter (609.6 mm) and thickness (14.7 mm). The fitted polynomial and the corresponding parameters aregiven in Table 5.4.

$$
\begin{aligned}
f(x, y) = {} & p_{00} + p_{10} * x + p_{01} * y + p_{20} * x^2 + p_{11} * x * y + p_{02} * y^2 + p_{30} * x^3 \\
& + p_{21} * x^2 * y + p_{12} * x * y^2 + p_{03} * y^2 + p_{40} * x^4 + p_{31} * x^3 * y \\
& + p_{22} * x^2 * y^2 + p_{13} * x * y^3 + p_{04} * y^4 + p_{50} * x^5 + p_{41} * x^4 * y \\
& + p_{32} * x^3 * y^2 + p_{23} * x^2 * y^3 + p_{14} * x * y^4 + p_{05} * y^5
\end{aligned}
$$

	C_1	C_2	$F\left(\dfrac{a}{L}\right)$	$\dfrac{\sigma_0}{K_I(a)}$
p_{00}	-0.3124	0.1519	0.7421	7.35
p_{10}	204.3	-253	38.89	-525.2
p_{01}	-71.77	97.69	-11.49	-81.38
p_{20}	5374	-8225	-401.8	1.59E+04
p_{11}	-1.59E+04	2.09E+04	-1633	1.45E+04
p_{02}	5321	-7361	579.9	-1032
p_{30}	-2.66E+04	4.81E+04	4481	-1.68E+05
p_{21}	-1.75E+05	3.30E+05	3.45E+04	-5.02E+05

p_{12}	4.26E+05	-5.83E+05	2.76E+04	-1.33E+05
p_{03}	-1.33E+05	1.86E+05	-1.09E+04	3.41E+04
p_{31}	3.65E+06	-5.09E+06	-1.08E+04	4.59E+06
p_{22}	1.04E+05	-1.92E+06	-6.48E+05	5.07E+06
p_{13}	-4.24E+06	6.16E+06	-1.41E+05	1.61E+05
p_{04}	1.38E+06	-1.95E+06	9.11E+04	-2.88E+05
p_{32}	-2.54E+07	3.89E+07	2.25E+04	-2.95E+07
p_{23}	8.98E+06	-3.49E+06	3.71E+06	-1.63E+07
p_{14}	1.42E+07	-2.21E+07	-7.96E+04	2.17E+06
p_{05}	-5.01E+06	7.22E+06	-2.61E+05	7.68E+05
R-Square	0.9980	0.9975	0.999	0.9994

Table 5.4. The parameters of the fitted polynomial.
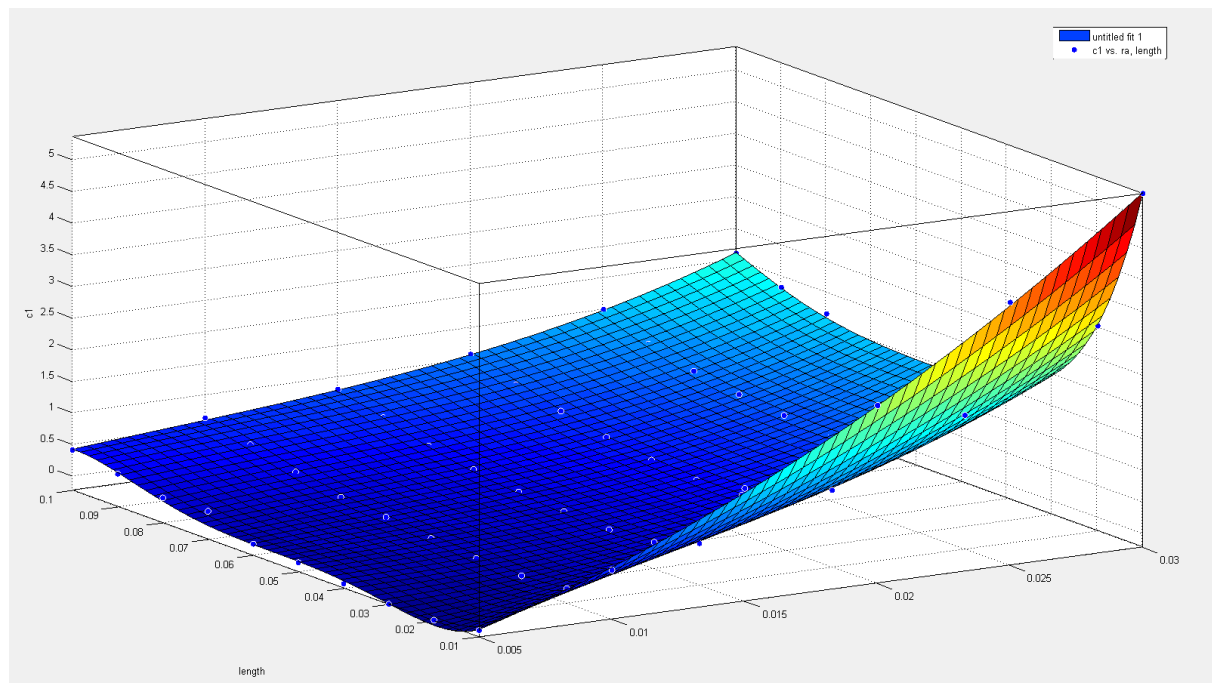
Figure 5.14. Graphic presentation of the fitted curved for weight function parameter C1 (R-square = 0.998).
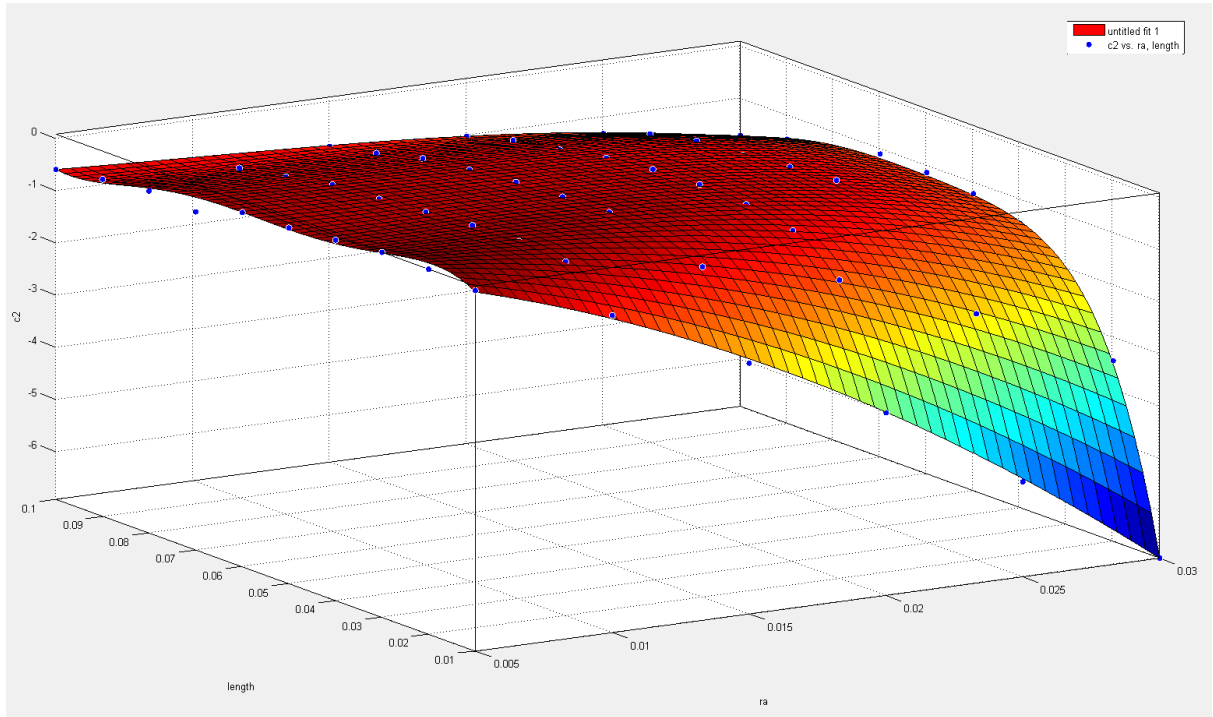
Figure 5.15. Graphic presentation of the fitted curved for weight function parameter C2 (R-square = 0.997).
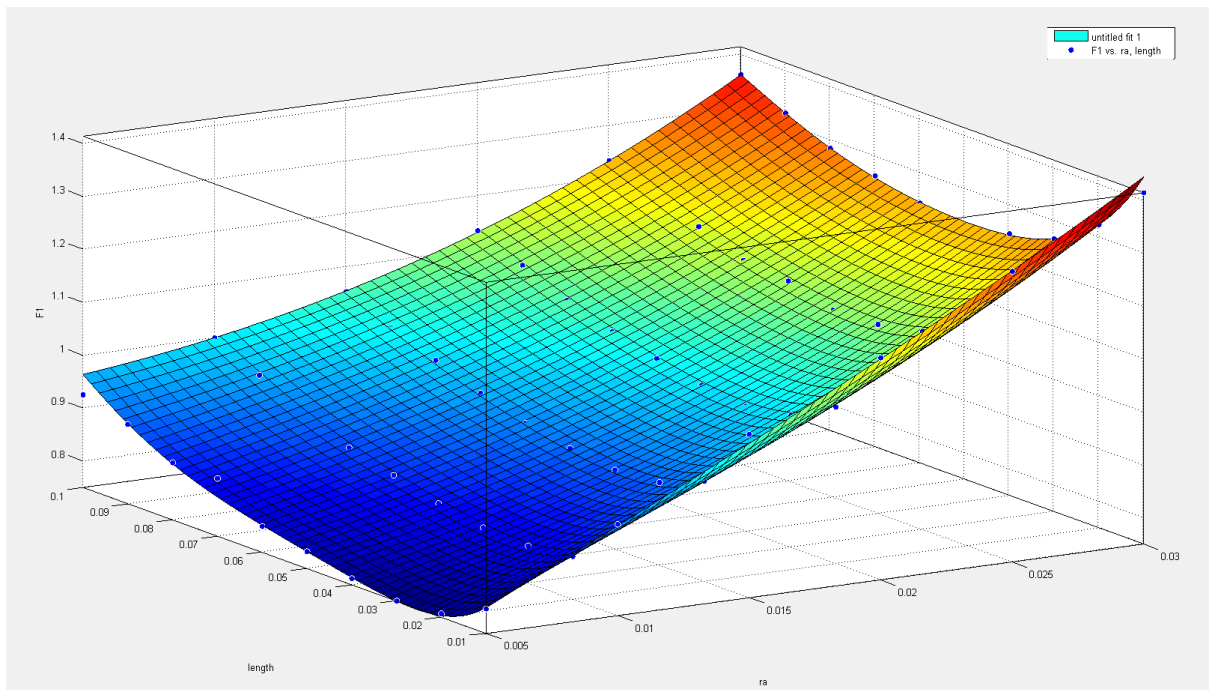
Figure 5.16. Graphic presentation of the fitted curved for weight function parameter $F\left(\dfrac{a}{L}\right)$ **(R-square = 0.999).**
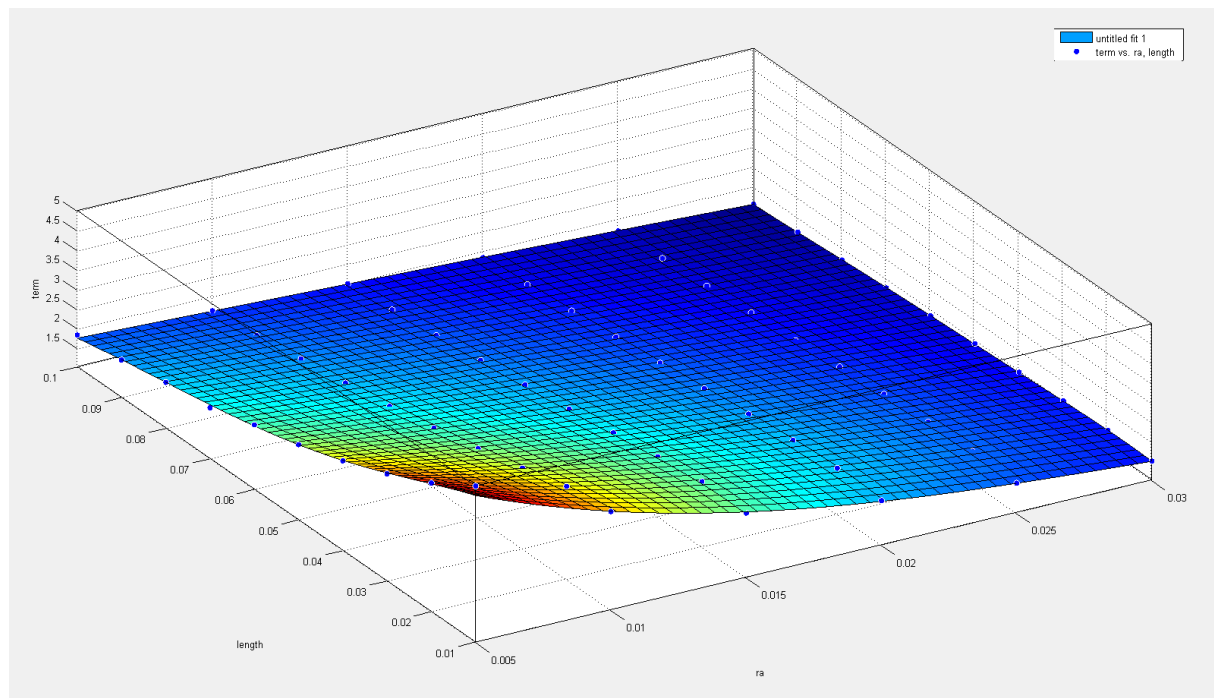
Figure 5.17. Graphic presentation of the fitted curved for weight function parameter $\dfrac{\sigma_0}{K_I(a)}$ (R-square = 0.999).

The fitted weight functions are validated against the result of the Abaqus FEA. Table 5.5 shows a comparison of the results. The maximum difference between the SIF calculated using the fitted weight function and the Abaqus FEA is less than 4%. Hence, the fitted weight function can be employed to couple with the CFD and heat transfer models.

Puncture Radius (mm)	Crack Length (mm)	Abaqus SIF (MPa m$^{0.5}$)	WF SIF (MPa m$^{0.5}$)	% Difference between WF and Abaqus
35	50	1.72E+06	1.67E+06	-3.10
35	100	2.19E+06	2.14E+06	-2.32
2	45	1.04E+06	1.04E+06	-0.25

Table 5.5. Comparison of the Stress Intensity Factor obtained using the Abaqus FEA and the fitted weight function method (WF).

5.4. Integration of the Fluid Dynamics, Heat Transfer and Fracture Mechanics

The fluid dynamics, pipe wall heat transfer and crack tip fracture mechanics sub-modules are coupled together to perform low-temperature-inducedbrittle fracture analysis. For a given geometry, the weight function parameters are firstly calculated using Abaqus. The parameters database is then fitted into polynomial equations described in the previous section. The polynomial equations are then put into the combined CFD (described in Chapter 3) - heat transfer (as in Chapter 4) code to carry out the simulation. Figure 5.18 shows the corresponding calculation algorithm for determining the defect length while accounting for the pertinent fluid dynamics, heat transferand fracture mechanics.

Initial values (T, P, fluid composition, pipeline dimensions, puncture size, geometry and location, etc.)

Use the CFD model to determine fluid properties within and exiting the pipe

Obtain the temperature profile around the puncture using the heat transfer model

Temperature at crack tip below DBTT?

Yes

Calculate crack tip SIF, K_I

No

$K_I > K_{IC}$ at below DBTT

No

Crack does not propagate

Yes

Crack propagates into warmer metal and arrests when $K_{IC} \geq K_I$

$K_I > K_{IC}$ at above DBTT

No

Crack does not propagate

Yes

Unstable crack propagation. END.

Figure 5.18. Crack propagation calculation flow algorithm.

5.5 Summary

In this chapter, the development of a fracture model for simulating thebrittle fractureof pressurised pipelines was presented. This model combines the FEA and the weight function methods,accounting for real pipe/puncture geometries.The integration of the CFD, heat transfer and fracture model isalso presented. The coupled model is usedfor the analysis presented in the next chapter.

CHAPTER 6: APPLICATION OF THE LOW TEMPERATURE-INDUCED BRITTLE FRACTURE PROPAGATION MODEL — CASE STUDIES

6.1 Introduction

This chapter presents and discusses the simulation results obtained using the integrated brittle fracture model based on the coupling of the heat transfer, the Computational Fluid Dynamics (CFD) and the fracture mechanics models presented in chapters 3, 4 and 5 for a series of hypothetical test cases involving the pipeline transportation of pure CO_2 and its various mixtures.

The pipeline is assumed 10-km long, 609.6-mm OD, transporting gas or dense phase CO_2. A 10-km long pipeline is implied to reduce the computational runtimes to practical levels. The fracture toughness measurements above and below the Ductile-Brittle-Transition Temperature (DBTT) are taken as 95 MPa $m^{0.5}$ and 40 MPa $m^{0.5}$ respectively. These values are assumed constant at any temperature diverging from the DBTT.

The two pipeline scenarios considered are as follows:

1) exposed pipeline which lies above ground
2) buried pipeline

As part of the analysis, the pipe wall thickness, DBTT and defect shape are varied in order to investigate their impact on the fracture propagation behaviour. The examined flow conditions included isolated (i.e., no flow within the pipeline upon failure) and unisolated flows.

Unless otherwise stated, the initial defect shape is assumed to be a 20-m dia. circular puncture with a 20-mm hairline fracture extending from one side parallel to the main axis of the pipeline. The inventory is assumed to be pure CO_2. Table 6.1 presents the prevailing conditions for the simulation tests conducted.

Inventory	100% CO_2
Feed pressure (bara)	34 (gas phase), 150 (dense phase)
Ambient and feed temperature (K)	283.15
Overall pipeline length (km)	10
Pipeline thickness (mm)	5, 6, 9, 14.7
Pipeline external diameter (mm)	609.6
Failure mode	puncture
Puncture diameter (mm)	20
Equation of state	Modified Peng Robinson
Pipe material	British Gas LX/1
Pipe roughness (mm)	0.05
Pipe wall thermal conductivity (W/(m K))	53.65
Pipe wall heat capacity (J/(kg K))	434
Feed flow rate (m/s)	0, 0.2 m/s
DBTT (°C)	0, −10
K_{Ic}(MPa m$^{0.5}$)	95 (ductile), 40 (brittle)

Table 6.1 Pipeline Characteristics and prevailing condition for the test cases

6.2 Crack Propagation in Exposed Pipelines

Two types of simulations have been conducted for the exposed pipeline. These include 1) pipeline transporting gas and 2) dense phase CO_2. CO_2 is considered in the dense phase when it is transported above its critical pressure (73.8 bara) and below its critical temperature (31.1 °C). To satisfy the 50% Specified Minimum Yield Strength (SMYS) requirement for the operating pressures (see table 6.1), the respective pipe wall thicknesses for each case are

taken as 6 mm and 14.7 mm respectively. The pipeline material is assumed to comply with British Gas LX/1 specification corresponding to a DBTT of 0 ℃. In both cases, the pipeline is assumed to be isolated upon failure corresponding to zero feed flow.

Figure 6.1 shows the transient axial pipe temperature profiles at different time intervals in the proximity of the puncture plane for gas phase CO_2 at 10 ℃. It is clear that the rapid expansion of the escaping inventory results in significant cooling of the pipe wall with the effect becoming more pronounced with time and distance towards the puncture plane. According to the data, the pipe wall temperature reaches the DBTT of 0 ℃ some 60 s following the puncture, dropping to a minimum temperature of −23 ℃.

Figure 6.2 shows the corresponding variation of the crack length against time following the puncture. As it may be observed, crack growth occurs when the temperature at any point at the defect/pipeline boundary drops below the DBTT and $K_c > K_{mat}$. At ca. 1,000 s following puncture, the crack reaches the critical length that the pipe wall toughness can withstand, thus becoming unstable leading to catastrophic pipeline failure.
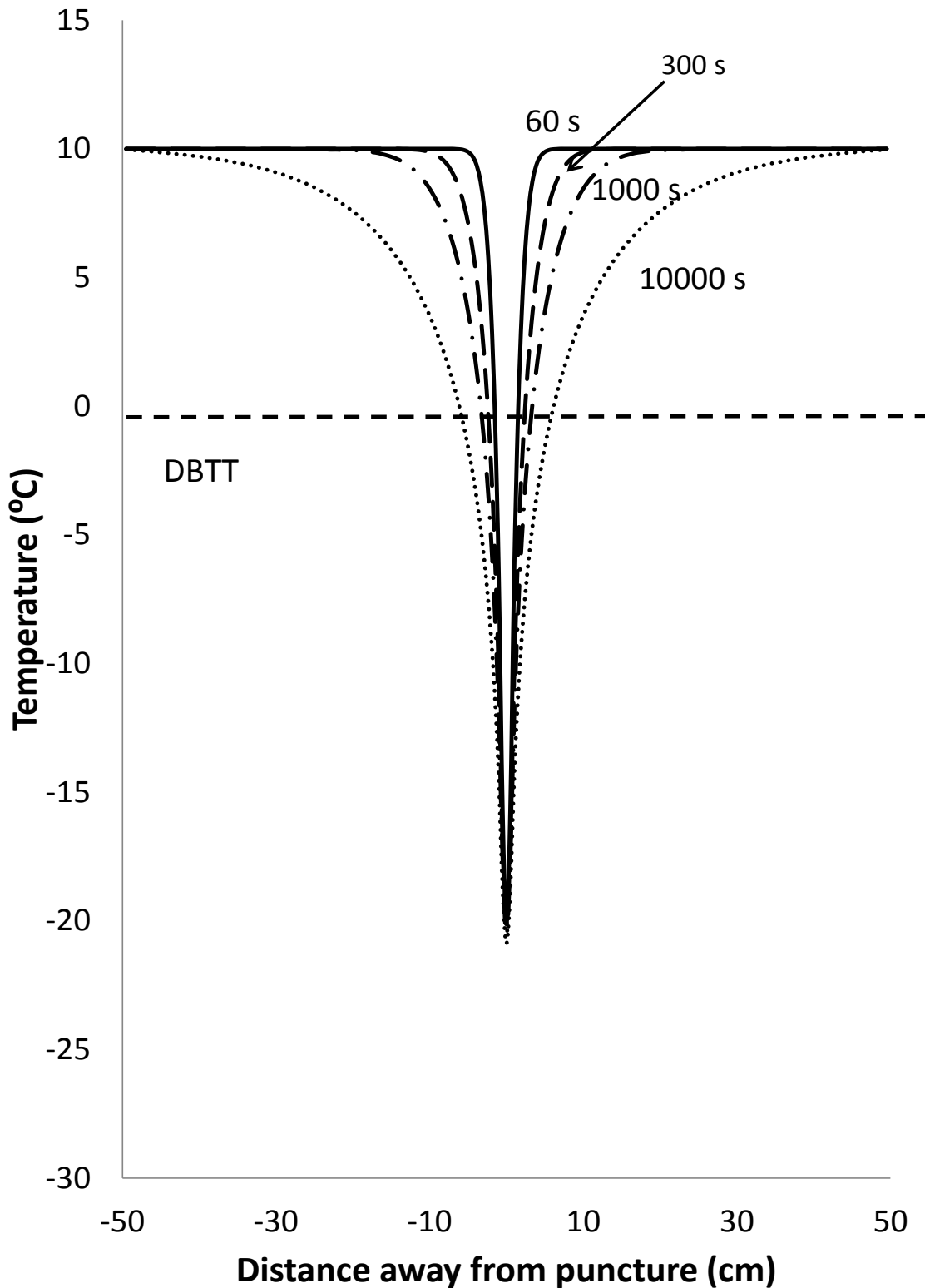
Figure 6.1. The variation of the pipe wall temperature in the proximity of the puncture with time for gas phase CO$_2$ (34 bara, 10 ℃; exposed pipeline)
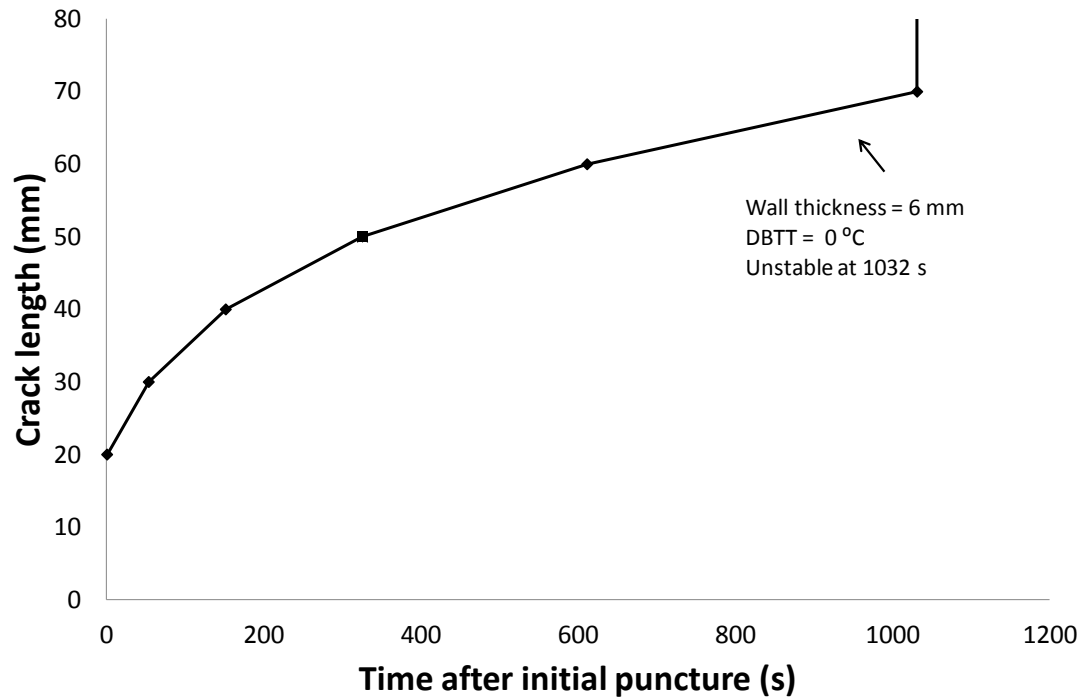
Figure 6.2. Variation of the crack length against time following the puncture of the gas phase CO$_2$ pipeline (34 bara, 10 ℃; exposed pipeline)

Figures 6.3 and 6.4 respectively show the same data as in figures 6.1 and 6.2, but this time for a pipeline containing dense phase CO$_2$ at 150 bara. It is clear from figure 6.3 that the minimum temperature only reaches −2 ℃ (c.f. −23 ℃ for gas phase CO$_2$). The initial crack tip temperature 20mm away from the puncture always stays above the DBTT. Hence, for the conditions tested, crack propagation will not occur in the exposed pipeline containing dense phase CO$_2$.
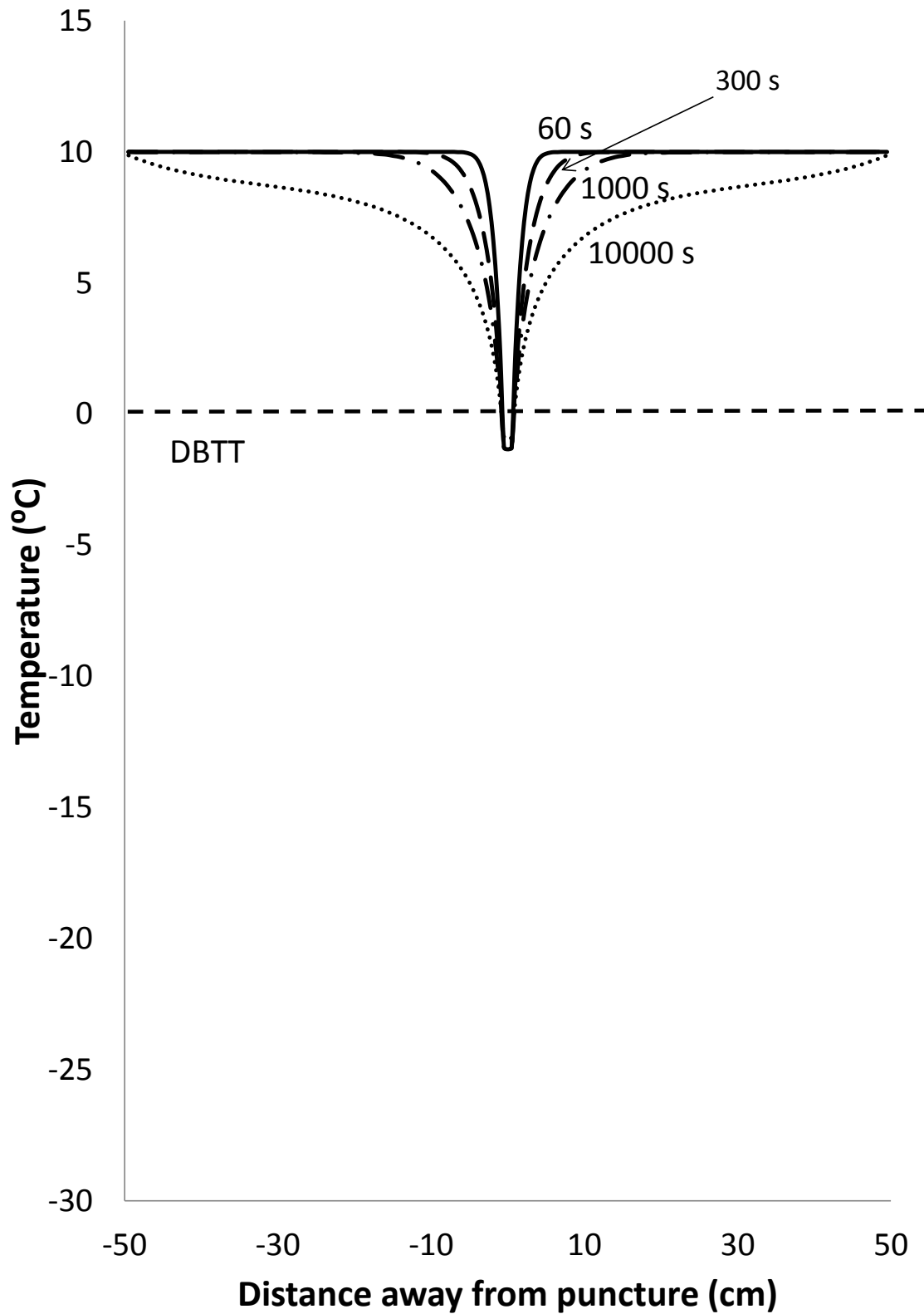
Figure 6.3. The variation of the pipe wall temperature in the proximity of the puncture with time for gas phase CO₂ (150 bara, 10 ℃, exposed pipeline)
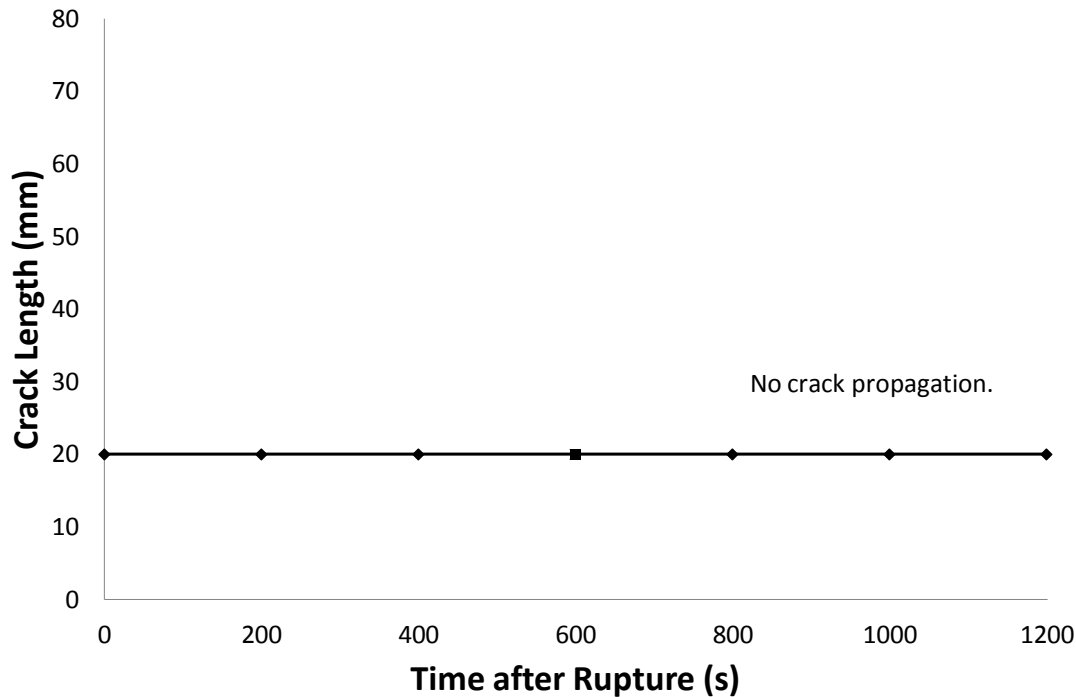
Figure 6.4. Variation of the crack length against time following the puncture of the dense phase CO_2 pipeline (150 bara, 10 ℃, exposed pipeline).

6.3 Crack Propagation in Buried Pipelines

In the simulation presented in this section, all of the pipe properties remain the same as those in table 6.1 with the exception that the pipeline is assumed to be buried. The backfill soil is assumed to be sand with thermal conductivity and mean particle size of 0.95 W/mK and 1.35 mm respectively. Furthermore, it is assumed that there is no blowout of the soil following the initial puncture due to its small diameter. The simulation results for two tests are presented, including gas and dense phase CO_2 inventories.

Figure 6.5 shows the transient pipe wall temperature in the proximity of the puncture at different time intervals up to 10,000 s following puncture for the pipeline transporting gas phase CO_2 at 34 bar and 10 °C. Figure 6.6 shows the same data as in figure 6.5 but for the dense phase CO_2 at 150 bar and 10 ℃. In both cases, the pipeline is assumed to be isolated upon failure corresponding to zero feed flow.

Returning to figure 6.5 for gas phase CO_2, the following observations can be made:

i)   the minimum pipe wall temperature at the puncture location remains at $-20\ ^{\circ}C$ for at least the duration of the release period of 10, 000 s under consideration.

ii)   In the first 1,000 s following puncture, the minimum pipe wall temperature corresponds to the release location. Also, the pipe wall temperature away from the puncture plane decreases with the passage of time.

iii)   At around 5,000 s, a switchover takes place where the pipe wall temperature away from the puncture plane drops further than that at the puncture plane, falling to a minimum temperature of $-55\ ^{\circ}C$ at ca 1,000 s. This switchover is due to the eventual secondary cooling of the pipe wall by the surrounding soil in turn cooled by the low temperature (ca. -70 $^{\circ}C$) escaping CO_2.

Similar trends in the data may be observed for dense phase CO_2 with the exception that the minimum rupture plane temperature before the switch over takes place is -2 $^{\circ}C$ (c.f -20 $^{\circ}C$ for gas phase; see figure 6.5). On the other hand the minimum temperature away from the puncture plane at 10,000 s following puncture is ca $-42\ ^{\circ}C$ (c.f $-55\ ^{\circ}C$ for gas phase CO_2: see figure 6.5).
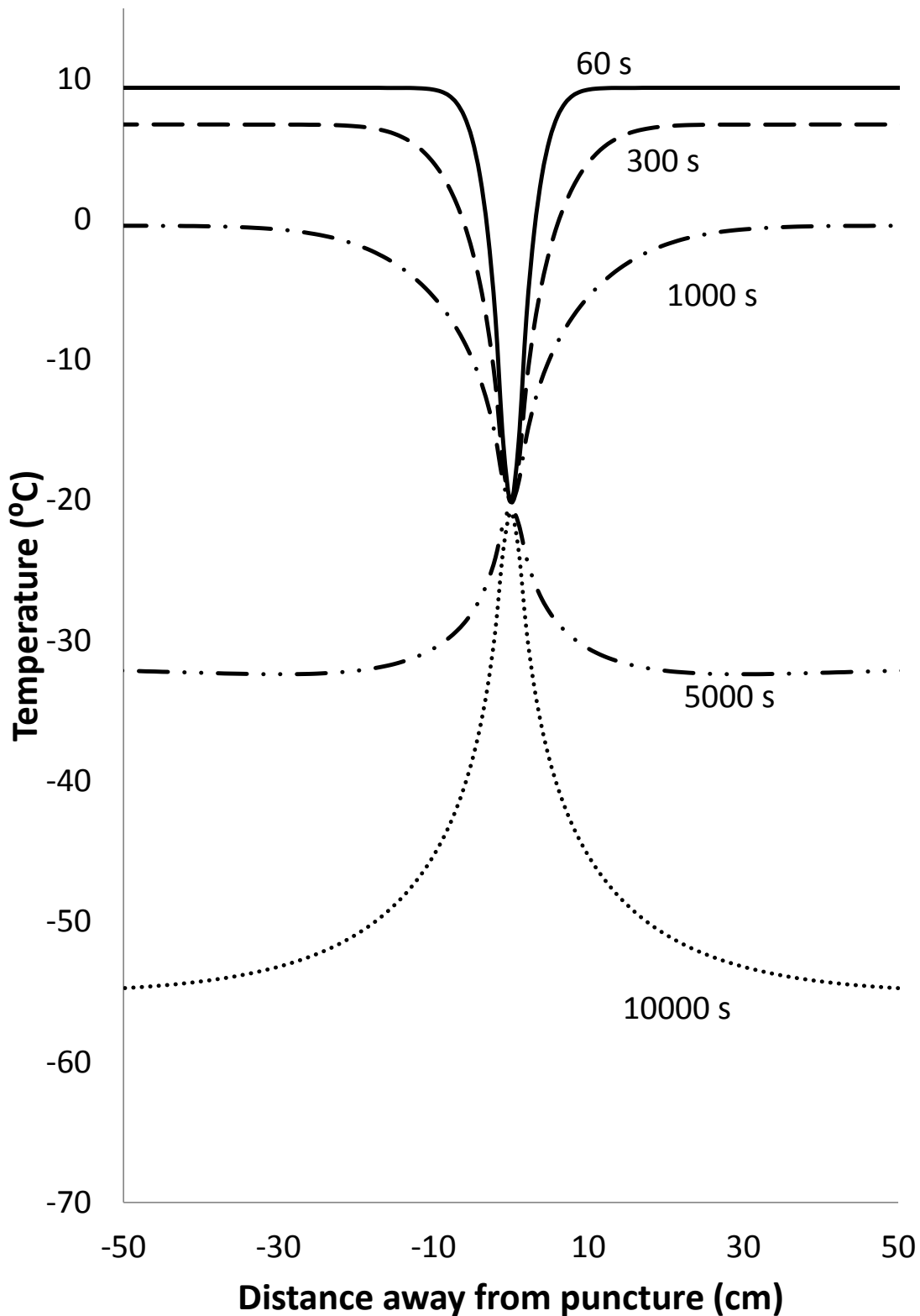
**Figure 6.5. The variation of the pipe wall temperature in the proximity of the puncture with time for the gas phase CO$_2$ pipeline (34 bara, 10 °C; buried pipeline, no soil blow out)**
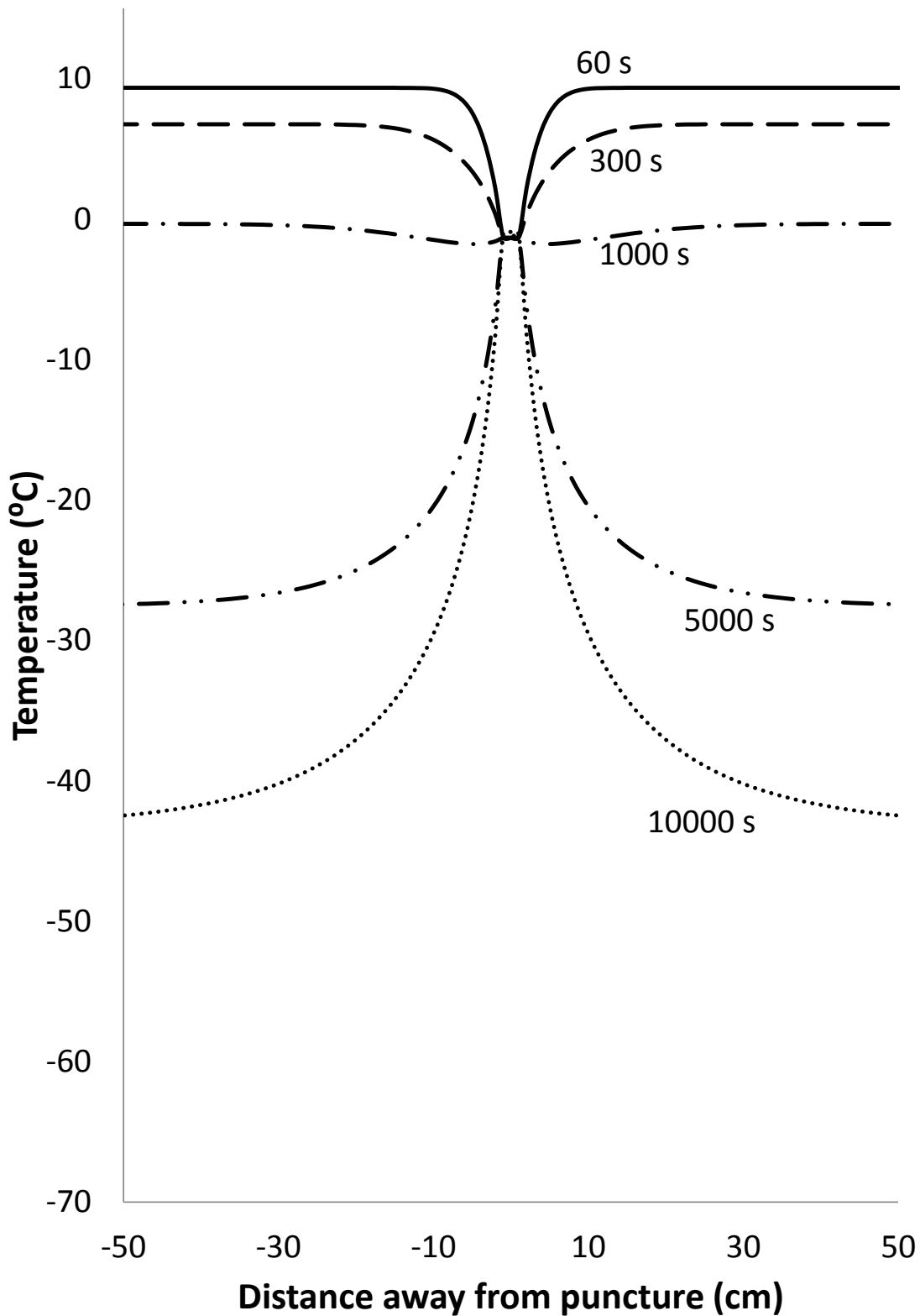
Figure 6.6. The variation of the pipe wall temperature in the proximity of the puncture with time for the dense phase CO_2 pipeline (150 bara; 10 $°C$, buried pipeline, no soil blow out)

Figure 6.7 shows the corresponding variation of the crack length against time following the puncture of the buried pipeline transporting gas and dense phase CO_2. As it may be observed, for the gas phase buried pipeline, it only takes 360 s following the initial puncture for the crack to become unstable. This compares to ca. 1,000 s for the exposed pipeline (see figure 6.2). The considerably shorter time span to reach unstable crack in the former case is due to the secondary cooling of the pipe wall by the surrounding soil exposed to the escaping low temperature CO_2. The same process is also responsible for promoting crack propagation in the dense phase CO_2 pipeline, where the crack starts to propagate ca.774 s following puncture. As it may be recalled, no crack propagation was observed in the case of the exposed pipeline transporting dense phase CO_2 (see figure 6.4).
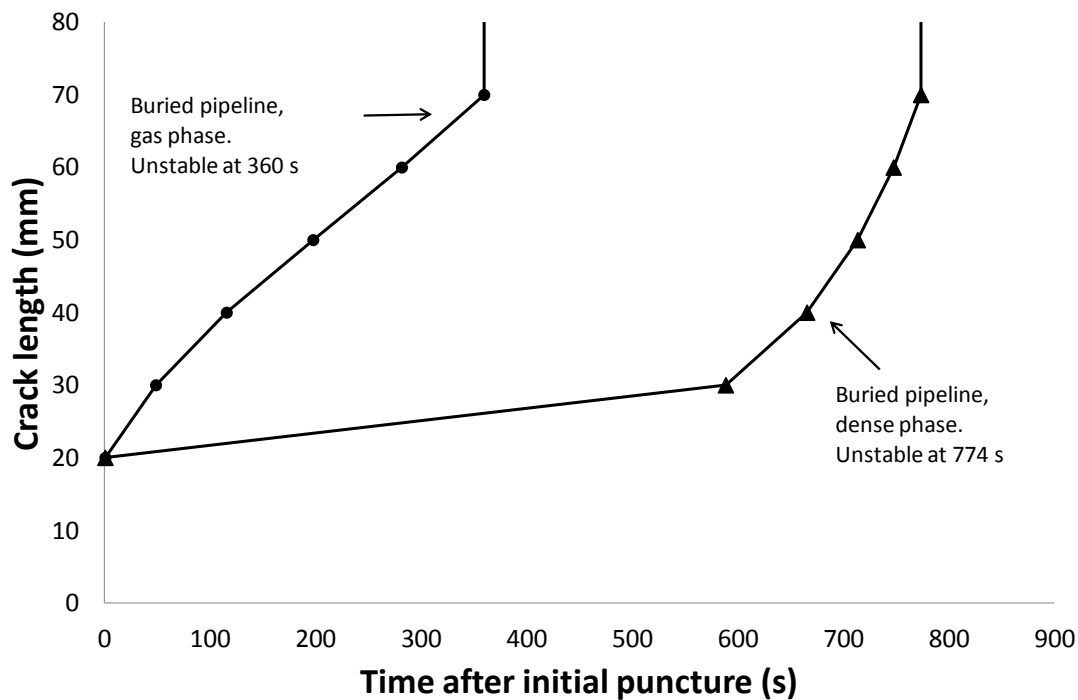
Figure 6.7. Variation of the crack length against time following the puncture for pipeline transporting gas and dense phase CO_2 (34 bara and 150 bara; 10 ℃, buried pipeline, no soil blow out).

6.4 Sensitivity Analysis

6.4.1 Impact of Pipe Wall Thickness

Figure 6.8 shows the impact of the pipe wall thicknesses (5, 6 and 9 mm) on the crack propagation behaviour against time for the exposed gas phase CO_2 pipeline. The results for

the 6-mm wall thickness are the same as in figure 6.2, where the crack becomes unstable at ca. 1,000 s following puncture. When the pipe wall thickness was reduced from 6 to 5 mm, the critical crack length after which the crack became unstable decreased from 70 mm to 50 mm, corresponding to 326 s following puncture.

Increasing the pipe wall thickness to 9 mm on the other hand results in no crack propagation despite the fact that crack tip temperature drops below the DBTT (see figure 6.1). For the same operating condition, increasing the pipe wall thickness results in a reduction in the hoop stress, and thus the crack driving force. In this case, K_I does not exceed the K_{IC}, hence there is no crack growth.
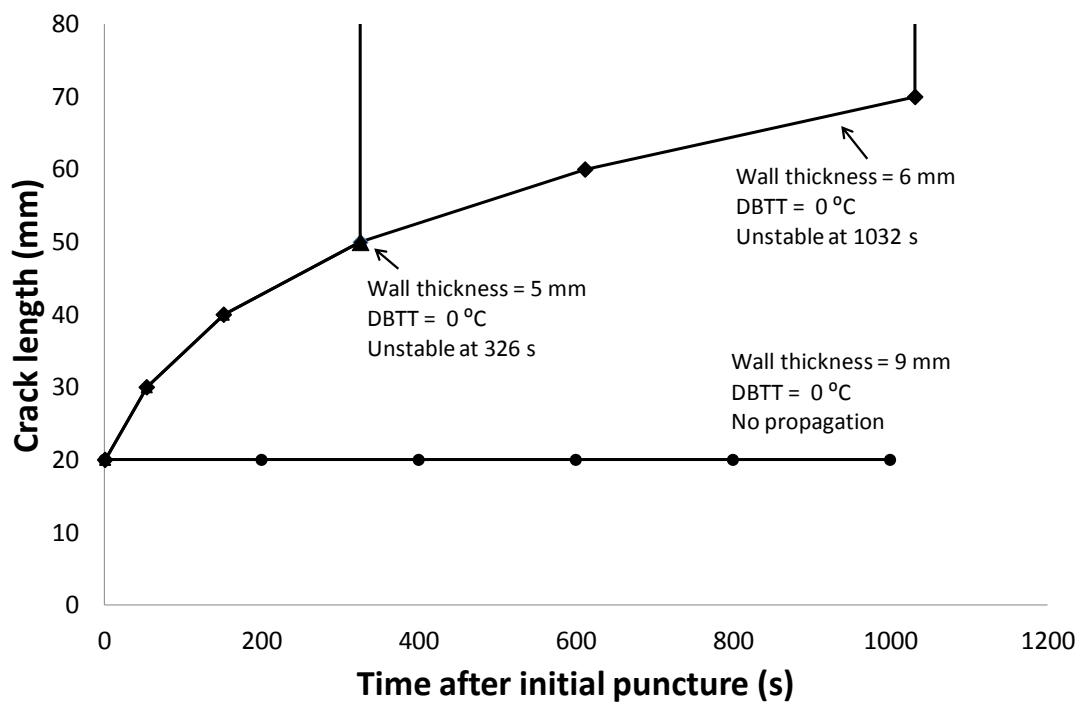
Figure 6.8. Comparison of the variation of the crack length against time after puncture with various pipe wall thicknesses; exposed pipeline, gas phase CO₂

6.4.2 Impact of Ductile-Brittle-Transition Temperature

Figure 6.9 shows the effect of varying the DBTT of the pipe material on the crack propagation behaviour following puncture for the gas phase CO_2 pipeline (see table 6.1). As it may be observed, when the DBTT is 0 °C, it takes 326 s and 1036 s for the cracks to reach

the critical condition for the 5 mm and 6 mm pipe wall thicknesses respectively. However, reducing the pipe wall material DBTT to -10 ℃ has a dramatic impact on the fracture propagation behaviour. For both pipe wall thicknesses, the initial crack grows by only 10 mm, arresting ca. 2,900 s after the initial puncture. Noting that modern pipelines normally have a DBTT of -70 ℃, it is very unlikely that the brittle fracture will occur in a gas phase exposed CO_2 pipeline.
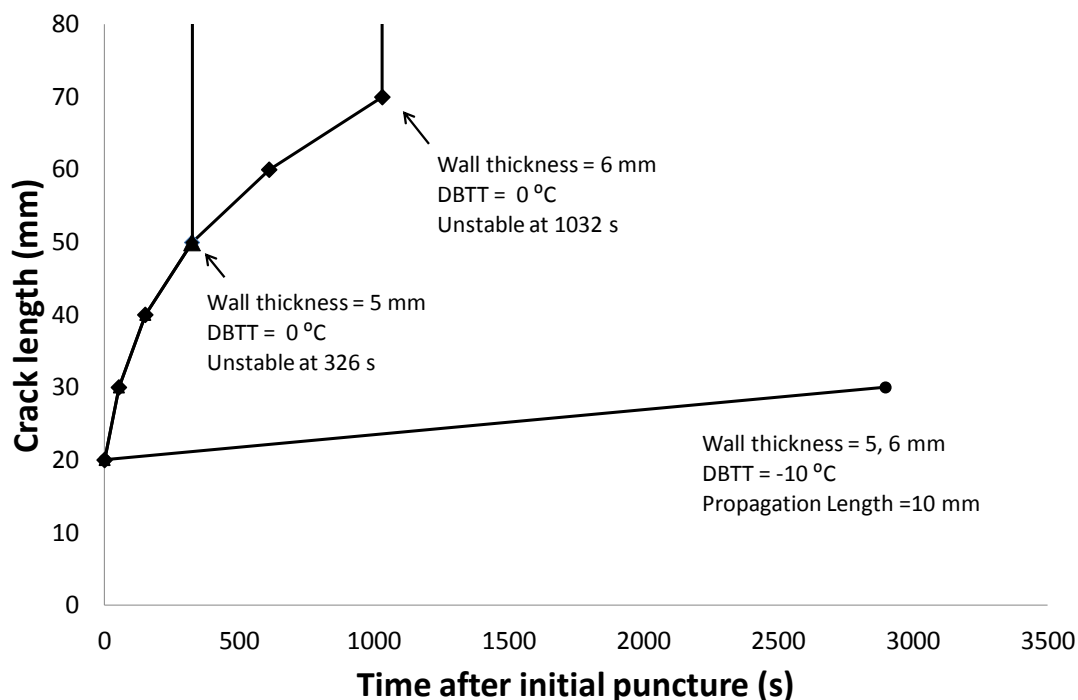
Figure 6.9. Comparison of the variation of the crack length against time following the puncture with various DBTT; exposed pipeline, gas phase CO_2.

6.4.3 Impact of Flow

Figure 6.10 shows the fracture propagation behaviour for the gas phase CO_2 pipeline (DBTT = 0 ℃ and pipe thickness of 6 mm; table 6.1), for both isolated and unisolated flows. In the latter case, the feed flow into the pipe is assumed to remain at 0.2 m/s throughout. As it may be observed, in the case of unisolated flow, the crack arrests after 247 s following puncture. This compares to unstable crack propagation at 1,032 s following puncture for the isolated pipeline. Remarkably and counter-intuitively, the above observation means that for the case

considered, emergency isolation of the flow following the formation of the initial defect results in unstable facture propagation.

The above observation may be explained by reference to figure 6.11 showing the corresponding variation of the pipe wall temperature profile in the proximity of the puncture at two time intervals of 300 s and 5,000 s following puncture for both the isolated and unisolated flow scenarios. As it may be observed, at 300 s, both the isolated and unisolated flow scenarios show similar temperature profiles. However, at 5,000 s following the initial puncture, the initial feed flow in the unisolated pipeline results in a lower degree of cooling of the pipe wall as compared to the isolated case (cf -18 $^{\circ}$C with -23 $^{\circ}$C). This suggests that the relatively warm (10 $^{\circ}$C) bulk fluid flowing within the pipe reduces the amount of localised cooling of the pipe wall, thus increasing its resistance to brittle fracture propagation.
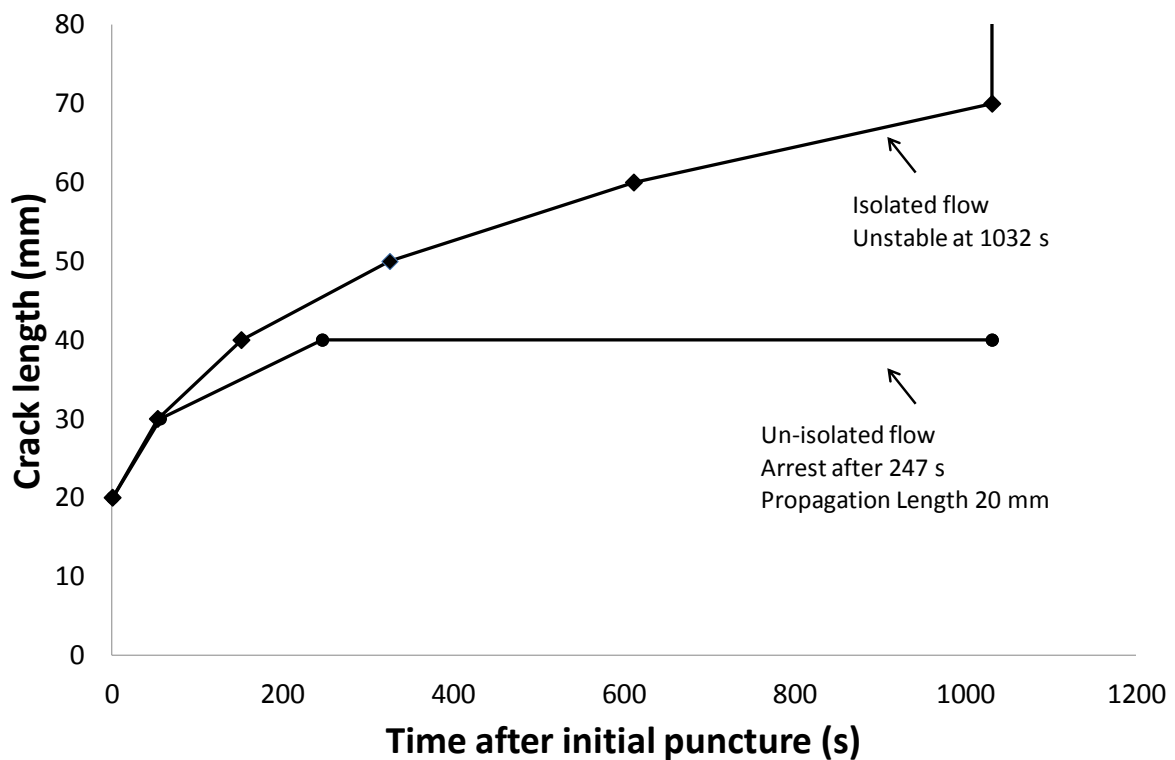
Figure 6.10. Variation of the crack length against time following the puncture of the gas phase pipeline for isolated and unisolated flows
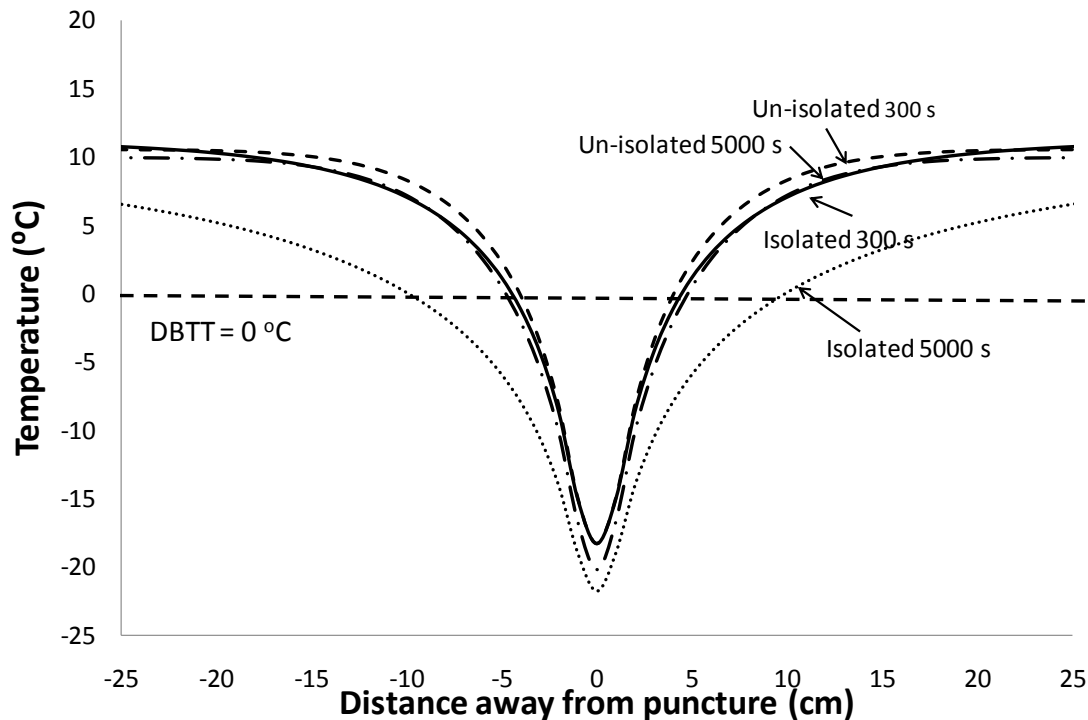
Figure 6.11. Comparison of pipe wall temperature profiles 300 s and 5,000 s following puncture of the gas phase pipeline for isolated and unisolated flows

6.4.4 Impact of Initial Temperature

In this section, the impact of the feed temperature on the crack propagation is investigated. All of the pipe properties remain the same as in table 6.1 except that the feed temperature is assumed to be 0 ℃. The DBTT is assumed to be -10 ℃ to avoid immediate crack propagation.

Figure 6.12 shows the transient pipe wall temperature in the proximity of the puncture at different time intervals up to 10,000 s following puncture for the pipeline transporting dense phase CO_2 at 150 bar and 0°C. The pipeline is assumed to be isolated upon failure corresponding to zero feed flow.

Returning to figure 6.12 for dense phase CO_2, the minimum pipe wall temperature at the puncture location remains at -17 °C for at least the duration of the release period of 10,000 s under consideration. In the first 1,000 s following puncture, the minimum pipe wall temperature corresponds to the release location, and the pipe wall temperature away from the

puncture plane decreases with the passage of time, staying at approx. −6 ℃. At approx. 5,000s, the temperature at the puncture drops towards the DBTT. At around 10,000 s, the pipe wall temperature drops below the DBTT to approx. −17 ℃.

However, no crack propagation is observed. Figure 6.13 shows the variation of the corresponding crack length against time.
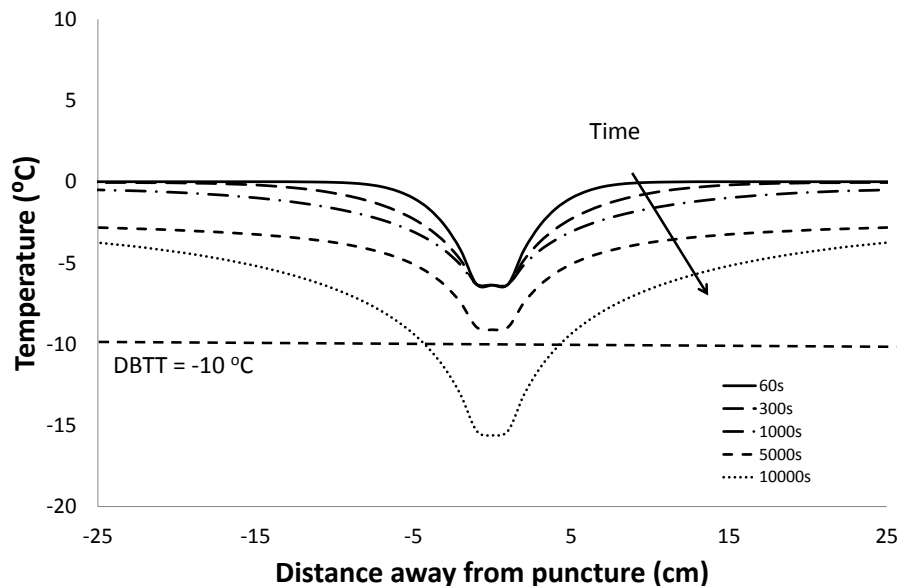
Figure 6.12. The variation of the pipe wall temperature in the proximity of the puncture with time for the dense phase CO$_2$ pipeline (150 bara, 0 ℃, exposed pipeline, DBTT = -10 ℃)
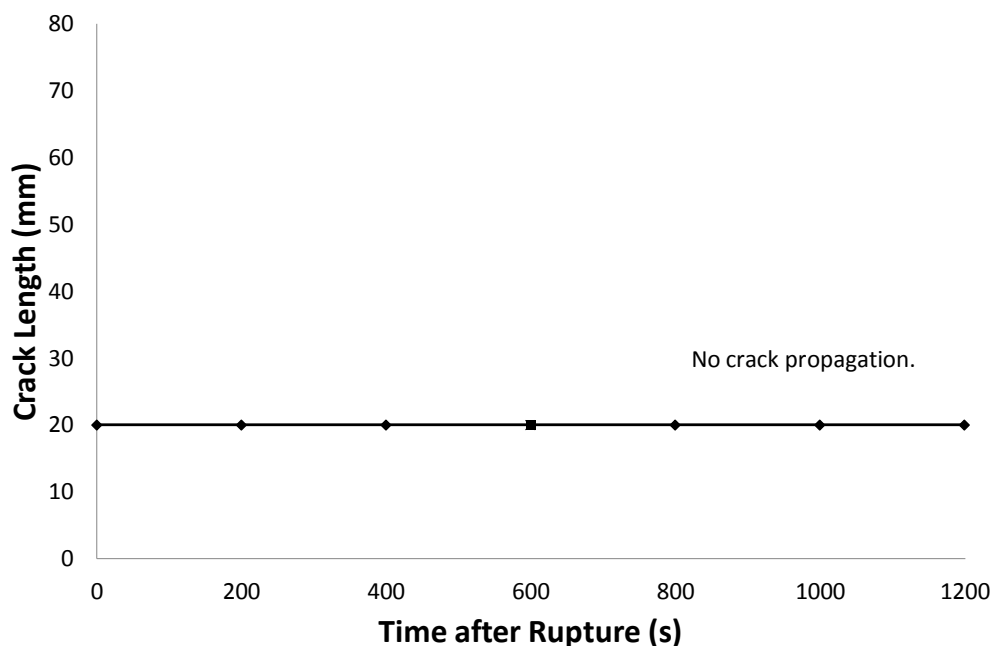
Figure 6.13. Variation of the crack length against time following the puncture of the dense phase CO$_2$ pipeline (150 bara, 0 ℃, exposed pipeline, DBTT = -10 ℃).

Figures 6.14 and 6.15 respectively show the variations of corresponding crack tip temperatures and crack tip intensity factor K_I as a function of the depressurisation time. The fluid phase at any time during the depressurisation is shown in the figures. As it may be observed, during the liquid/vapour phase change, the crack tip temperature drops below the DBTT of -10 ℃ at around 5,000 s following the formation of the initial through-wall defect (figure 6.14). The corresponding crack tip stress intensity factor is 20 MPa m0.5 (figure 6.15). Given that this value is well below the lower bound of the material critical crack intensity factor K_{IC} of 40 MPa m$^{0.5}$, fracture propagation will not occur in the dense (liquid) phase pipeline even though the crack tip temperature has dropped below the DBTT of -10 ℃.
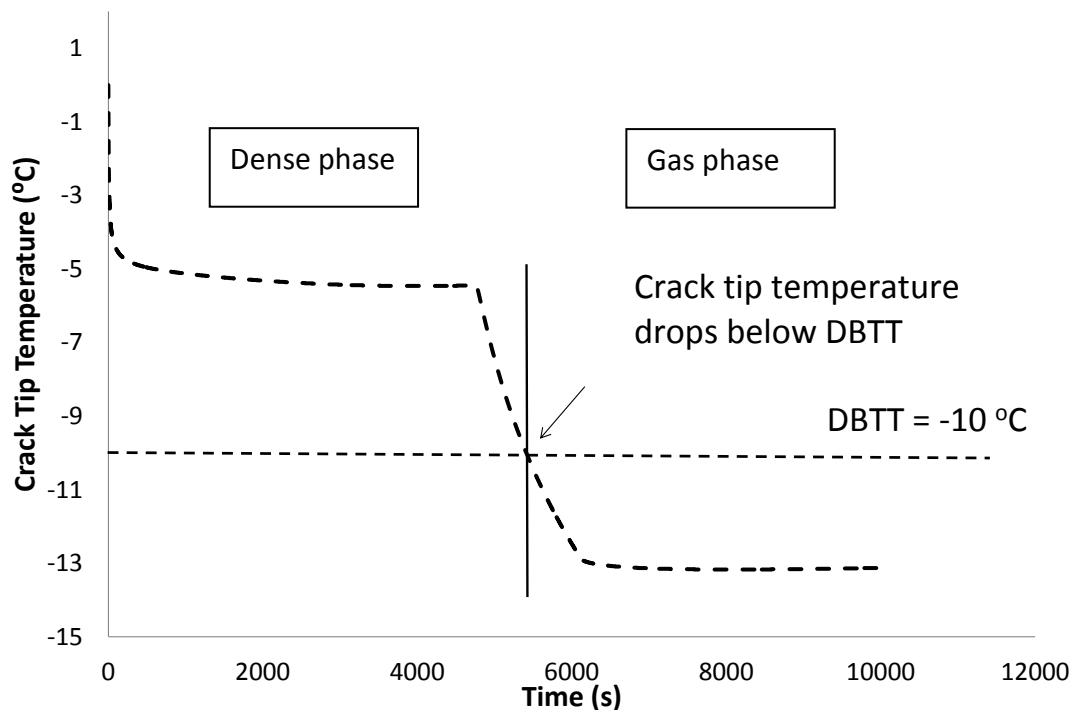
Figure 6.14. Variation of axial pipe wall temperature at different time intervals following the puncture of the dense phase pipeline
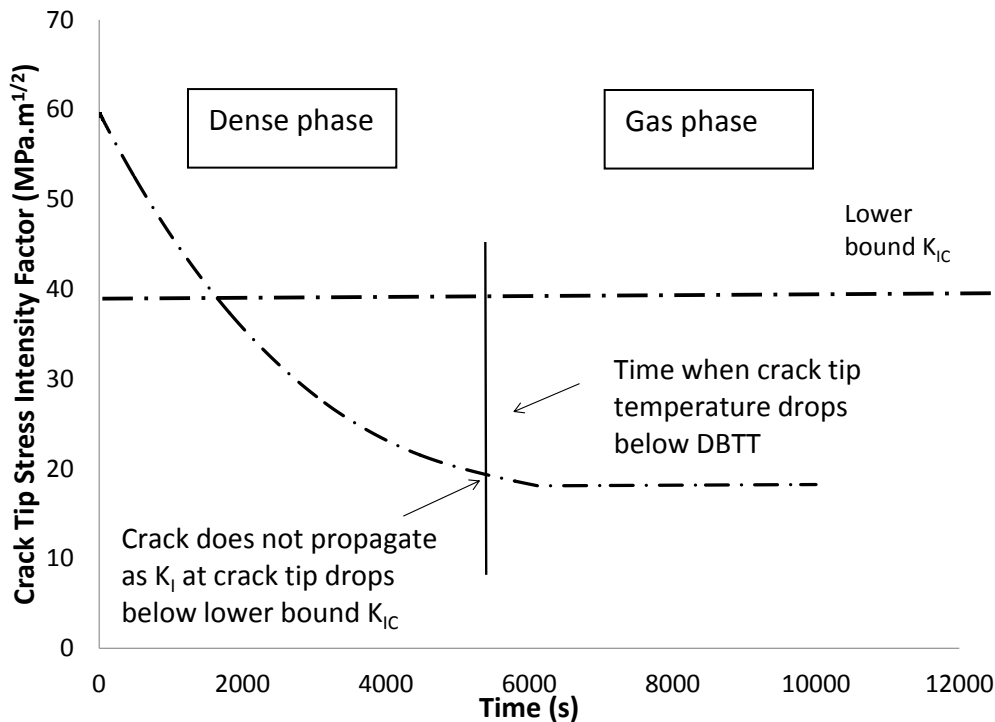
Figure 6.15. Variation of crack tip intensity factor against time following the puncture of the dense phase pipeline

6.4.5 Impact of Stream Impurities

Figure 6.16 shows the impact of the impurities in the dense phase CO_2 stream (150 bar and 10 °C) on the variation of the pipe wall temperature in the proximity of the puncture at 10,000 s following the initial puncture. The pipeline thickness is 14.7 mm. The corresponding composition of CO_2 mixtures tested are given in table 6.2. These cover pure CO_2, post-combustion, pre-combustion (Cosham et al., 2011) and two hypothetical mixtures of CO_2 and N_2 (5% v/v and 10%) representing cases of extreme impurity.

Returning to figure 6.16, as it may be observed, within the ranges tested, impurities have negligible impact on the resulting pipe wall temperature profile and hence the fracture propagation behaviour during the depressurisation process. As such they are no longer considered in this study.
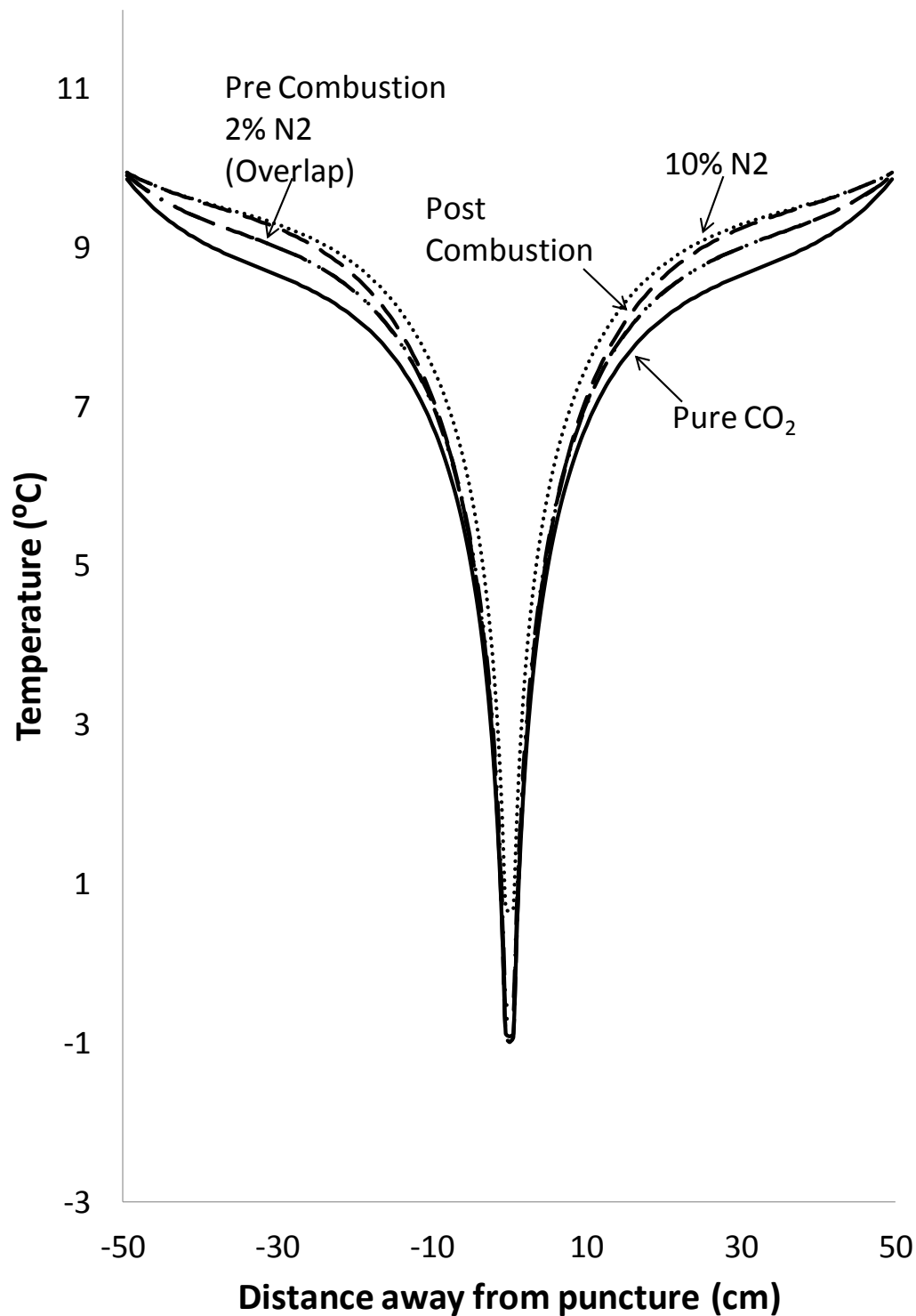
Figure 6.16. The impact of CO_2 composition on the pipe wall temperature profile in the proximity of the puncture plane at 10,000 s following puncture for dense phase CO_2

Feed (v/v)
100% CO_2
95.6% CO_2, 0.4% CO, 0.6% N_2, 3.4% H_2S
99.82% CO_2, 0.17% N_2, 0.01% O_2
95% CO_2, 5% N_2
90% CO_2, 10% N_2

Table 6.2. The % v/v composition of the various CO_2 impurities adopted for the fracture propagation simulations to investigate the impact of impurities

6.4.6 Impact of Defect Shape and Size

Figure 6.17 shows schematic representations and the characteristic dimensions (represented by a, b, and c) for four puncture geometries considered in this study in order to investigate the impact of the defect shape on the fracture propagation behaviour. These include circular and elliptical punctures with hairline fractures of finite equal lengths (a = 20 mm) extending from either one or both sides. Such through-wall defects may form, for example, as a result of damage by a mechanical digger.

Type 1	Type 2
Type 3	Type 4
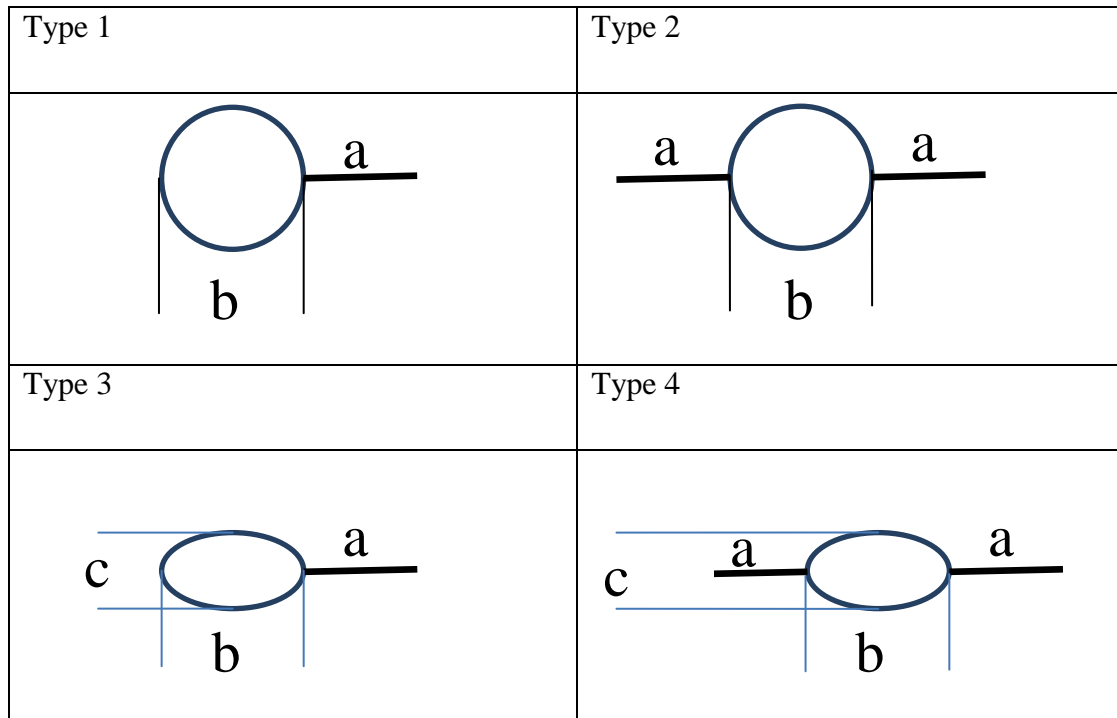
Figure 6.17. Various puncture geometries considered in the study, indicating the characteristic dimensions, a, b and c

Table 6.3 shows brittle fracture data for Type 1 defect geometry for different pipe wall thicknesses of 3.5, 4, 5 and 9 mm for the gas phase CO_2. Two puncture diameters of 10 and 20 mm are considered in order to investigate the impact of the defect size. A relatively high DBTT of 0 ℃ is assumed as the worst-case scenario.

As it may be observed, the larger initial puncture diameter (20 mm) results in a significant reduction in the pipeline's resistance to fracture. For all but the largest pipe wall thicknesses (9 mm), uncontrolled propagating fractures would be expected.

Table 6.4 shows the corresponding fracture data as in table 6.3 but for type 1 to type 4 defect shapes (see table 6.17). For consistency, a constant defect area of 3.14 cm^2 equivalent to a 20 mm dia. circular hole is assumed. Based on the data presented, it is clear that the initial defect geometry has a profound impact on the pipeline's resistance to brittle fracture. The elliptical defect geometries (Types 3 and 4) are worse than the circular defect geometries. Also, the presence of two initial cracks on either side of the defect dramatically reduces the pipe wall's resistance to brittle fracture propagation.

Wall thickness (mm)	Puncture diameter = 20 mm		Puncture diameter = 10 mm	
	Crack state	Time(s)	Crack state	Time(s)
3.5	Unstable	Instant	Unstable	2,458
4	Unstable	234	Unstable	24,632
5	Unstable	2,330	Arrest, 40 mm	25,300
9	No growth	-	No growth	-

Table 6.3. Gas phase brittle fracture propagation behaviour for Type 1 defect geometry

Wall thickness (mm)	Type 2		Type 3		Type 4	
	Crack state	Time(s)	Crack state	Time(s)	Crack state	Time(s)
3.5	Unstable	Instant	Unstable	Instant	Unstable	Instant
4	Unstable	40	Unstable	40	Unstable	Instant
5	Unstable	234	Unstable	2,330	Unstable	40
9	No growth	-	Arrest, 40 mm	43,818	Arrest, 40 mm	43,818

Table 6.4. Gas phase brittle fracture propagation behaviour for Types 2–4 defect geometries (defect area = 3.14 cm^2)

6.5 Conclusion

The application of the fracture model to hypothetical but realistic failure scenarios using British Gas LX/1 pipeline materials reveals significant, and to some extent, unexpected findings. For example:

- puncture in a gas phase CO_2 pipeline results in a higher degree of expansion-induced cooling as compared to puncture in a dense phase CO_2 pipeline , despite the lower starting pressures in the former case.

- buried the pipeline without soil blowing out significant promotes the brittle fracture as the pipe wall temperature goes much lower.

- brittle fracture propagation in modern X70 dense phase CO_2 pipelines is unlikely given the relatively low DTBT ($-70\ ^oC$).

- isolation of the feed flow to the pipeline following the initial puncture promotes brittle fracture propagation.

- thin wall pipeline could develop catastrophic brittle fracture very quickly while thick wall pipeline could eliminate the brittle fracture regardless of the pipe wall temperature.

- starting feed temperature affects the brittle fracture propagation. The initial fracture may not grow due to over depressurisation.

- in all the circumstances examined in this study, the initial defect geometry in the pipeline plays a fundamentally important role in dictating whether or not a fracture will propagate in gas phase CO_2 pipelines.

- within the ranges tested, CO_2 stream impurities do not have an impact on the brittle fracture propagation behaviour.

CHAPTER 7: CONCLUSIONS AND FUTURE WORK

It is widely accepted that pressurised pipelines will be the main method for transporting captured CO_2 from fossil fuel power plants and other CO_2-intensive industries for subsequent storage. Given that CO_2 is an asphyxiant at high concentrations, the safety of such pipelines in the event of pipeline failure is of fundamental importance.

Given the relatively high Joule-Thomson expansion cooling of CO_2, coupled with its slow depressurisation, there is concern that a situation may arise in which a seemingly inconsequential small diameter through-wall defect may eventually transform into a catastrophic running brittle fracture.

In this study, a rigorous fluid/structure interaction model for simulating the above process was presented. The model accounts for most of the important processes governing the fracture propagation process, including the fluid/wall heat transfer effects, the pressure stresses in the pipe wall, and the initial defect geometry. Real fluid behaviour is considered using the Modified Peng Robinson equation of state for CO_2.

The key contributions of this work may be distilled in the following sequential stages:

- Development of a pipeline transient heat transfer model accounting for the flowing fluid /pipe wall/surrounding ambient heat transfer exchanges.

- Development, testing and verification of a crack tip fracture model accounting for pipeline fracture toughness and puncture geometry. This involved three steps: 1) Establishing the crack tip model using the Finite Element Mehtod (FEA). 2) Deriving the corresponding parameters of weight function from the FEA results. 3) Curve fitting the weight function parameter data to polynomials. The method provides an analytical expression of the weight function of any given pipeline and puncture geometry to calculate the Stress Intensity Factor, making it possible to couple the fracture model with the heat transfer and fluid outflow model.

- Development of the coupled fluid, heat transfer and fracture models.

The application of the brittle fracture model to hypothetical but realistic CO_2 pipelines suffering an initial through-wall defect or a puncture reveals significant, and to some extent, unexpected findings. For example:

- puncture in a gas phase CO_2 pipeline results in a higher degree of expansion-induced cooling of the escaping fluid and hence the pipe wall in contact with it as compared that for a dense phase CO_2 pipeline . This is despite the lower starting pressure in the former case.

- puncture in a buried pipeline where there is no blowout of the surrounding soil is more likely to lead to brittle facture propagation as compared to that for an exposed pipeline. In the former case, the cooling of the surrounding soil by the escaping CO_2 will result in the secondary cooling of the pipe wall thus facilitating brittle fracture. However, in the case of the exposed pipeline, most of the cooling takes place outside the pipe by the expanding escaping CO_2.

- brittle fracture propagation in modern X70 dense phase CO_2 pipelines is unlikely given the relatively low DTBT (-70 ^oC).

- isolation of the feed flow to the pipeline following the initial puncture promotes brittle fracture propagation.

- thin walled CO_2 pipelines may develop catastrophic brittle fracture very quickly. Increasing the pipe wall thickness may altogether eliminate such risk regardless of the pipe wall temperature.

- as expected, the lowering the starting feed temperature increases the risk of brittle fracture.

- in all the test cases examined in this study, the initial through-wall defect shape in the pipeline has been shown to play a fundamentally important role in

dictating whether or not a fracture will propagate and ultimately become unstable. Irregular defect geometries with hair line cracks pose the highest risk of brittle fracture due to stress concentration fields.

- within the ranges tested, CO_2 stream impurities do not have an impact on the brittle fracture propagation behaviour.

It should be noted that, for simplicity, the fluid decompression behaviour model employed in this study is based on the Homogenous Equilibrium Model (HEM) where the constituent phases are assumed to remain at thermal and mechanical equilibrium. The HEM has been shown to produce reasonably good agreement with the limited real pipeline rupture data available for hydrocarbons. In the case of dense phase CO_2 pipeline rupture release, heterogeneous stratified flow has been directly observed since the conclusion of this work through independent studies. The development of a heterogeneous flow model accounting for phase slip and temperature gradients between the constituent phases is therefore a very useful extension of this work. This will require the formulation of separate conservation equations for each constituent phase and their coupling through the appropriate empirically determined source terms. The latter will require the design of realistic experiments for the investigation of the various flow regimes and their transitions during pipeline failure.

Furthermore, in the case of buried pipelines, where there is no blowout, the heat transfer modelling in this study is based on the assumption that the surrounding soil reaches the adiabatically expanded temperature of the escaping CO_2. This is a conservative assumption as it results in lower pipe wall temperatures than realistically expected. A future study should consider a more realistic scenario that will consider the percolation/diffusion of the escaping CO_2 into the surrounding soil accounting for the relatively complex accompanying heat and mass transfer phenomena. An interesting analogy and perhaps a useful starting point is heat transfer in packed fluidised beds for which empirically derived correlations are available.

Finally, despite being computationally efficient and robust, the Modified Peng Robinson Equation of state employed in this study is not particularly suited to CO_2 and its mixtures. In addition, it cannot handle CO_2 below its triple point where the

transition to the solid phase will occur. The latter limitation is particularly important given the ~~very~~ likelihood of reaching the CO_2 triple point temperature (-56.6 ^{o}C) during the decompression process and the marked change in its heat transfer characteristics as compared to the gaseous phase CO_2. A future study should address the above limitation through the development of a dedicated robust and computationally efficient equation of state for CO_2 and its mixtures.

References

Anderson, T. L. (2005). FRACTURE MECHANICS Fundamentals and Applications Third Edition. Taylor & Francis Page 173-254.

Andrews, R., Haswell, J., Cooper, R., (2010). Will fractures propagate in a leaking CO2 pipeline? Journal of Pipeline Engineering 9. 277 – 287

ANSYS® Academic Research. (2011). ANSYS Release 14.0, Help System, Coupled Field Analysis Guide, ANSYS, Inc.

Assael, M. J., Trusler, J. P. M., & Tsolakis, T. F. (1996). Thermophysical properties of fluids.

Atti, O. F. (2006). Modelling outflow and low temperature induced crack propagation in pressurised pipelines. London: University College London.

Bai, Y., & Bai, Q. (2005). Subsea pipelines and risers. Elsevier.

Banks-Sills, L., & Sherman, D. (1986). Comparison of methods for calculating stress intensity factors with quarter-point elements. International Journal of Fracture, 32(2), 127–140. doi:10.1007/BF00019788

Barsoum, R. S. (1976). On the use of isoparametric finite elements in linear fracture mechanics. International Journal of Numerical Methods in Engineering, 10, 25–37.

Bendiksen, K. H., Malnes, D., Moe, R., & Nuland, S. (1991). The dynamic two-fluid model OLGA: theory and applications. SPE Production Eng.

Bilio, M., Brown, S., Fairwheather, M., Mahgerefteh, H., (2009). CO2 pipelines material and safety considerations, IChemE Symposium Series: HAZARDS XXI Process Safety and Environmental Protection. 423 – 429.

Brennan, F. (1994). Evaluation of stress intensity factors by multiple reference state weight function approach. Theoretical and Applied Fracture Mechanics, 20(3), 249–256. doi:10.1016/0167-8442(94)90017-5

Brown, S. (2011). CFD Modelling of Outflow and Ductile Fracture Propagation in Pressurised Pipelines. University College London.

Bueckner, H. F. (1970). A Novel Principle for the Computation of Stress Intensity Factors. Zeitschrift Fur Angewandte Mathematik und Mechanik.

Carpenter, W. C. (1983). Extrapolation techniques for determining stress intensity factors. Engineering Fracture Mechanics, 18, 325–332.

Cengel, Y. A. (2003). Heat Transfer: A Practical Approach. McGraw-Hill Higher Education.

Chan, S. K., Tuba, I. S., & Wilson, W. K. (1970). On the finite element method in linear fracture mechanics. Engineering Fracture Mechanics, 4, 1–17.

Chen, N. H. (1979). An explicit equation for friction factor in pipe. Industrial & Engineering Chemistry Fundamentals, 18(3), 296–297.

Chen, J. R., Richardson, S. M., & Saville, G. (1993). A simplified numerical method for transient two-phase pipe flow. Trans IChemE.

Chen, J. R., Richardson, S. M., & Saville, G. (1995a). Modelling of two-phase blowdown from pipelines – I. A hyperbolic model based on variational principles. Chem. Eng. Sci., 50.

Chen, J. R., Richardson, S. M., & Saville, G. (1995b). Modelling of two-phase blowdown from pipelines – II. A simplified numerical method for multi-component mixtures. Chem. Eng. Sci., 50.

Churchill, S. W., & Bernstein, M. (1977). A Correlating Equation for Forced Convection from Gases and Liquids to a Circular Cylinder in Cross Flow. Journal of Heat Transfer, 99, 300–306.

Churchill, S. W., & Chu, H. H. . (1975). Correlating Equations for Laminar and Turbulent Free Convection from a Horizontal Cylinder. International Journal of Heat Mass Transfer, 18.

Cosham, A., & Eiber, R. (2008). Fracture propagation in CO2 pipelines. Journal of Pipeline Engineering.

Courant, R., Friedrichs, K., & Lewy, H. (1967). Partial Difference Equations of Mathematical Physics. IBM Journal of Research and Development, 11(2).

Cruse, T. A. (1969). Numerical Solutions in Three-dimensional Elastostatics. International Journal of Solids and Structures.

Daubert, T. E., & Danner, R. P. (1990). Data Compilation - Physical and Thermodynamic Properties of Pure Compounds. Taylor and Francis.

Denton, G. (2009). CFD Simulation of Highly Transient Flowse. University College London.

Edwards, D. ., Denny, V. ., & Mills, A. . (1979). Transfer Processes. Washington,DC: Hemisphere.

Ely, J. F., & Hanley, H. J. M. (1981). Prediction of transport properties. 1. Viscosity of fluids and mixtures. Industrial & Engineering Chemistry Fundamentals, 20(4).

Ely, J. F., & Hanley, H. J. M. (1983). Prediction of transport properties. 2. Thermal conductivity of pure fluids and mixtures. Industrial & Engineering Chemistry Fundamentals, 22(1).

Fett, T., Mattheck, C., & Munz, D. (1989). Approximate weight function for 2D and 3D problems. Engineering Analysis with Boundary Elements, 6(1), 48–63.

Flatt, R. (1986). Unsteady compressible flow in long pipelines following a rupture. International Journal for Numerical Methods in Fluids, 6(2).

Gnielinski, V. (1976). New Equations for Heat and Mass Transfer in Turbulent Pipe and Channel Flow. Chemical Engineering, 16, 359–368.

Griffith, A. A. (1921). The phenomena of rupture and flow in solids. Philosophical transactions of the Royal society of London, 221, 163–198.

Huebner, K. H. (2001). The Finite Element Method in Engineering.

Inoue, T., Makino, H., Endo, S., Kubo, T., & Matsumoto, T. (2003). Simulation method for shear fracture propagation in natural gas transmission pipelines. Proceedings of the Thirteenth (2003) International Offshore and Polar Engineering Conference, Vol 4, 121–128,575.

Irwin, G. R. (1957). Analysis of Stresses and Strains near the End of a Crack Traversing a Plate. Journal of Applied Mechanics.

J.Janna, W. (2000). Engineering Heat Transfer. CRC Press.

Jones, D. G., & Gough, D. W. (1981). Rich gas decompression behaviour in pipelines. AGA EPRG Pipeline Research Seminar IV.

Johnson, D. M., Horner, N., Carlson, L., & Eiber, R. (2000). Full scale validation of the fracture control of a pipeline designed to transport rich natural gas. Pipeline Technology, 1, 331.

Kersten, M. S. (1949). Thermal properties of soils. Mineapolis: Engineering Experiment Station, Bulletin 2.

Kimambo, C. Z., & Thorley, A. (1995). Computer modelling of transients ruptured high-pressure natural gas pipelines: a review of experimental and numerical studies. IMechE, C502/003.

Kruse, H., & Tekiela, M. (1996). Calculating the consequences of a CO2 Pipeline rupture. En. Conv. Man.

Leis, B. N., Forte, T. P., & Clark, E. B. (2005). Modeling running fracture in pipelines – past, present, and plausible future directions. Proc. 11th Int.Conf. Frac.

Leveque, R. J. (2002). Finite Volume Methods for Hyperbolic Problems. Cambridge University Press.

Li, H., & Yan, J. (2009). Evaluating cubic equations of state for calculation of vapor–liquid equilibrium of CO2 and CO2-mixtures for CO2 capture and storage processes. Applied Energy, 86(6), 826–836. doi:10.1016/j.apenergy.2008.05.018

Lim, I. L., & Choi, S. K. (1992). Comparison between various displacement-based stress intensity factor computation techniques Nodal lettering. International Journal of Fracture, 193–210.

Mahgerefteh, H., & Atti, O. (2006). Modeling low-temperature–induced failure of pressurized pipelines. AIChE Journal, 52(3), 1248–1256. doi:10.1002/aic.10719

Mahgerefteh, H., Brown, S., Denton, G., (2012). Modelling the impact of stream impurities on ductile fractures in CO2 pipelines. Chemical Engineering Science 74, 200–210.

Mahgerefteh, H., Brown, S., Zhang, P., (2011). A dynamic boundary ductile-fracture-propagation model for CO2 pipelines. Journal of Pipeline Engineering 9, 265–276.

Mahgerefteh, H., Denton, G., & Rykov, Y. (2008a). A hybrid multiphase flow model. Aiche Journal, 54(9), 2261–2268. doi:Doi 10.1002/Aic.11569

Mahgerefteh, H., Denton, G., & Rykov, Y. (2008b). CO2 Pipeline Rupture. HAZARDS XX Process Safety and Environmental Protection, IChemE Sympsium, 896–882.

Mahgerefteh, H., Rykov, Y., & Denton, G. (2009). Courant, Friedrichs and Lewy (CFL) impact on numerical convergence of highly transient flows. Chemical Engineering Science, 64(23).

Mahgerefteh, H., Saha, P., & Economou, I. G. (1999). Fast numerical simulation for full-bore rupture of pressurized pipelines. AIChE J., 45, 1191.

Mahgerefteh, H., & Wong, S. M. A. (1999). A numerical blowdown simulation incorporating cubic equations of state. Computers in Chemical Engineering, 23(9).

Mahgerefteh, H., Saha, P., & Economou, I. G. (1997). A study of the dynamic response of emergency shutdown valves following full-bore rupture of gas pipelines. Trans. Inst. Chem. Eng., 75, 201.

Makino, H., Sugie, T., Watanabe, H., Kubo, T., Shiwaku, T., Endo, S., Machida, S. (2001). Natural gas decompression behavior in high pressure pipelines. ISIJ International, 41(4), 389–395.

Maxey, W. A. (1974). Fracture Initiation , Propagation and arrest. Houston.

NG, S. . (1998). Crack surface displacement methods for determining stress intensity factors involving a semi-infinite crack model. The Hong Kong Polytechnic University.

Nordsveen, M., & Haerdig, A. (1997). Simulation of severe slugging during depressurisation of an oil/gas pipeline, modelling, identification and control. Modeling, Identification and Control, 18(1).

Niu, X., & Glinka, G. (1990). Weight Function for Edge and Surface Semi-Elliptical Cracks in Flat Plates and Plates with Corners. Engineering Fracture Mechanics, 36, 459–475.

Odonoghue, P. E., Green, S. T., Kanninen, M. F., & Bowles, P. K. (1991). The Development of a Fluid Structure Interaction-Model for Flawed Fluid Containment Boundaries with Applications to Gas Transmission and Distribution Piping. Computers & Structures, 38(5-6), 501–513.

Ojdrovic, P., & Petroski, H. (1991). Weight functions from multiple reference states and crack profile derivatives. Engineering Fracture Mechanics, 39, 105–111.

Oke, A., Mahgerefteh, H., Economou, I. G., & Rykov, Y. (2003). A transient outflow model for pipeline puncture. Chem Eng Sci, 58.

Oke, A. (2004). An efficient numerical simulation for modelling outflow following rupture or puncture of pressurised pipeline networks. University College London.

Orowan, E. (1949). Fracture and Strength of Solids. Reports on Progress in Physics.

Parks, D. M. (1974). A stiffness derivative finite element technique for determination of elastic crack tip stress intensity factors. International Journal of Fracture, 10, 478–502.

Parfomak, P.W., Fogler, P., (2007). Carbon Dioxide (CO2) Pipelines for Carbon Sequestration: Emerging Policy Issues. Congressional Research Service: Washington, DC.

Peng, D. Y., & Robinson, D. B. (1976). A New Two-Constant Equation of State. Industrial & Engineering Chemistry Fundamentals, 15(1).

Petroski, H., & Achenbach, J. (1978). Computation of the weight function from a stress intensity factor. Engineering Fracture Mechanics, 10(2), 257–266. doi:10.1016/0013-7944(78)90009-7

Picard, D. J., & Bishnoi, P. R. (1988). The importance of real fluid behaviour and non-isentropic effects in modelling compression characteristics of pipeline fluids for application in ductile fracture propagation analysis. Can. J. Chem. Eng., 66(3).

Pook, L. P. (2000). Linear Elastic Fracture Mechanics for Engineers: Theory and Applications. WIT Press.

Rahman, S., Brust, F. W., Ghadiali, N., & Wilkowski, G. (1998). Crack-opening-area analyses for circumferential through-wall cracks in pipes — part I: analytical models. Int. J.Press. Vessels Pip., 75, 357–373.

Richardson, S. M., Saville, G., Fisher, A., Meredith, A. J., & Dix, M. J. (2006). Experimental Determination of Two-Phase Flow Rates of Hydrocarbons Through Restrictions. Trans IChemE, Part B: Process Safety and Environmental Protection, 84.

Rice, J. R. (1968). Path Independent Integral and the Approximate Analysis of Strain Concentration by Notches and Cracks. Journal of Applied Mechanics, 35, 379–386.

Rice, J. R. (1972). Some Remarks on Elastic Crack-Tip Stress Fields. International Journal of Solids and Structures.

Seevam, P.N., Race, J.M., Downie, M.J., Hopkins, P., (2008). Transporting the next generation of CO2 for carbon,capture and storage: the impact of impurities on supercritical CO2 pipelines, 7th International Pipeline Conference, Calgary. 39–51.

Serpa, J., Morbee, J., Tzimas, E., (2011). Technical and Economic Characteristics of a CO2 Transmission Pipeline Infrastructure. JRC Scientific and Technical Reports. European Commission Joint Research Centre Institute for Energy. 51.

Shen, G., & Glinka, G. (1991). Determination of weight functions from refeerence stress intensity factors. Journal of Theoratical Applied Fracture Mechanics, 15, 237–245.

Shih, C. F., & Asaro, R. J. (1988). Elastic-Plastic Analysis of Cracks on Bimaterial Interfaces: Part I—Small Scale Yielding. Journal of Applied Mechanics.

Shih, C. F., DeLorenzi, H. G., & German, M. D. (1976). Crack extension modelling with singular quadratic isoparametric elements. International Journal of Fracture, 12, 647–651.

SIMULIA. (2010). Abaqus Theory Manual (6.10).

SIMULIA. (2011). ABAQUS FEA. Dassault Systemes.

Sneddon, I. N. (1946). The Distribution of Stress in the Neighbourhood of a Crack in an Elastic Solid. Proceedings, Royal Society of London.

Soave, G. (1972). Equilibrium constants from a modified Redlich-Kwong equation of state. Chemical Engineering Science, 27(6).

Steiner, D., & Taborek, J. (1992). Flow boiling heat transfer in vertical tubes correlated by an asymptotic method. Heat Transfer Engineering, 13(2).

Suehiro, Y.; Nakajima, M.; Yamada, K.; Uematsu, M., (1996), Critical parameters of {xCO2 + (1 - x)CHF3} for x = (1.0000, 0.7496, 0.5013 , and 0.2522), The Journal of Chemical Thermodynamics 28, 1153-1164.

Tada, H., Paris, P. C., & Irwin, G. R. (2000). The Stress Analysis of Cracks Handbook.

Takeuchi, I., Makino, H., Okaguchi, S., Takahashi, N., & Yamamoto, A. (2006). CRACK ARRESTABILITY OF HIGH-PRESSURE GAS PIPELINES BY X100 OR X120. Amsterdam.

Terenzi, A. (2005). Influence of real-fluid properties in modelling decompression wave interacting with ductile fracture propagation. Oil Gas Sci.Tech, 60(4), 711–719.

Toro, E. F. (2009). Riemann Solvers and Numerical Methods for Fluid Dynamics - A Practical Introduction (3rd ed.). Springer - Verlag.

Walas, S. M. (1985). Phase equilibria in chemical engineering. Boston: Butterworth.

Westergaard, H. M. (1939). Bearing Pressures and Cracks. Journal of Applied Mechanics.

Williams, M. L. (1957). On the Stress Distribution at the Base of a Stationary Crack. Journal of Applied Mechanics.

Wilson, W. K. (1973). Finite Element Methods for Elastic Bodies Containing Cracks.

Wu, D., & Chen, S. (1997). A Modified Peng-Robinson Equation of State. Chemical Engineering Communications, 156(1).

Wu, X. R., & Carlsson, A. J. (1991). Weight Functions and Stress Intensity Factor Solutions. Pergamon Press.

Wylie, E. B., & Streeter, V. L. (1993). Fluid Transients in systems. Englewood, NJ: Prentice-Hall.

Zhuang, Z., & Guo, Y. J. (1999). Analysis of dynamic fracture mechanisms in gas pipelines. Engineering Fracture Mechanics, 64(3), 271–289.

Zucrow, M. J., & Hoffman, J. D. (1976). Gas Dynamics, Volume I and II. Wiley, New York,.

Appendix

Fortran Source Code for the Heat Transfer Model

```
! -------------------------------------------------
! THIS IS THE PIPEWALL HEAT TRANSFER SIMULATION CODE WRITTEN
! BY PENG (GRASSZHANG@GMAIL.COM) STARTED ON 22, APR,2010
! HEAT FLOW MODEL
! -------------------------------------------------
! --------------DECLARATION----------------------
        SUBROUTINE PIPEWALLHT
    IMPLICIT REAL*8 ( A-H,O-Z)
    PARAMETER (NPHYS=10,NCMAX=71, PI=3.141592654D0, PUNIT=101325.D0, &
    &      RGAS=8.31439D0, ACGRAV=9.8066352D0)
    PARAMETER (ISP = 5000)
    PARAMETER (EPS = 1.D-5,EPSA = 1.0541855751231137D-6)
    PARAMETER (EPS1 = 0.5D0, NPIPE = 10,EPSB = 1.D-6)
    PARAMETER (NMESH = 2, NSGRID = 5)
    PARAMETER (N1MESH = 2, NS1GRID = 5)
    PARAMETER (NF1NGRD = N1MESH*NS1GRID, NFNGRD = NMESH*NSGRID)
    PARAMETER (NCOMPONENTS = 71)
    COMMON /FEEDCOMP1 / XU
    COMMON/PIPED/DPIPE, LPIPE, RF
        COMMON/HTTRANS/ PIPETHCK,TNODE,DNODEDIS,VORIF,DT,REND11,TORIF,HTWMT, &
    &  HTN,PORIF,PIPETHCOL,PIPEHCP,PIPEDENS,TCONGAS
    COMMON /ORIFICE3/ORDIAMT,ORHEIGHT,PLENGTH,IORIENT,DIS1,IZ3
    COMMON/ENVRM/ PEXTB, TINFC, HTC
    COMMON/ TEMPER3 / T,TS1,TS
    COMMON/ DENSXXX / R,RS1,RS
    COMMON/ VELOCIT3 / U,US1,US
    COMMON/ PRESS3 / P,PS1,PS
    COMMON/TVISC/VIS
    COMMON /CARRYON/ ISWITCH2,SNT,HNT,ZT1,WMT1,CPT1,CVT1
```

```
COMMON /TWOPHASES/DENGS,DENLQ,VISGS,VISLQ,XQLT,WMGS,WMLQ, &

&          XLQ(NCMAX),YGS(NCMAX),TCONGS,TCONLQ

COMMON /TCONGS/ TCONGS1


DOUBLE PRECISION R(NPIPE,2,0:ISP),T(NPIPE,2,0:ISP),U(NPIPE,2,0:ISP),P(NPIPE,2,0:ISP)

DIMENSION ZFEED(NCMAX),XU(NCMAX),TCUMDIS(NCMAX),XO2(NCMAX)




!    Real*8,allocatable,dimension(:,:,:)::TNODE  ! TEMPERATURE AT EACH NODE IN K

Real*8 TNODE(0:5,0:1000,0:2000)

Real*8,allocatable,dimension(:,:,:)::HNODE  ! HEAT FLOW AT EACH NODE

REAL DX,DY,DZ  ! STEP LENGTH IN RADIAL(X) TANGENTIAL (Y) AND AXIAL (Z)

Real*8,allocatable,dimension(:)::TFEED ! FEED TEMPATURE AT EACH INNER NODE IN K

REAL *8 :: NU,PR,RE ! Nusselt, Prandtl, Reynolds number

REAL *8 :: FFACTOR ! FANNING FRICTION FACTOR

REAL *8 :: HORIF,HAMP,HPIPE ! HEAT TRANSFER COEFFICIENTS AT ORIFICE AND AMBIENT AND
FLUID-PIPE(W/M2K)

REAL *8 :: HNAT,HFOR ! NATURAL AND FORCED HEAT TRANSFER COEFFICIENT   (W/M2K)

REAL *8 :: RA  ! RAYLEIGH NUMBER IN NATURAL CONVECTION CAL

REAL *8 :: TAIR(7)=(/123,173,223,273,293,313,333/)  ! IN C

REAL *8 :: VAIR(7)=(/0.00000308,0.00000595,0.00000955,0.00001330,0.00001511,0.00001697,0.00001890/)

        ! IN M2/S

REAL *8 :: KAIR(7)=(/0.0116,0.0160,0.0204,0.0243,0.0257,0.0271,0.0285/) ! IN W/M.K

REAL *8 :: PRAIR(7) = (/0.76,0.74,0.725,0.715,0.713,0.711,0.709/)

    !TEMPERATURE, KINETIC VISCOSITY,CONDUCTIVITY PR AIR PROPERTY TABLE

    !FROM http://www.engineeringtoolbox.com/air-properties-d_156.html

    !IN ACCORDANCE WITH PERRY'S BOOK

INTEGER :: IT !POINTER USED IN AIR TABLE

REAL *8 :: TFILM ! FILM TEMPERATURE IN NATURAL CONVECTION CAL

REAL *8 :: DT ! TIME STEP IN S

INTEGER :: MIDNODE !NODE NUMBER AT CENTRAL LINE

INTEGER :: ORIY,ORIZ ! ORIFICE NODES IN Y AND Z DIRECTION

REAL *8 :: K2,K3,K4,K5,K6,K7  ! CONDUCTANCE IN 6 DIRECTION  NUMBERING IN FEMI'S MODEL NODE
NUMBERING
```

```
      REAL *8 :: T2,T3,T4,T5,T6,T7  !TEMPERATURE DIFFERENCE IN HEAT FLOW CALCULATION

      REAL *8 :: KFEEDPIPE,KFEEDORI,KPIPE !THERMAL CONDUCTIVITY OF FLUID,FLUID AT ORIFICE, PIPE
W/(MK)




          PIPETH    = PIPETHCK/1000.D0 ! PIPE THICKNESS IN M

      PIPEDO    = DPIPE + 2.D0*PIPETH !PIPE OUTTER DIAMETER IN M

      PIPEDI    = DPIPE ! PIPE INNER DIAMETER IN M

      PIPELEN   = 1 ! CALCULATING PIPE LENGTH IN M

      ORID      = ORDIAMT ! ORIFICE DIAMETER IN M

!    TOTALT    = 1000.0 ! TOTAL SIMULATION TIME IN SECOND

      TAMB      = TINFC+273.15  ! AMBIENT TEMPERATURE IN K

      TORI      = TORIF ! FLUID EXIT TEMPETATURE AT ORIFICE IN K




      NUMX      = 3 ! NUMBER OF NODE IN X

      DX                      = PIPETH / (NUMX-1)!NODE X DIMENSION IN M

      DY              = 0.0025d0 !NODE Y DIMENSION IN M

      DZ        = 0.0025d0 !NODE Z DIMENSION IN M

      NUMY      = CEILING(PIPEDI*PI/4/DY) ! NUMBER OF NODE IN Y, ONLY MODEL 1/4 OF THE PIPE
CIRCULAR

      NUMZ      = CEILING(PIPELEN/DZ) ! NUMBER OF NODE IN Z




!$$$$$$ !   DIFFU     = 1.172*0.00001 ! THERMAL DIFFUSIVITY IN M2/S FOR CARBON STEEL FROM WIKI

!$$$$$$      RHOEXIT   = 1001 ! Fluid density at orifice  kg/m3

!$$$$$$      RHOPIPE   = 50 ! FLUID DENSITY IN PIPE PRIOR ORIFICE kg/m3

!$$$$$$      UEXIT     = 10 ! Fluid exit velocity in m/s

!$$$$$$      UPIPE     = 5 ! fluid velocity in pipe

!$$$$$$      VISFEXIT  = 1.3*0.0001 ! Fluid viscosity at orifice pa.s

!$$$$$$      VISFPIPE  = 1.3*0.0001 ! FLUID VISCOSITY IN PIPE PRIOR ORIFICE
```

!$$$$$$ CPEXIT   = 2300 ! specific heat at orifice J/(Kg.K)

!$$$$$$ CPPIPE   = 2300 ! SPECIFIC HEAT at pipe prior orifice

   CPIPEWALL = PIPEHCP*PIPEDENS !VOLUMATRIC HEAT CAPACITY OF PIPE WALL J/M3K

   KPIPE   = PIPETHCOL ! thermal conductivity of pipe W/(m K)

!$$$$$$ KFEED   = 0.1 ! thermal conductivity of fluid W/(m K)

!$$$$$$ KFEEDORI = 0.05 ! THERMAL CONDUCTIVITY OF FLUID AT ORIFICE W/(M K)

   G   = 9.81 !gravity

! -------------INITIATION---------------------

!$$$$$$ DY = PIPEDI*PI/4/ (NUMY-1) ! ONLY MODELS QUARTER PIPE

!$$$$$$ DZ = PIPELEN / (NUMZ-1)

!   ALLOCATE (TNODE(0:NUMX+1,0:NUMY+1,0:NUMZ+1))

   ALLOCATE (HNODE(0:NUMX+1,0:NUMY+1,0:NUMZ+1))

   ! 3 NODE (2 CELLS)IN X 21NODES (20CELLS)IN Y, 1001NODES 1000CELLS IN Z

   ! TNODE(1,:,:) ARE THE INNER SURFACE TNODE(3,:,:) ARE OUTER SURFACE

   ! TNODE(:,1,:) AND TNODE(:,NUMY,:)ARE EDGES OF QUARTER PIPE

   ! TNODE(:,:,1) ARE NEAREST NODE TO ORIFICE

   ! ORIFICE CENTER TNODE(:,1,1)

   ! +1 for any fictional nodes

   ALLOCATE (TFEED(0:NUMZ+1))

!$$$$$$ TNODE = TAMB

!---------------SET TFEED ------------------------------------

         TFEED(0) = T(1,1,1)

          IF (PIPELEN .LE. DNODEDIS) THEN

         TFEED = T(1,1,1)

   ELSE

     I = 1

         DO WHILE (PIPELEN .GT. DNODEDIS*I)

      J = (I-1)*IFIX(DNODEDIS/DZ)

      K = I*(CEILING(DNODEDIS/DZ)-1)

```
      TFEED (J:K) = T(1,1,I)

     I=I+1

    END DO

    TFEED (K+1:NUMZ+1) = T(1,1,I+1)

   END IF




!---------------------------------------------------------------

!    TFEED = TAMB ! STEADY STATE,test

   HNODE = 0

!    DT = 0.1  ! TIME STEP IN S



!---------------DETERMINE ORIFICE NODES------------------------

   ORIY = NINT(ORID/2.0 / DY)

   IF (ORIY .EQ. 0) ORIY =1

   ORIZ = NINT(ORID/2.0 /DZ)

   IF (ORIZ .EQ. 0) ORIZ =1

   ! ORIFICE AREA (:,1+ORIY,1),(:,1+ORIY,1+ORIZ)

   !PRINT *, DY,DZ, ORID, ORIY,ORIZ

   !PAUSE

!---------------------------------------------------------------



!$$$$$$    TIME= 0

!$$$$$$    DO WHILE (TIME<TOTALT)




!--------------------Coefficients----------------------------------

   CALL PHASES (TORIF,PORIF,0,SPECIN,IPS)

        VTHER=1.D6*HTWMT/REND11

   VISFEXIT = VIS

   KFEEDORI = TCONGS1

!    CALL THERVISV(XU,TORIF,VTHER,HTN,KFEEDORI,VISFEXIT)

        RE = REND11*VORIF*ORID/VISFEXIT
```

```
CPEXIT = CPT1 * RGAS/HTWMT


PR =  CPEXIT*VISFEXIT/KFEEDORI

FFACTOR = (1/(1.7372*ALOG(RE/(1.964*ALOG(RE)-3.8215))))**2

NU = (RE-1000)*PR*FFACTOR/2/(1+(12.7*sqrt(FFACTOR/2))*(PR**(0.6666)-1))

HORIF = KFEEDORI / ORID * NU    ! COEFFICIENT FOR ORIFICE FLOW TO PIPE WALL




        RHOPIPE = R(1,1,1)

UPIPE = U(1,1,1)

PPIPE = P(1,1,1)

TPIPE = T(1,1,1)

CALL PHASES (TPIPE,PPIPE/1.D5,0,SPECIN,IPS)

VISFPIPE = VIS

KFEEDPIPE = TCONGS1

        CPPIPE = CPT1 *RGAS / HTWMT

RE = RHOPIPE*UPIPE*PIPEDI/VISFPIPE

PR = CPPIPE*VISFPIPE/KFEEDPIPE

IF (RE .LT. 2000) THEN

   IF (RE .LT. 0) RE=0

   NU = 3.66+0.0668*(PIPEDI/PIPELEN)*RE*PR/(1+0.04*(PIPEDI/PIPELEN*RE*PR)**(0.666))

   ELSE

   FFACTOR = (1/(1.7372*ALOG(RE/(1.964*ALOG(RE)-3.8215))))**2

   NU = (RE-1000)*PR*FFACTOR/2/(1+(12.7*sqrt(FFACTOR/2))*(PR**(0.6666)-1))

END IF

HPIPE = KFEEDPIPE / PIPEDI * NU
```

!---

!--------------------Calculate outter surface heat flow--------------------

!   MIDNODE = NUMY/2 + 1

  DO I = 1, NUMY

    DO J= 1, NUMZ

        IT =1

        TFILM = (TNODE(NUMX,I,J)+TAMB)/2

        DO WHILE (TFILM>TAIR(IT))

          IT=IT+1

        END DO

        RA = (G* (1/TFILM)* ABS(TNODE(NUMX,I,J)-TAMB) * PIPEDO**3)/VAIR(IT)**2*PRAIR(IT)

        IF (RA == 0) THEN

          NU = 0.36

          ELSE

          NU = (0.6+0.387*RA**(0.1666667)/(1+(0.559/PRAIR(IT))**(0.5625))**(0.296296))**2

        END IF

        HNAT = KAIR(IT)*NU/PIPEDO

        K2 = DX*DY/DZ*KPIPE/2

        K3 = K2

        K4 = DX*DZ/DY*KPIPE/2

        K5 = K4

        K6 = DY*DZ/DX*KPIPE

        K7 = DY*DZ*HNAT

        T2 = TNODE(NUMX,I,J-1)-TNODE(NUMX,I,J)

        T3 = TNODE(NUMX,I,J+1)-TNODE(NUMX,I,J)

        T4 = TNODE(NUMX,I+1,J)-TNODE(NUMX,I,J)

        T5 = TNODE(NUMX,I-1,J)-TNODE(NUMX,I,J)

        T6 = TNODE(NUMX-1,I,J)-TNODE(NUMX,I,J)

        T7 = TAMB-TNODE(NUMX,I,J)

        HNODE(NUMX,I,J) = K2*T2+K3*T3+K4*T4+K5*T5+K6*T6+K7*T7

```
     END DO

   END DO  ! ALL SURFACE NODE



   I = 1+ORIY  ! UPPER ORIFICE BOUNDARY

   DO J = 1, ORIZ+1

!$$$$$        RE = RHOEXIT*UEXIT*ORID/VISFEXIT

!$$$$$        PR =  CPEXIT*VISFEXIT/KFEEDORI

!$$$$$        FFACTOR = (1/(1.7372*ALOG(RE/(1.964*ALOG(RE)-3.8215))))**2

!$$$$$        NU = (RE-1000)*PR*FFACTOR/2/(1+(12.7*sqrt(FFACTOR/2))*(PR**(2/3)-1))

!$$$$$        HORIF = KFEED / PIPEDI * NU

        IT =1

        TFILM = (TNODE(NUMX,I,J)+TAMB)/2

        DO WHILE (TFILM>TAIR(IT))

           IT=IT+1

        END DO

        RA = (G* (1/TFILM)* ABS(TNODE(NUMX,I,J)-TAMB) * PIPEDO**3 )/VAIR(IT)**2*PRAIR(IT)

        IF (RA == 0 ) THEN

           NU = 0.36

          ELSE

          NU = (0.6+0.387*RA**(0.1666667)/(1+(0.559/PRAIR(IT))**(0.5625))**(0.296296))**2

        END IF

        HNAT = KAIR(IT)*NU/PIPEDO


        K2 = DX*DY/DZ*KPIPE/4

        K3 = K2

        K4 = DX*DZ/DY*KPIPE/2

        K5 = DX*DZ*HORIF/2

        K6 = DY*DZ/DX*KPIPE/2

        K7 = DY*DZ*HNAT/2

        T2 = TNODE(NUMX,I,J-1)-TNODE(NUMX,I,J)

        T3 = TNODE(NUMX,I,J+1)-TNODE(NUMX,I,J)

        T4 = TNODE(NUMX,I+1,J)-TNODE(NUMX,I,J)
```

```
        T5 = TORI-TNODE(NUMX,I,J)

        T6 = TNODE(NUMX-1,I,J)-TNODE(NUMX,I,J)

        T7 = TAMB-TNODE(NUMX,I,J)

        HNODE(NUMX,I,J) = K2*T2+K3*T3+K4*T4+K5*T5+K6*T6+K7*T7

    END DO



!-----------------Corner Point-------------------------------------
    I=1+ORIY

    J=1+ORIZ

!$$$$$$    RE = RHOEXIT*UEXIT*ORID/VISFEXIT

!$$$$$$    PR =  CPEXIT*VISFEXIT/KFEEDORI

!$$$$$$    FFACTOR = (1/(1.7372*ALOG(RE/(1.964*ALOG(RE)-3.8215))))**2

!$$$$$$    NU = (RE-1000)*PR*FFACTOR/2/(1+(12.7*sqrt(FFACTOR/2))*(PR**(2/3)-1))

!$$$$$$    HORIF = KFEED / PIPEDI * NU

    IT =1

    TFILM = (TNODE(NUMX,I,J)+TAMB)/2

    DO WHILE (TFILM>TAIR(IT))

        IT=IT+1

    END DO

    RA = (G* (1/TFILM)* ABS(TNODE(NUMX,I,J)-TAMB) * PIPEDO**3 )/VAIR(IT)**2*PRAIR(IT)

    IF (RA == 0 ) THEN

        NU = 0.36

        ELSE

        NU = (0.6+0.387*RA**(0.1666667)/(1+(0.559/PRAIR(IT))**(0.5625))**(0.296296))**2

    END IF

    HNAT = KAIR(IT)*NU/PIPEDO



    K2 = DX*DY/DZ*KPIPE/4

    K22= DX*DY*HORIF/4

    K3 = DX*DY/DZ*KPIPE/2

    K4 = DX*DZ/DY*KPIPE/2

    K5 = DX*DZ/DY*KPIPE/4

    K52= DX*DZ*HORIF/4
```

K6 = DY*DZ/DX*KPIPE*3/4

K7 = DY*DZ*HNAT*3/4

T2 = TNODE(NUMX,I,J-1)-TNODE(NUMX,I,J)

T3 = TNODE(NUMX,I,J+1)-TNODE(NUMX,I,J)

T4 = TNODE(NUMX,I+1,J)-TNODE(NUMX,I,J)

T5 = TORI-TNODE(NUMX,I,J)

T6 = TNODE(NUMX-1,I,J)-TNODE(NUMX,I,J)

T7 = TAMB-TNODE(NUMX,I,J)

HNODE(NUMX,I,J) = K2*T2+K3*T3+K4*T4+K5*T5+K6*T6+K7*T7+(K22+K52)*T5

```
!-------------------------------------------------------------------
! LEFT PART
   J = 1+ORIZ
   DO I= 1,1+ORIY
!$$$$$$      RE = RHOEXIT*UEXIT*ORID/VISFEXIT
!$$$$$$      PR =  CPEXIT*VISFEXIT/KFEEDORI
!$$$$$$      FFACTOR = (1/(1.7372*ALOG(RE/(1.964*ALOG(RE)-3.8215))))**2
!$$$$$$      NU = (RE-1000)*PR*FFACTOR/2/(1+(12.7*sqrt(FFACTOR/2))*(PR**(2/3)-1))
!$$$$$$      HORIF = KFEED / PIPEDI * NU
      IT =1
      TFILM = (TNODE(NUMX,I,J)+TAMB)/2
      DO WHILE (TFILM>TAIR(IT))
        IT=IT+1
      END DO
      RA = (G* (1/TFILM)* ABS(TNODE(NUMX,I,J)-TAMB) * PIPEDO**3 )/VAIR(IT)**2*PRAIR(IT)
      IF (RA == 0 ) THEN
        NU = 0.36
        ELSE
        NU = (0.6+0.387*RA**(0.1666667)/(1+(0.559/PRAIR(IT))**(0.5625))**(0.296296))**2
      END IF
      HNAT = KAIR(IT)*NU/PIPEDO


      K2 = DX*DY*HORIF/2
```

```
        K3 = DX*DY/DZ*KPIPE/2

        K4 = DX*DZ/DY*KPIPE/4

        K5 = K4

        K6 = DY*DZ/DX*KPIPE/2

        K7 = DY*DZ*HNAT/2

        T2 = TORI-TNODE(NUMX,I,J)

        T3 = TNODE(NUMX,I,J+1)-TNODE(NUMX,I,J)

        T4 = TNODE(NUMX,I+1,J)-TNODE(NUMX,I,J)

        T5 = TNODE(NUMX,I-1,J)-TNODE(NUMX,I,J)

        T6 = TNODE(NUMX-1,I,J)-TNODE(NUMX,I,J)

        T7 = TAMB-TNODE(NUMX,I,J)

        HNODE(NUMX,I,J) = K2*T2+K3*T3+K4*T4+K5*T5+K6*T6+K7*T7

   END DO




!----------------------------------------




!---------MIDDLE NODE---------------------


DO K=2,NUMX-1

 DO I = 1,  NUMY

  DO J= 1, NUMZ


      K2 = DX*DY/DZ*KPIPE

      K3 = K2

      K4 = DX*DZ/DY*KPIPE

      K5 = K4

      K6 = DY*DZ/DX*KPIPE

      K7 = K6

      T2 = TNODE(K,I,J-1)-TNODE(K,I,J)

      T3 = TNODE(K,I,J+1)-TNODE(K,I,J)

      T4 = TNODE(K,I+1,J)-TNODE(K,I,J)

      T5 = TNODE(K,I-1,J)-TNODE(K,I,J)
```

```
    T6 = TNODE(K-1,I,J)-TNODE(K,I,J)

    T7 = TNODE(K+1,I,J)-TNODE(K,I,J)

    HNODE(K,I,J) = K2*T2+K3*T3+K4*T4+K5*T5+K6*T6+K7*T7


  END DO

 END DO  ! ALL MID NODE

!---------------------------------------------------------------------

  I = 1+ORIY  ! UPPER ORIFICE BOUNDARY

  DO J = 1, ORIZ+1

!$$$$$$        RE = RHOEXIT*UEXIT*ORID/VISFEXIT

!$$$$$$        PR =  CPEXIT*VISFEXIT/KFEEDORI

!$$$$$$        FFACTOR = (1/(1.7372*ALOG(RE/(1.964*ALOG(RE)-3.8215))))**2

!$$$$$$        NU = (RE-1000)*PR*FFACTOR/2/(1+(12.7*sqrt(FFACTOR/2))*(PR**(2/3)-1))

!$$$$$$        HORIF = KFEED / PIPEDI * NU


      K2 = DX*DY/DZ*KPIPE/2

      K3 = K2

      K4 = DX*DZ/DY*KPIPE

      K5 = DX*DZ*HORIF

      K6 = DY*DZ/DX*KPIPE/2

      K7 = K6

      T2 = TNODE(K,I,J-1)-TNODE(K,I,J)

      T3 = TNODE(K,I,J+1)-TNODE(K,I,J)

      T4 = TNODE(K,I+1,J)-TNODE(K,I,J)

      T5 = TORI-TNODE(K,I,J)

      T6 = TNODE(K-1,I,J)-TNODE(K,I,J)

      T7 = TNODE(K+1,I,J)-TNODE(K,I,J)

      HNODE(K,I,J) = K2*T2+K3*T3+K4*T4+K5*T5+K6*T6+K7*T7

  END DO

! ---------------------CORNER --------------------------------------

  I=1+ORIY

  J=1+ORIZ

!$$$$$$    RE = RHOEXIT*UEXIT*ORID/VISFEXIT
```

```
!$$$$$$     PR =  CPEXIT*VISFEXIT/KFEEDORI

!$$$$$$     FFACTOR = (1/(1.7372*ALOG(RE/(1.964*ALOG(RE)-3.8215))))**2

!$$$$$$     NU = (RE-1000)*PR*FFACTOR/2/(1+(12.7*sqrt(FFACTOR/2))*(PR**(2/3)-1))

!$$$$$$     HORIF = KFEED / PIPEDI * NU

   K2 = DX*DY/DZ*KPIPE/2

   K22= DX*DY*HORIF/2

   K3 = DX*DY/DZ*KPIPE

   K4 = DX*DZ/DY*KPIPE

   K5 = DX*DZ/DY*KPIPE/2

   K52= DX*DZ*HORIF/2

   K6 = DY*DZ/DX*KPIPE*3/4

   K7 = K6

   T2 = TNODE(K,I,J-1)-TNODE(K,I,J)

   T3 = TNODE(K,I,J+1)-TNODE(K,I,J)

   T4 = TNODE(K,I+1,J)-TNODE(K,I,J)

   T5 = TORI-TNODE(K,I,J)

   T6 = TNODE(K-1,I,J)-TNODE(K,I,J)

   T7 = TNODE(K+1,I,J)-TNODE(K,I,J)

   HNODE(K,I,J) = K2*T2+K3*T3+K4*T4+K5*T5+K6*T6+K7*T7+(K22+K52)*T5


!-------------------------------------------------------------------

!-------------------------------------------------------------------

! LEFT PART

   J = 1+ORIZ

   DO I= 1,1+ORIY

!$$$$$$      RE = RHOEXIT*UEXIT*ORID/VISFEXIT

!$$$$$$      PR =  CPEXIT*VISFEXIT/KFEEDORI

!$$$$$$      FFACTOR = (1/(1.7372*ALOG(RE/(1.964*ALOG(RE)-3.8215))))**2

!$$$$$$      NU = (RE-1000)*PR*FFACTOR/2/(1+(12.7*sqrt(FFACTOR/2))*(PR**(2/3)-1))

!$$$$$$      HORIF = KFEED / PIPEDI * NU

      K2 = DX*DY*HORIF

      K3 = DX*DY/DZ*KPIPE

      K4 = DX*DZ/DY*KPIPE/2
```

```
        K5 = K4

        K6 = DY*DZ/DX*KPIPE/2

        K7 = K6

        T2 = TORI-TNODE(K,I,J)

        T3 = TNODE(K,I,J+1)-TNODE(K,I,J)

        T4 = TNODE(K,I+1,J)-TNODE(K,I,J)

        T5 = TNODE(K,I-1,J)-TNODE(K,I,J)

        T6 = TNODE(K-1,I,J)-TNODE(K,I,J)

        T7 = TNODE(K+1,I,J)-TNODE(K,I,J)

        HNODE(K,I,J) = K2*T2+K3*T3+K4*T4+K5*T5+K6*T6+K7*T7

     END DO



!---------------------------------------



END DO  !MID NODE



!-------------------INNER NODE -------------------------------------
K = 1



  DO I = 1,  NUMY

    DO J= 1, NUMZ
!$$$$$$        RE = RHOPIPE*UPIPE*PIPEDI/VISFPIPE

!$$$$$$        PR = CPPIPE*VISFPIPE/KPIPE

!$$$$$$        NU = 3.66+0.0668*(PIPEDI/PIPELEN)*RE*PR/(1+0.04*(PIPEDI/PIPELEN*RE*PR)**(2/3))

!$$$$$$        HPIPE = KFEED / PIPEDI * NU



        K2 = DX*DY/DZ*KPIPE/2

        K3 = K2

        K4 = DX*DZ/DY*KPIPE/2

        K5 = K4

        K7 = DY*DZ/DX*KPIPE

        K6 = DY*DZ*HPIPE
```

```
        T2 = TNODE(K,I,J-1)-TNODE(K,I,J)

        T3 = TNODE(K,I,J+1)-TNODE(K,I,J)

        T4 = TNODE(K,I+1,J)-TNODE(K,I,J)

        T5 = TNODE(K,I-1,J)-TNODE(K,I,J)

        T7 = TNODE(K+1,I,J)-TNODE(K,I,J)

        T6 = TFEED(J)-TNODE(K,I,J)

        HNODE(K,I,J) = K2*T2+K3*T3+K4*T4+K5*T5+K6*T6+K7*T7
!$$$$$$          IF ((I .EQ. 1).AND.(J .EQ.4)) THEN

!$$$$$$          PRINT *,hnode(k,i,j)

!$$$$$$          END IF


      END DO

    END DO  ! ALL INNER SURFACE NODE


    I = 1+ORIY ! UPPER ORIFICE BOUNDARY

    DO J = 1, ORIZ+1

!$$$$$$          RE = RHOEXIT*UEXIT*ORID/VISFEXIT

!$$$$$$          PR =  CPEXIT*VISFEXIT/KFEEDORI

!$$$$$$          FFACTOR = (1/(1.7372*ALOG(RE/(1.964*ALOG(RE)-3.8215))))**2

!$$$$$$          NU = (RE-1000)*PR*FFACTOR/2/(1+(12.7*sqrt(FFACTOR/2))*(PR**(2/3)-1))

!$$$$$$          HORIF = KFEED / PIPEDI * NU

!$$$$$$          RE = RHOPIPE*UPIPE*PIPEDI/VISFPIPE

!$$$$$$          PR = CPPIPE*VISFPIPE/KPIPE

!$$$$$$          NU = 3.66+0.0668*(PIPEDI/PIPELEN)*RE*PR/(1+0.04*(PIPEDI/PIPELEN*RE*PR)**(2/3))

!$$$$$$          HPIPE = KFEED / PIPEDI * NU


        K2 = DX*DY/DZ*KPIPE/4

        K3 = K2

        K4 = DX*DZ/DY*KPIPE/2

        K5 = DX*DZ*HORIF/2

        K7 = DY*DZ/DX*KPIPE/2

        K6 = DY*DZ*HPIPE/2

        T2 = TNODE(K,I,J-1)-TNODE(K,I,J)
```

```
            T3 = TNODE(K,I,J+1)-TNODE(K,I,J)

            T4 = TNODE(K,I+1,J)-TNODE(K,I,J)

            T5 = TORI-TNODE(K,I,J)

            T6 = TFEED(J)-TNODE(K,I,J)

            T7 = TNODE(K+1,I,J)-TNODE(K,I,J)

            HNODE(K,I,J) = K2*T2+K3*T3+K4*T4+K5*T5+K6*T6+K7*T7

    END DO



!-----------------Corner Point-------------------------------------

    I=1+ORIY

    J=1+ORIZ

!$$$$$$    RE = RHOEXIT*UEXIT*ORID/VISFEXIT

!$$$$$$    PR =  CPEXIT*VISFEXIT/KFEEDORI

!$$$$$$    FFACTOR = (1/(1.7372*ALOG(RE/(1.964*ALOG(RE)-3.8215))))**2

!$$$$$$    NU = (RE-1000)*PR*FFACTOR/2/(1+(12.7*sqrt(FFACTOR/2))*(PR**(2/3)-1))

!$$$$$$    HORIF = KFEED / PIPEDI * NU

!$$$$$$    RE = RHOPIPE*UPIPE*PIPEDI/VISFPIPE

!$$$$$$    PR = CPPIPE*VISFPIPE/KPIPE

!$$$$$$    NU = 3.66+0.0668*(PIPEDI/PIPELEN)*RE*PR/(1+0.04*(PIPEDI/PIPELEN*RE*PR)**(2/3))

!$$$$$$    HPIPE = KFEED / PIPEDI * NU



    K2 = DX*DY/DZ*KPIPE/4

    K22= DX*DY*HORIF/4

    K3 = DX*DY/DZ*KPIPE/2

    K4 = DX*DZ/DY*KPIPE/2

    K5 = DX*DZ/DY*KPIPE/4

    K52= DX*DZ*HORIF/4

    K7 = DY*DZ/DX*KPIPE*3/4

    K6 = DY*DZ*HPIPE*3/4

    T2 = TNODE(K,I,J-1)-TNODE(K,I,J)

    T3 = TNODE(K,I,J+1)-TNODE(K,I,J)

    T4 = TNODE(K,I+1,J)-TNODE(K,I,J)

    T5 = TORI-TNODE(K,I,J)
```

T6 = TFEED(J)-TNODE(K,I,J)

T7 = TNODE(K+1,I,J)-TNODE(K,I,J)

HNODE(K,I,J) = K2*T2+K3*T3+K4*T4+K5*T5+K6*T6+K7*T7+(K22+K52)*T5

```
!--------------------------------------------------------------------

! LEFT PART

  J = 1+ORIZ

  DO I= 1,1+ORIY

!$$$$$$       RE = RHOEXIT*UEXIT*ORID/VISFEXIT

!$$$$$$       PR =  CPEXIT*VISFEXIT/KFEEDORI

!$$$$$$       FFACTOR = (1/(1.7372*ALOG(RE/(1.964*ALOG(RE)-3.8215))))**2

!$$$$$$       NU = (RE-1000)*PR*FFACTOR/2/(1+(12.7*sqrt(FFACTOR/2))*(PR**(2/3)-1))

!$$$$$$       HORIF = KFEED / PIPEDI * NU

!$$$$$$       RE = RHOPIPE*UPIPE*PIPEDI/VISFPIPE

!$$$$$$       PR = CPPIPE*VISFPIPE/KPIPE

!$$$$$$       NU = 3.66+0.0668*(PIPEDI/PIPELEN)*RE*PR/(1+0.04*(PIPEDI/PIPELEN*RE*PR)**(2/3))

!$$$$$$       HPIPE = KFEED / PIPEDI * NU


      K2 = DX*DY*HORIF/2

      K3 = DX*DY/DZ*KPIPE/2

      K4 = DX*DZ/DY*KPIPE/4

      K5 = K4

      K7 = DY*DZ/DX*KPIPE/2

      K6 = DY*DZ*HPIPE/2

      T2 = TORI-TNODE(K,I,J)

      T3 = TNODE(K,I,J+1)-TNODE(K,I,J)

      T4 = TNODE(K,I+1,J)-TNODE(K,I,J)

      T5 = TNODE(K,I-1,J)-TNODE(K,I,J)

      T6 = TFEED(J)-TNODE(K,I,J)

      T7 = TNODE(K+1,I,J)-TNODE(K,I,J)

      HNODE(K,I,J) = K2*T2+K3*T3+K4*T4+K5*T5+K6*T6+K7*T7

  END DO
```

```
!---------------------------------------
 !  PRINT*, TNODE(1,3,1),TNODE(1,1,3)



    DO K=1, NUMX

        DO I=1,NUMY

            DO J=1,NUMZ

                ! IF (K==2 .AND. I==11 .AND. J==2) THEN

                ! PAUSE

                ! END

                TNODE(K,I,J)=TNODE(K,I,J)+DT/(CPIPEWALL*DX*DY*DZ)*HNODE(K,I,J)



            END DO

        END DO

    END DO


DO K=0,NUMX+1

    DO J=0,NUMZ+1

        TNODE(K,0,J)=  TNODE(K,2,J)

    END DO

END DO

DO K=0,NUMX+1

    DO I = 0,NUMY+1

        TNODE(K,I,0)=TNODE(K,I,2)

    END DO

END DO


DO K=0,NUMX

    DO I=1,ORIY

        DO J=1,ORIZ

            TNODE(K,I,J) = TORI

        END DO
```

```
   END DO

END DO



!PRINT *, TIME

!PRINT *, TNODE(2,3,4),TNODE(2,3,3),TNODE(2,3,2),TNODE(2,3,1)

!PRINT *, TNODE(2,2,3),TNODE(2,2,2),TNODE(2,2,1)

!PRINT *, TNODE(2,1,3),TNODE(2,1,2),TNODE(2,1,1)

!          WRITE (89,*) TIME




!$$$$$$    TIME=TIME+DT

!$$$$$$  ! REMEMBER TO SET SYMENTICAL NODE

!$$$$$$    END DO

!------------------------------------------------------------------------



END
```

MATLAB Source Code for calculating the weight function parameters

```
clear;


STRESS3 = 1000000;
K = 0.0;
STEP = 0.0001;
Pres = 100000;
thick = 0.0147;
radiu = 0.6096 / 2.0 - thick / 2.0;
STRESS1 = Pres*radiu / thick;
STRESS2 = 1;
CRACKL = [0.02];
K1 = [6.74E+05];


K2 = [4.72E+05];


syms x;
for i=1:180

if i <= 180
    thick = 0.005;
end;
if i <= 120
    thick = 0.006;
end;
if i <= 60
    thick = 0.009;
end;
radiu = 0.6096 / 2.0 - thick / 2.0;
STRESS1 = Pres*radiu / thick;


F10 =  STRESS1*(1.-x / CRACKL(i))^(-0.5);
F11 =  STRESS1*(1.-x / CRACKL(i))^(0.5);
F12 =  STRESS1*(1.-x / CRACKL(i))^(1.5);
F20 =  STRESS2*STRESS1/CRACKL(i)*x*(1.-x / CRACKL(i))^(-0.5);
F21 =  STRESS2*STRESS1/CRACKL(i)*x*(1.-x / CRACKL(i))^(0.5);
F22 =  STRESS2*STRESS1/CRACKL(i)*x*(1.-x / CRACKL(i))^(1.5);

W10 = int(F10,x,0,CRACKL(i));
W20 = int(F20,x,0,CRACKL(i));
W11 = int(F11,x,0,CRACKL(i));
W12 = int(F12,x,0,CRACKL(i));
W21 = int(F21,x,0,CRACKL(i));
W22 = int(F22,x,0,CRACKL(i));

F1(i) = K1(i)/STRESS1/sqrt(3.1415*CRACKL(i));
Q1 = F1(i)/2.0*(K1(i)*sqrt(3.1415*CRACKL(i)/2.0)-W10);
Q2 = F1(i)/2.0*(K2(i)*sqrt(3.1415*CRACKL(i)/2.0)-W20);


C1(i) = (Q1*W22-Q2*W12)/(W11*W22-W21*W12);
C2(i)= (Q2*W11-Q1*W21)/(W11*W22-W21*W12);
c1(i) = double(C1(i));
c2(i) = double(C2(i));
term (i) = STRESS1 / K1(i);
```

```
end
```

```
orit = 0.005;
lent = 0.15;
cracklt = orit*2 + lent;
cc1 = fittedmodelc1(orit,lent);
cc2 = fittedmodelc2(orit,lent);
ff1 = fittedmodelf1(orit,lent);
term1 = fittedmodelterm(orit,lent);
Fm = STRESS1*2* term1 * sqrt(2)*(ff1/2*(1.0-x/cracklt)^(-0.5)+cc1*(1.0-
x/cracklt)^(0.5)+cc2*(1.0-x/cracklt)^(1.5));
Kq = int(Fm,x,0,cracklt);
double(Kq)
```